TWO-PHASE BUBBLY FLOW STRUCTURE IN LARGE DIAMETER PIPES

BY

IHAB EDWARD GERGES,
B.Sc. (Engineering)

In memory of my father

TWO-PHASE BUBBLY FLOW STRUCTURE

IN LARGE DIAMETER PIPES

TWO-PHASE BUBBLY FLOW STRUCTURE

IN LARGE DIAMETER PIPES

By

Ihab Edward Gerges, B.Sc. (Engineering)

A Thesis

Submitted to the School of Graduate Studies

in Partial Fulfilment of the Requirements

for the Degree

Master of Engineering

McMaster University

MASTER OF ENGINEERING (1999)	McMaster University
(Mechanical)	Hamilton, Ontario

TITLE: Two-Phase Bubbly Flow Structure in Large Diameter Pipes.

AUTHOR: Ihab Edward Gerges, B.Sc. (Mechanical Engineering)

(Cairo University)

SUPERVISOR: Professor M. Shoukri

NUMBER OF PAGES: xviii, 117

ABSTRACT

Two-phase flow structure of an air-water, bubbly, upward, cocurrent flow in a large diameter pipe, 20 cm, was investigated experimentally. Local flow parameters such as void fraction, bubble velocity, bubble diameter and interfacial area concentration were measured using a dual fiber optic probe.

A well calibrated air-water testing loop was used to conduct the present experimental work. A computerized data acquisition system was used to analyze the probe output signals and so measuring the different flow parameters.

The local time-averaged bubble diameter was measured using a direct averaging method and Uga's statistical method. The interfacial area concentration was measured using two methods; the bubble diameter-based method and the direct method proposed by Kataoka et al. (1985).

Results of the present tests were compared with available data obtained for flow in small diameter pipes under the same flow conditions. Also, selected existing correlations based on data from small diameter pipe flows were applied to the present data to check their applicability to flows in large diameter pipes.

The results indicated the following under the same flow conditions,

- The local void fractions were in good agreement with those of Stankovic (1992) obtained using the same experimental setup.
- The bubble diameter results obtained using the direct average method and Uga's statistical method were in good agreement. The present work showed that the bubble diameter was generally insensitive to changing the flow rate. Unlike the

small diameter pipes results, the present work showed an increase in bubble diameter near the wall.

Local Interfacial Area Concentration (IAC) results obtained using the two measuring methods were in good agreement. The IAC values measured in the present work were higher than those obtained in small diameter pipes under the same flow conditions. Also, the existing IAC correlations underestimated the area-averaged values significantly, particularly at low air flow rates.

ACKNOWLEDGMENTS

I would like to express my sincere thanks to Dr. M. Shoukri for his patience, support, understanding and guidance throughout this project.

Also, I would like to express my sincere gratitude and appreciation to my wife for her help and support.

Many thanks to Marilyn Paterson assistant to the dean, the departmental administrative assistants Rebecca, Jane, Alyson and Betty and to the departmental technicians Dave and Joe for their great help.

Thanks to colleagues and friends, Jim Cotton, Tony Robinson, Harland Mackenzie and Chris Norris for their advice and assistance.

TABLE OF CONTENTS

LIST OF TABLES

LIST OF FIGURES

NOMENCLATURE

Symbol	Description	Units
a_i	Interfacial Area Concentration IAC	1/m
A	Pipe cross section area	m^2
A_b	Mean bubble surface area	m^2
A_g	Cross sectional area for the gas phase	m^2
A_l	Cross sectional area for the liquid phase	m^2
A_o	Orifice area	m^2
A_{sg}	Surface area of the gas phase	m^2
C	Flow coefficient	
	Statistical factor	
C_D	Drag coefficient	N.sec
d_{crit}	Critical bubble diameter	m
D	Pipe diameter	cm
D_b	Bubble diameter	mm, m
e	Internal energy per unit mass	N.m/Kg
f	Bubble frequency	bubble/sec
F	Drag force	N
g	Gravitational acceleration	m/sec^2
G	Mass flux	$Kg/sec.\ m^2$
h	heat transfer coefficient	W/m.k

H	Enthalpy	N.m/Kg
j	Superficial velocity	m/sec
L	Tests section axial position	m
Lv	Vertical distance between probe tips	mm
$\dot{m}$	Mass flow rate	Kg/sec
$\dot{m}_k$	Mass exchange per unit area for the phase k	$Kg/m^2.sec$
M_i	Generalized interfacial drag	N/m^3
$\vec{n}$	Unit vector normal to the interface	
N_b	Bubble concentration per unit volume	bubble/m3
N_r	Number of records	
Ns	Number of successful bubbles per sapling time	bubble/sec
P	Pressure	N/m^2
$\vec{q}$, q"	Heat flux	W/m^2
r	Radial location	cm
R	Bubble radius / Pipe radius	mm / cm
S	Slip ratio	
$S(r)$	Local standard deviation	
SN	Sampling number of records	
SR	Sampling rate	scan/sec
t	Probe time	sec
T	Sampling time	sec
T_l , T_g	Liquid and Gas phase temperature	K

$\bar{u}$	Velocity vector	m/sec
u_g	Actual gas phase velocity	m/sec
u_l	Actual liquid phase velocity	m/sec
u_r	Relative velocity	m/sec
U_b	Bubble velocity	m/sec
V	Probe signal volt	mv
V	Total flow volume	m^3
V_b	Mean bubble volume	m^3
V_g	Volume occupied by gas phase	m^3
V_i	Interfacial velocity	m/sec
V_l	Volume occupied by liquid phase	m^3
$\dot{V}_g$	Gas volumetric flow rate	m^3/sec
$\dot{V}_l$	Liquid volumetric flow rate	m^3/sec
X	penetration length measured by front probe	mm
Y	penetration length measured by rear probe	mm

<u>Greek</u>

$< >$	Volume-averaged
α	Void fraction
	Volumetric concentration
α_o	Maximum inclination angle for interfacial velocity
$\bar{\bar{\delta}}$	Unit tensor.

θ	Angle between velocity vector and vertical axis	degree
ρ	Density	Kg/m^3
σ	Surface tension	N/m
$\overline{\overline{\sigma}}$	Viscosity stress tensor	N/m^2
τ	Shear stress	N/m^2
	Time delay	sec
$\overline{\overline{\tau}}_k$	Average viscous stress tensor	N/m^2
ΔP	Pressure drop	$N/\ m^2$
Δt	Time limits	sec
Φ	Dissipation	$N/sec.\ m^2$
Γ	Mass generation or transfer rate	Kg/m^3 sec

Subscript

f	Front sensor
g	Gas phase
i	Interfacial
k	Gas or liquid phase
l	Liquid phase
min	Minimum
max	Maximum
op	Orifice plate
r	Rear sensor

TS	Test section

Superscript

t	Turbulent
-	vector
	time averaged

CHAPTER 1

INTRODUCTION

Two-phase flows have received much attention in the past few decades due to its importance in the power and process industries, to name a few. Consequently, there is a continuous need to enhance knowledge of the parameters affecting two-phase flows in piping systems. Although a significant body of knowledge on two-phase flow was generated, available experimental data tend to be limited to two-phase flow in small diameter pipes.

In the analysis of two-phase flow thermal-hydraulics, various formulations such as the homogeneous flow model, drift flux model, and two-fluid model have been proposed. The two-fluid model considers each phase separately, in terms of two sets of conservation equations which govern the balance of mass, momentum and energy of each phase, and accounts for interface exchange through additional interfacial terms in the governing equations. Because of its detailed treatment of phase interactions, the two-fluid model can be considered the most accurate. However, the accuracy of the two-fluid model, and thus its usefulness in applications, depends on accurate modelling of the interfacial transfer terms. The Interfacial Area Concentration (IAC) is the main parameter in the interface exchange formulation and its importance can explicitly be seen in the basic conservation equations of the two-fluid model.

Many models and empirical relations have been proposed to formulate the IAC in terms of flow parameters such as gas and liquid superficial velocities, void fraction and pressure drop. However, available models are based on limited data for flows in small-diameter pipes. The validity of these models for use in large-diameter pipes have not yet been determined.

The present work was driven by the need to obtain data on two-phase flow structure in large diameter vertical pipes in support of the design of a proposed passive cooling system for CANDU reactors (Canadian heavy-water cooled and moderated reactors, using natural uranium as a fissile fuel). Thermal-hydraulic codes used for the design and analysis of such systems are typically based on the two-fluid model formulation for which knowledge of the interfacial area concentration (IAC), in terms of other flow parameters, is required. Available IAC correlations are based on data obtained in small diameter pipes and hence the need for data in large diameter pipes ($D \geq 20$ cm).

1.1 Objectives:

The main objectives of the present work are to provide further knowledge concerning the structure of two-phase flows in large-diameter vertical pipes, and to check the applicability of existing IAC correlations for large-diameter pipes, thus providing information that is necessary for the designers of the Passive Moderator Cooling System (PMCS). These objectives were achieved through the following steps,

a) Modification of an existing test facility for investigating two-phase flow structure in a large-diameter vertical pipe (20 cm).

b) Extensive experimental work specifically designed to cover a sufficient range of parameters which are known to affect the flow structure.

c) Data Processing utilizing a visual C++ program which calculated the void fraction, bubble velocity, bubble diameter and IAC.

d) Comparing the experimental results of the IAC with existing correlations under the same flow conditions.

e) Comparing the IAC results with existing IAC values for small diameter-pipes under the same flow parameters.

CHAPTER 2

INTRODUCTORY CONCEPTS ON ADIABATIC TWO-PHASE FLOW IN VERTICAL PIPES

2.1 Definitions And Relations.

This section presents definitions of the two-phase flow parameters that will be used in the discussion of the present work.

The area averaged void fraction α is the area of the flow occupied by the gas phase, in proportion to the total flow area.

$$\alpha = \frac{A_g}{A} \tag{2.1}$$

The volume averaged void fraction $<\alpha>$ is the volume fraction of the flow occupied by the gas phase, as compared to the total flow volume,

$$<\alpha> = \frac{V_g}{V_l + V_g} = 1 - \frac{V_l}{V_l + V_g} \tag{2.2}$$

where V_g, V_l, A_g, and A are the volume occupied by the gas phase, the volume occupied by the liquid phase, the cross sectional area for the gas, and the pipe cross section area respectively.

The mass flux of the phase k, G_k is given by,

$$G_k = \frac{m_K}{A} \tag{2.3}$$

where m_K is the mass flow rate of the phase K.

The actual phase velocity of the gas and liquid phases, u_g and u_l respectively, are the space-averaged velocities for the given phase. It is also defined as the velocity that the phase would reach if it move separately in the portion of the pipe cross sectional area that is occupied by this phase alone,

$$u_g = \frac{\dot{V}_g}{A_g} = \frac{\dot{V}_g}{\alpha A} \tag{2.4a}$$

$$u_l = \frac{\dot{V}_l}{A_l} = \frac{V_l}{(1-\alpha)A} \tag{2.4b}$$

where $\dot{V}_g$ and $\dot{V}_l$ are the gas and liquid volumetric flow rates respectively.

The superficial velocity j (volumetric flux) for each phase, which is defined as the velocity that the phase would reach if it was flowing alone in the pipe is defined as,

$$\dot{j}_g = \frac{\dot{V}_g}{A} \tag{2.5a}$$

$$j_l = \frac{\dot{V}_l}{A} \tag{2.5b}$$

or,

$$j_g = \alpha \; u_g \tag{2.6a}$$

$$j_l = (1-\alpha) \; u_l \tag{2.6b}$$

The slip ratio S is the ratio between the gas and liquid velocities,

$$S = \frac{u_g}{u_l} \tag{2.7}$$

For homogeneous flows, S=1

The interfacial area concentration a_i is defined as the ratio between the gas phase surface area and the total flow volume,

$$a_i = \frac{A_{sg}}{V} \tag{2.8}$$

where A_{sg} is the surface area of the gas phase.

The relative velocity u_r is the velocity of the gas phase with respect to the liquid phase.

$$u_r = (u_g - u_l) \tag{2.9}$$

For homogenous flow $u_r = 0$.

2.2 Flow Patterns in Vertical Co-current Two-Phase Flow.

The relative velocity and momentum transfer between the phases gives rise to various flow patterns. These patterns influence most of the two-phase quantities such as, void fraction and heat transfer coefficient. Also, it is required to quantify the interfacial area concentration what turns to be the key point for calculating the interfacial transport of the mass, momentum, and energy. Although the present work is solely concerned with the bubbly flow regime, each flow regime for vertical upward co-current two-phase flows will be discussed.

For the case of interest the flow patterns are classified into four main patterns as shown by Figure 2.1. These are as follows:

a) **Bubbly flow** is distinguished by the presence of approximately uniformly distributed gas bubbles in a continuous liquid column. The critical diameter for the bubbles d_{crit} can be defined as the diameter below which the bubbles remain spherical and translate in a rectilinear motion in the static liquid medium. Above the critical diameter the bubbles start to move in a Sinusoidal or Zigzag fashion [Taitel 1980]. The critical diameter can be represented by the following equation:

$$d_{crit} = \left[\frac{0.4 * \sigma}{(\rho_l - \rho_g) * g}\right]^{1/2} \tag{2.10}$$

where σ is the surface tension for the bubble-liquid interface, g is the gravitational acceleration, ρ_l is the liquid phase density, and ρ_g is the gas phase density.

Bubbly flow is classified, depending upon the bubble size, as bubbly flow and finely dispersed bubbly flow. In the dispersed bubbly flow regime, which occurs at high liquid superficial velocities j_l, bubble diameters do not exceed the critical diameter d_{crit}. Taitel et al. 1980, also found that bubbly flow will occur as long as the following condition is satisfied.

$$D > \frac{(4.36)^2}{\rho_l}\left[\frac{(\rho_l - \rho_g)\sigma}{g}\right]^{1/2} \tag{2.11}$$

where D is the pipe diameter

For an air-water flow near atmospheric pressure, equation 2.11 is satisfied for pipe diameters of 50 mm or higher.

b) **Slug flow** is characterized by the appearance of large, bullet-shaped bubbles, which have diameters nearly equal to the pipe diameter and move uniformly upward this is shown by Figure 2.1. These are typically designated as "Taylor bubbles" [Taitel et al. 1980]. Usually the Taylor bubbles are separated by regions of the continuous liquid phase (slugs) which bridge the pipe cross section and contain relatively small gas bubbles. In the thin region between the Taylor bubbles and the pipe wall, the liquid may flow downward as a thin film. At low flow rates, this flow pattern also known as plug (piston) flow having well-defined phase boundaries. However, at higher flow rates the phase boundaries are less distinguishable clear and the pattern known as slug flow.

c) **Churn flow** is characterized by the appearance of bullet-shaped bubbles, as for the slug flow regime, but is much more unstable, foamy, and disordered. It appears at a higher gas flow rates compared to the slug flow regime. The bullet-shaped Taylor bubbles are narrower, their shape is disordered, and the continuity of the liquid slugs between successive Taylor bubbles is continuously disrupted by a high local gas concentration. Between the bubbles, the liquid accumulates forming a bridge which is lifted once again by the gas. This describes the typical motion observed by Taitel et al. (1980) for the churn flow. At higher liquid flow rates a foamy flow pattern is observed.

d) **Annular flow** is characterized by the presence of a continuous column or core of gas along the pipe, which is surrounded by a continuous annulus of the liquid phase. The liquid phase moves upwards both as a wavy liquid film surrounding the gas core, and as droplets entrained in the gas core for sufficiently high gas velocity. A wispy-annular flow pattern describes annular flows with a liquid phase in form of large lumps or wisps.

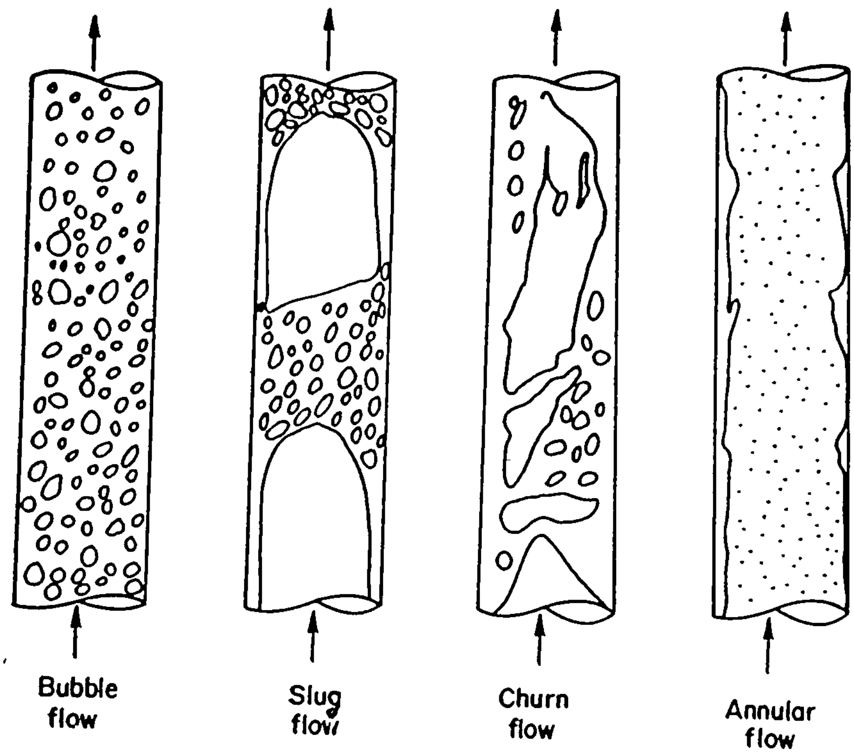

Figure 2.1: Two-Phase Flow Patterns in Vertical Co-current Flow

2.3 Flow regime maps.

Flow maps is a simple method of determining flow regimes based upon known flow parameters. The most common maps are plotted with superficial velocities as the main coordinates, or as a combination of parameters which include velocities. The flow regimes are presented as specified areas on the graph separated by lines to separate the different regimes.

The maps are greatly simplified to present the flow pattern in only two variables, as it is very complicated to characterize the flows in accordance with every parameter which influences them. There are several reported maps for upward two-phase flows, however only a few of these maps are widely used. These include the maps prepared by Hewitt and Roberts (1969), Taitel et al. (1980), Weisman and Kang (1981), Mishima and Ishii (1984) and Ohnuki et al. (1995).

The flow regime map of Taitel et al (1980) is the most widely used flow regime map. This map was developed through modelling of the mechanisms contributing to the transition boundaries between the various flow regimes. As reported by Taitel et al (1980), the flow regime map predictions are in good agreement with the actual data obtained from air-water flow in vertical pipes of 25mm and 51 mm diameters. Figure 2.2 shows a flow regime map for air-water at 25° C and 0.1 MP in a 50 mm diameter vertical pipes. The five lines (A, B, C, D and E) represent the transition boundaries between the five flow regimes, (I) bubbly; (II) finely-dispersed bubbly; (III) slug; (IV) churn and (V) annular.

Stankovic (1997) showed that slug flow is not encountered in large diameter pipes (D=20 cm). In such pipes, increasing the gas velocity causes a transition from bubbly to churn flow directly.

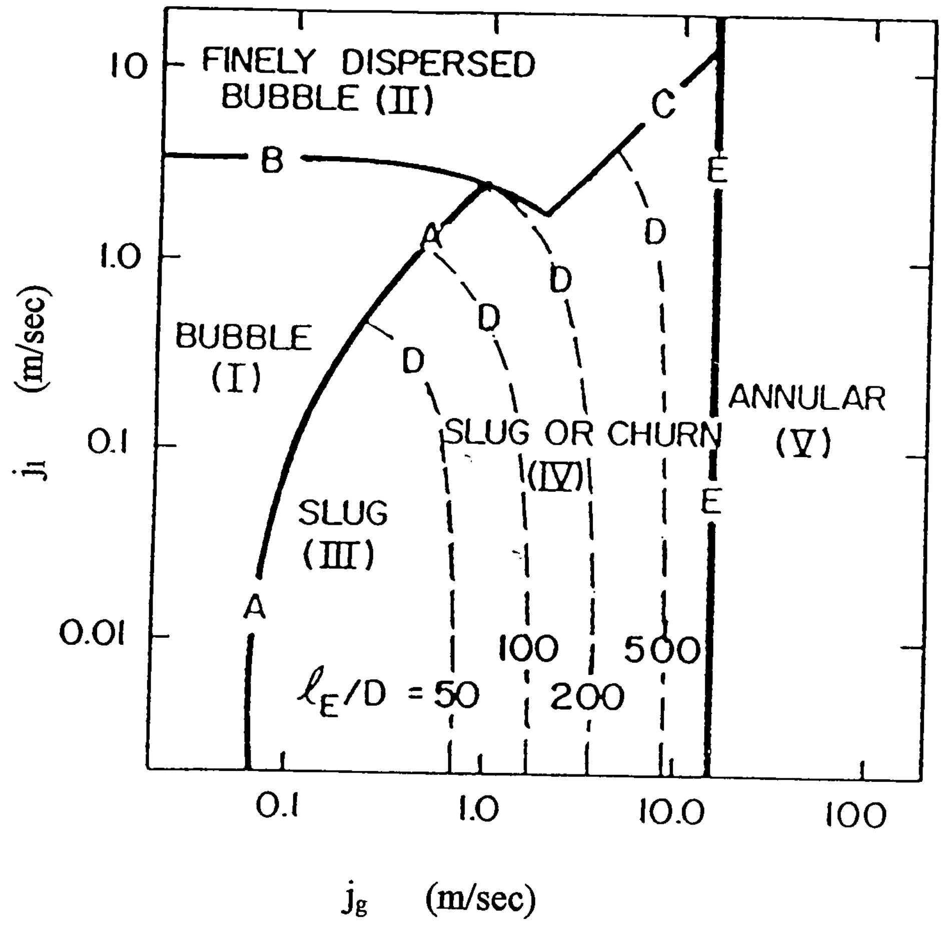

Figure 2.2 Flow Regime Map of Taitel et al. (1980) for Air-Water at 25° C and 0.1 MPa in 50 mm Diameter Vertical Pipes

CHAPTER 3

LITERATURE REVIEW

3.1 Two-phase flow modeling.

The formulation of appropriate models for two-phase flow has been the subject of interest for the last three decades. The main difficulty in modeling two-phase flow, as compared to single-phase flow, is the presence of moving and deformable interfaces through which mass, momentum and energy are exchanged.

A number of modeling approaches have been used based on assumptions made regarding the relative motion between the phases and the interfacial conditions. These approaches range from describing the two-phase flow as a pseudo single-phase fluid, i.e. homogeneous mixture, to a multi-field model, in which separate conservation equations are written for each flow field, e.g. liquid, vapour, droplets etc.

The homogeneous equilibrium model (HEM) is the simplest two-phase flow model. It assumes that the two phases flow at the same velocity and are always in thermodynamic equilibrium. The HEM is useful in limited applications. Other mixture models add some complexity through empirical or semi-empirical correlations to account for relative motion and / or thermal non-equilibrium between the phases.

In the two-fluid model, separate conservation equations are written for each phase and interfacial transport of mass, momentum and energy are incorporated as additional terms in the phasic conservation equations. The model can predict many more details, as compared with mixture models, but requires more constitutive relations for interfacial transport phenomena. The two-fluid model is the closest practical model to rigorous mathematical representation of two-phase flow as shown below.

The fundamentals of continuum mechanics can be used to develop a general mathematical model for two-phase flow as shown by Ishii (1975) and Delhaye (1981). It can be shown that two-phase flow can be represented by two sets of local instantaneous conservation equations, one for each phase, and interfacial conditions in the following general forms

(i) Local instantaneous equations;

$$\frac{\partial}{\partial t}(\rho_k \Psi_k) + \nabla \cdot (\rho_k \Psi_k \vec{u}_k) + \nabla \quad \vec{J}_k - \rho_k \Phi_k = 0 \qquad k=1, 2 \qquad (3.1)$$

(ii) Interfacial conditions;

$$\sum_{k=1,2} (\dot{m}_k \; \Psi_k + \vec{n}_k \cdot \vec{J}_k) = 0 \qquad (3.2)$$

where $\dot{m}_k$ is the mass transfer rate across the interface;

$$\dot{m}_k = \rho_k(\bar{u}_k \quad \bar{u}_i) \cdot \bar{n}_k \qquad (3.3)$$

where $\bar{u}_i$ is the interface velocity and $\bar{n}_k$ is the unit vector normal to the interface.

The definition of the variables Ψ_k, $\bar{J}_k$ and Φ_k ,as shown by Shoukri (1994a), will vary according to the conservation equation as given in the following table.

Balance	Ψ_k	$\bar{J}_k$	Φ_k
Mass	1	0	0
Momentum	$\bar{u}_k$	$\bar{\bar{\sigma}}_k = - P_k \bar{\bar{\delta}}_{ij} + \bar{\bar{\tau}}_k$	$\vec{g}_k$
Energy	$e_k + \frac{1}{2} u_k^2$	$\vec{q}_k - \bar{\bar{\sigma}} \quad \bar{u}_k$	$\vec{g}_k \cdot \bar{u}_k$

Table 3.1 : definitions of conservation quantities.

where $\bar{u}_k$, $\bar{\bar{\sigma}}_k$, P_k, $\bar{\bar{\tau}}_k$, $\vec{g}_k$, e_k and $\vec{q}_k$ are velocity vector, viscosity stress tensor, pressure, average viscous stress tensor, gravitational acceleration, internal energy per unit mass and heat flux of the phase k respectively. While $\bar{\bar{\delta}}_{ij}$ is the unit tensor.

The local instantaneous equations can be used to address simple problems with defined flow fields e.g. single bubble growth in liquid. However, in most two-phase problems, the local instantaneous equation cannot be applied directly due to two main difficulties: (i) existence of moving and deformable interfaces which lead to discontinuity in the flow field, and (ii) fluctuations of the flow variables caused by turbulence and moving interfaces. Accordingly, an averaging approach is used. It is based on averaging the local instantaneous equations in time, space or both.

Volume or time averaging can be used for averaging the local instantaneous equations. However, using one method alone keeps the continuity difficulties unsolved. This approach, as reported by Delhaye (1981), leads to the necessity of using composite averaging.

For example, time averaging of the phasic conservation equations (equation 3.1) over a period of time T yields;

$$\frac{\partial}{\partial t}\alpha_k\overline{(\rho_k\,\Psi_k)} + \nabla\,.\,\alpha_k\overline{(\rho_k\,\Psi_k\,u_k)} + \nabla\quad\alpha_k\bar{J}_k\ -\ \alpha_k\overline{\rho_k\,\Phi_k}$$

$$=\sum_{j=1}^{N_i} l_j^{-1}(\dot{m}_k\Psi_k\ +\ J_k\ .\ n_k)_j \tag{3.4}$$

where j denotes the j $^{\text{th}}$ interface passing through a point at the time T. With α_k is the residence time fraction of phase k, n_k is the unit vector normal to the interface, and l_j is expressed as;

$$l_j\ =\ T\left|v_i\ .\ n_k\right|_j \tag{3.5}$$

The RHS of equation (3.4) represents the interfacial transport terms which appear as a result of the averaging process. For example, for the mass conservation equation where $\Psi_k\ =\ 1$ and $J_k\ =\ 0$, the RHS represent the rate of interfacial mass transfer across the interface per unit volume, where $\dot{m}_k$ is the mass flux and $\sum_{j=1}^{N_i} l_j^{-1}$ represents the averaged interfacial area concentration.

Applying composite averaging and making assumptions regarding the distributions, i.e. the relation between the average of the products and the product of averages, one may develop a practical set of conservation equations representing the two-fluid model as shown below (Ishii 1980)

Continuity:

$$\frac{\partial}{\partial t}(\alpha_k \rho_k) + \nabla . (\alpha_k \rho_k u_k) = \Gamma_k \tag{3.6}$$

Momentum:

$$\begin{aligned}\frac{\partial}{\partial t}(\alpha_k \rho_k u_k) + \nabla \ (\alpha_k \rho_k u_k^2) &= - \alpha_k \nabla P_k - \nabla . \alpha_k (\bar{\bar{\tau}}_k + \tau_k^t) \\ &+ \alpha_k \rho_k g + u_{ki} \Gamma_k + M_{ik} - \nabla \alpha_k . \tau_i\end{aligned} \tag{3.7}$$

Energy:

$$\begin{aligned}\frac{\partial}{\partial t}(\alpha_k \rho_k H_k) + \nabla .(\alpha_k \rho_k u_k H_k) &= - \nabla . \alpha_k (\bar{\bar{q}}_k + q_k^t) \\ &+ \alpha_k \frac{d_k}{dt} P_k + H_{ki} \Gamma_k + a_i q_{ki}'' + \Phi_k\end{aligned} \tag{3.8}$$

Where Γ_k, M_{ik}, τ_i, $q_{ki}^{\cdot}$, and Φ are the mass generation, generalized interfacial drag, interfacial shear stress, interfacial heat flux, and dissipation, respectively. The subscript k denotes the "k" phase, and *i* stands for the value at the interface. The variables α_k, ρ_k, u_k, P_k, and H_k denote the volumetric concentration, density, velocity, pressure and enthalpy of the k phase, where as $\bar{\bar{\tau}}_k$, τ_k^t, $\bar{\bar{q}}_k$, q_k^t, g, H_{ki} stand for average viscous stress, turbulent stress, mean conduction heat flux, turbulent heat flux, acceleration due to gravity and enthalpy of phase k at the interface.

In general, the interfacial transfer terms can be modelled in terms of the interfacial area concentration a_i (m^2/m^3) and a driving force as shown by Ishii (1977). Interfacial transfer terms are a function of IAC and a driving force. For mass transfer, $\Gamma_k = a_i\ \dot{m}_k$ where $\dot{m}_k$ is the mass exchange rate per unit area. Similarly, the interfacial heat exchange rate can be expressed as $q''_{ki} = a_i\, h_i\, (T_l - T_g)$ and the momentum exchange term (drag) can take the form, $F_i = a_i\, C_D\, (u_g - u_l)$.

3.2 IAC Measurement Methods and Techniques.

In general, the interfacial area concentration is measured either directly or indirectly, through the measurement of other flow parameters from which the IAC can be calculated. Direct methods include the Chemical method, described below, in which the volume averaged IAC can be obtained directly from the rate of a chemical reaction across the interfaces.

A commonly used indirect method for measuring IAC in bubbly flow is through the measurement of the average bubble diameter $\overline{D}_b$ and the void fraction α or bubble concentration per unit volume N_b. Assuming spherical and uni-directional bubbles, the IAC can be calculated by either,

$$a_i = 6\alpha / \overline{D}_b \tag{3.9}$$

or

$$a_i = \Pi\ \overline{D_b^2}\ N_b \tag{3.10}$$

In support of this method, many studies were concerned with the measurement of $\overline{D}_b$, N_b and α using a variety of techniques including photography and local probes.

More recently, specific attention was given to using the formulation suggested by equations (3.4) and (3.5) for measuring IAC. As shown, the local interfacial area concentration can be defined as:

$$a_i(r) = \frac{1}{T}\sum_{j=1}^{N_i}\frac{1}{\left|V_i \cdot \bar{n}_i\right|_j} \qquad 1/m \tag{3.11}$$

This requires the measurements of the interfacial velocity and surface direction. Dual probes are used for this purpose as suggested by Herringe and Davis (1976) and Kataoka et al. (1985) among others. This method is described in detail in the next chapter.

A summary of the various techniques used in support of the above methods for measuring IAC are given below.

a) **Chemical Method**

Most of the early experiments concerning the interfacial area measurements utilized the chemical method or the chemical absorption technique. Examples include Kasturi et al (1974), Shilmkan et al (1977), Tomida et al (1978), Dejesus and Kawaji (1990) and many others.

This method is based on the theory of gas absorption with chemical reactions. In this situation the rate of mass transfer, i.e. the amount of gas absorbed, is independent of the liquid side mass transfer coefficient and is governed solely by the contact surface, i.e. interfacial area. By diluting the gas phase with a tracer gas, which would chemically react with the liquid phase, and measuring the rate of gas absorption, one can infer the interfacial area concentration. For example, Dejuses and Kawaji (1990) used the absorption of Co_2 diluted in air into aqueous sodium hydroxide solution to measure the interfacial area concentration in air-water flow.

The advantages of this method are that it is reliable and simple. The main disadvantage is the temperature effect on the reaction and readings. Therefore, the Chemical method requires a temperature controlled environment. This method is limited to measuring the volumetric average interfacial area in the flow.

b) **Light Scattering Method**

The light scattering measuring method for interfacial area concentration basically depends upon the light scattering technique. When a parallel beam of light is passed through a transparent test section, light is scattered by the particles of the dispersed phase e.g., gas bubbles in bubbly flow, by reflection, refraction, and diffraction. The optical device (light source) must be arranged so that only light scattered by diffraction is received by the photocell so that any light scattered by reflection and refraction must be eliminated. To satisfy this condition the photocell must be placed a large enough distance away from the optical device to ensure a small solid angle between them. The remaining scattered light passes outside the photocell so that only the portion of the incident parallel beam that passes through the mixture without meeting any obstacle is recorded. For cases with dispersed particles which are within 10 diameters from one another, multiple scattering exists causing a false reading. Consequently, larger distances are required for the photocell to generate accurate readings.

The dispersed phase, as viewed by the photocell, appears as an assembly of black spots. The amount of light received does not depend on the refractive indices of the two phases or on whether or not the dispersed phase is opaque. The amount of light transmitted to the photocell depends only on the projected area of the dispersed phase.

Calderbank (1958) proposed a correlation for converting the projected measured area at the photocell into an interfacial area.

This technique is comparably simple but clearly limited to highly dispersed two-phase flow regimes, i.e. bubbly and droplet flows. The measurement accuracy depends on the particle size. The light scattering technique is applicable only when interference due to multiple and forward light scattering is negligibly small. This method is also recommended for flows with phase change (Calderbank 1958).

c) **Photographic Method**

The photographic method is considered the most accurate method and has been used to compare and evaluate the accuracy of other methods. It is, however, limited to highly dispersed two-phase flows, i.e. bubbly and droplet flows. Through photography, the average bubble diameter can be obtained. The interfacial area can then be obtained if an independent measurement of bubble frequency or void fraction as shown by equations (3.9) and (3.10),

Zeitoun et al. (1994) used this method for obtaining the IAC in flow boiling applications. To improve the accuracy of measuring bubble diameter, he used a high speed video camera and a visualization system which allowed the simultaneous photography of two orthogonal views of individual bubbles.

d) **Local Probe Methods**

The local probe method allows for local measurement of void fraction, interfacial area as well as bubble size and velocity along with their radial distribution in pipe flow.

This measuring technique depends on the difference of the thermal-physical properties of the gas and liquid phases that allows the recognition of the phase in contact with the probe tip. The probe output is typically a time history of the phase contact with the probe tip. The output data can be analyzed by several methods to determine the local flow characteristics. Traversing the probe along the test cross-section area, the local distribution of the flow parameters can be obtained and volume, or area, averaged. The main source of error associated with this technique is the trigger voltage level which must be checked and adjusted periodically during experiments (Delhaye 1981). There are two common probe types or techniques; electrical resistivity probe and optical probe.

1) Electrical Resistivity Probe

This method was first proposed by Nael and Bankoff (1963) and by Akagawa (1963). It is relatively simple and reliable. A typical probe is shown in Figure 3.1, where the probe tip and the housing tube are the two electrodes.

The electrical resistivity probe measures the instantaneous and local electrical resistivity in two-phase flow mixture by means of the sensor electrode. For a gas liquid flow the gas is electrically insulating, while the liquid is conducting. When the probe tip is in contact with the liquid phase, the circuit is closed, and when it is in contact with a gas phase, the circuit is open. The voltage drop across the sensor fluctuates between a maximum and a minimum values depending on whether it is exposed to liquid or gas. The output signal of the probe shows the voltage variation with respect to the time. This not only indicates which phase is contacting the probe, but also the time it takes for the particular phase to move along the probe tip. For double-sensor probes, shown in Figure 3.2, each sensor gives a separate signal and thus a separate time trace. By correlating the two signals one can estimate important flow parameters such as bubble velocity.

Analysis of the output signals can yield parameters such as, void fraction, bubble diameter and velocity. A detailed description of the analysis method will be discussed later in chapter 4 of this thesis.

This method is known to be one of the most accurate methods. However, this is an intrusive method which can disturb the flow and thus add error to the measurement.

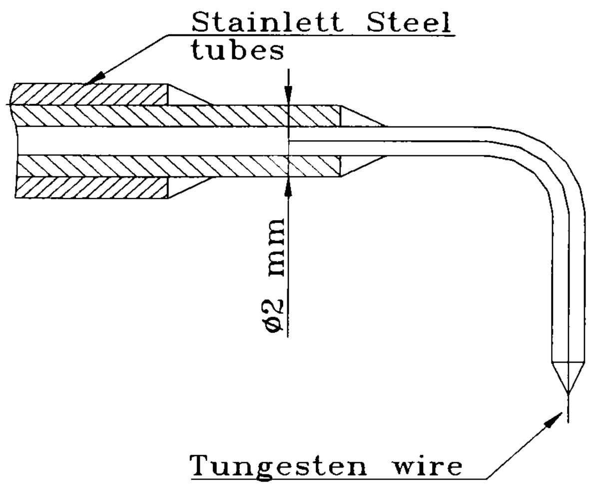

Figure 3.1 Single-Sensor Electrical Resistivity Probe (Delhaye 1981)

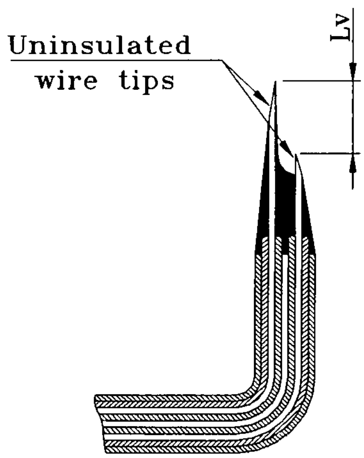

Figure 3.2 Double-Sensor Electrical Resistivity Probe

2) Optical Fiber Probe

The operation of optical probes is based on the difference of the optical properties of the two phases. The fiber sensor is a group of fibers tied together so that a light beam passes down the probe through one half of the optic fibers and is reflected, totally or partially, at the probe tip through the other half. As shown in Figure 3.3, a light beam passing down the probe into the flow is totally reflected when the probe is in contact with the gas while only partially reflected when in contact with the liquid. The phase interface change affects the reflection of the light into the probe as shown by Figure 3.3. The intensity of the reflected light determines the phase in contact with the probe tip. The returning light signals can be converted into voltage signals via a photo-multiplier. This signal can then be processed in the same manner as for the resistivity probes to obtain the desired flow characteristics.

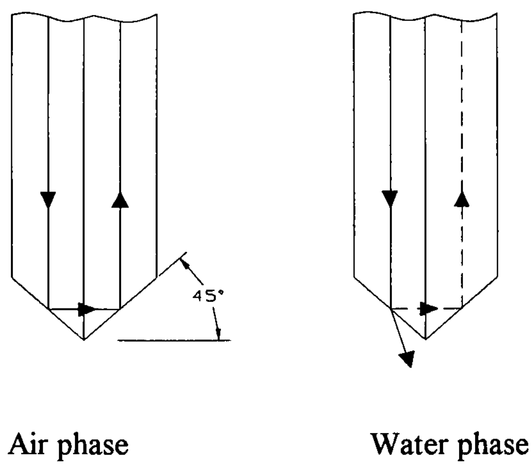

Figure 3.3 Effect of Tip-Touching Phase on Light Reflection

3.3 Interfacial Area Concentration Correlations and their Limitations

As indicated earlier, the two-fluid model is, in theory, the most accurate model for simulating two-phase flows. Design and analysis tools used for design and safety analysis of two-phase systems in industry, particularly the nuclear industry, are based on two-fluid models. The most limiting factor in applying two-fluid models is the lack of appropriate closure, or constitutive equations. The most critical of these are correlations for interfacial area concentration. A brief summary of available correlations is given below.

In order to correlate the interfacial area concentration, an earlier approach was followed by the work of Banerjee et al (1970) and Jespen (1970). The approach requires correlating the interfacial area concentration in terms of frictional pressure drop as well as a measure for the flow velocity which takes into consideration the fact that the interfacial area and interfacial mass transfer are dependent on energy dissipated in the fluid. With the same approach, Kasturi and Stepanek (1974), Shilimkan and Stepanek (1977), Tomida et al (1978) and Dejuses and Kawaji (1990) correlated the interfacial area concentration in terms of frictional or total pressure drops. These correlations were based on the analysis of the data from slug and annular flow regimes in upward co-current flows, except for Dejesus and Kawaji (1990) which covered a wider range of flow regimes from bubbly to annular flow.

Other investigators empirically correlated the IAC in terms of other flow parameters and the thermo-physical properties of the fluid. Therefore, several correlations have been reported, and most of these correlations were restricted to certain flow regimes and flow conditions in relatively small pipes. The following table (3.2) shows the published correlations of interfacial area concentration and their limitations.

Author	Correlation	Measuring technique	Test section dim. / diameter	Flow regime	limitations
Kasturi and Stepank (1974)	$a_i(\dot{V}_l/\alpha_l) = 2.26 \times 10^{-5}\left(\Delta P/L\right)_f^{1.07}$	Chemical	0.6 cm	All	
Akita and Yoshida (1974)	$a_i D_h = \frac{1}{3}(g\ D_h^2\ \frac{\rho_f}{\sigma})^{0.5}(g\frac{D_h^3}{\upsilon_f^2})^{0.1}\alpha^{1.13}$	Photographic	15 cm	Bubbly and Churn	$\alpha < 0.14$
Shilimkan and Stepank (1977)	$a_i(\dot{V}_l/\alpha_l) = 3.61 \times 10^{-5}\left(\Delta P/L\right)_f^{1.31}$	Chemical	0.1 cm	All	
Tomida et al (1978)	$a_i = 0.22(\Delta P / L)_T\,\alpha$	Chemical	1.65 cm	Slug to Annular	jg < 8 m/sec
Kelly and Kazimi (1981)	$a_i = (\frac{6\ \alpha\,\rho_f\ U_r^2}{W_e\sigma})$			Bubbly	$\alpha < 0.3$ and We=50 $G_l > 2700\ Kg / m^2\ s$
Tabie et al (1989)	$a_i = 2100(\alpha)^{1.25}\ (1-\alpha)^{0.75}$	Chemical	10.2 cm	All	
Dejuses and Kawaji (1990)	$a_i = 1.535(\Delta P / L)_T^{0.12} J_g^{1.2} J_l^{-0.14}(\alpha_l)^{1.6}$	Chemical	2.54 and .267 cm	All	
Zeitoun and Shoukri (1994)	$a_i = 3.24(\alpha)^{0.757}(g\ \Delta\rho / \sigma)^{0.55}(\frac{\mu}{G_l})^{0.1}$	Photographic	I.D =12 mm O.D=25 mm	Bubbly with phase change	$G_l \le 550\ Kg / m^2 s$ $\alpha < 0.3$ $P \approx 1$ atm

Table 3.2 Interfacial Area Correlations

As discussed earlier, all of the reported IAC correlations were based on measurements of two-phase flows in small diameter pipes. The applicability of these correlations to flows in large diameter pipes needs to be evaluated.

CHAPTER 4

EXPERIMENTAL TEST LOOP AND MEASUREMENTS.

The present experimental work was performed to measure the flow structure parameters such as void fraction, bubble diameter, bubble velocity, and interfacial area concentration in upward two-phase bubbly flow in a 20 cm diameter pipe. To achieve this goal a two-phase loop and an optical fiber probe were used along with measuring data acquisition equipment. This chapter describes in detail the two-phase loop, measurement instrumentation and data acquisition technique.

4.1 Description of the Two-Phase Loop.

A low pressure air-water loop was used to obtain local two-phase parameters measurements under different flow conditions. Figure 4.1 shows a schematic diagram of the loop. The loop was designed to operate in a natural circulation mode, as an air lift pump, or in a forced circulation mode using a centrifugal water pump as shown in the figure. The loop description could be divided into two main parts, the main components and the instrumentation. The main components are as follows,

a) Riser, Downcomer and Stand-by Pump

The riser is a transparent acrylic pipe with a height and diameter of 10m and 0.2m respectively. Its transparency facilitates flow visualization along the pipe. The downcomer portion was made of 0.1m PVC pipes including a 1.5 m long transparent acrylic pipe to ensure only single-phase water flow in the downcomer. Both the downcomer and riser have the same height and both are connected at the top to an air separation tank. The riser was extended approximately 0.5 m into the tank to discharge the two-phase mixture at a level higher than the water level to promote phase separation.

The bottom part of the riser and the downcomer were connected by a 0.1 m diameter PVC pipe and a gate valve (V_1) for controlling the circulated water flow rate. A stainless-steel centrifugal pump with a rating of 450 USGPM at 10 m head was installed in a by-pass line together with gate valves V_2 and V_3. These two valves served to start the pump and adjust the water flow rate during testing in the forced circulation mode.

b) Air Separation Tank

A 2.25 m long, 0.93 m wide and 0.79 m high air-water stainless-steel separation tank was constructed to separate the air from the two-phase flow mixture incoming into the tank. This tank is illustrated in Figure 4.2. Complete separation was ensured by having long separation path and large separation interface area. As mentioned, the riser pipe was extended into the tank to a height of about 0.5 m to discharge the two-phase flow mixture to a level higher than the water level in the tank. This height is necessary for achieving a successful separation of the phases. For the experiments with low mass flux, the flow mixture was discharged just at the riser end so the air is naturally separated and flows up while the liquid falls down as a free film wetting the riser. For the experiments with high mass flux, a reflector plate helped separate the two phases. The reflector plate was installed at a higher elevation in the tank than the flow exit, as shown in Figure 4.2.

To reduce flow disturbances and improve air separation, a baffle was welded in the middle of the tank with a 2.5 cm gap between the plate and the bottom of the tank. The baffle plate improved phase separation by forcing any trapped bubbles to flow up and be separated from the water surface. The separated air at the upper part of the tank was finally vented out through four openings near the top of the tank. The ideal working conditions for the air separation tank were 20 cm and 40 cm water level for natural and forced circulation experiments respectively. In case of a tank overflow, or for the high mass flux experiments, a large-diameter hose was attached to an opening near the top of the tank. For monitoring the water level in the tank, a sight glass is attached to the tank side.

c) Air Injection Line.

Compressed air was supplied to the test loop by a 5.08cm (2") stainless-steel pipe inlet line. The air was filtered before injection into the loop. The air injection loop is shown schematically in Figure 4.3. The air pressure was manually controlled by a pressure regulator and then injected upstream of the riser at an elevation lower than the horizontal PVC pipe connecting the downcomer and the riser, as shown by Figure 4.1. A circular "shower head" like sieve, with a large number of 1 mm diameter holes was installed in the air injection pass. The disk covers the entire cross-sectional area of the lower part of the riser. A honey comb flow straightener and a coarse grid mesh were also installed downstream at the inlet of the riser to reduce swirling and to improve radial bubble distribution. The air flow rate was manually adjusted by a control valve (V_9). The air inlet line was also equipped with a non-reurn valve (V_{11}) and a stand-by stop valve (V_8) to ensure that there is no possibility of the air injection line being flooded with water from the test loop in case of a fully-close failure of the air control valve.

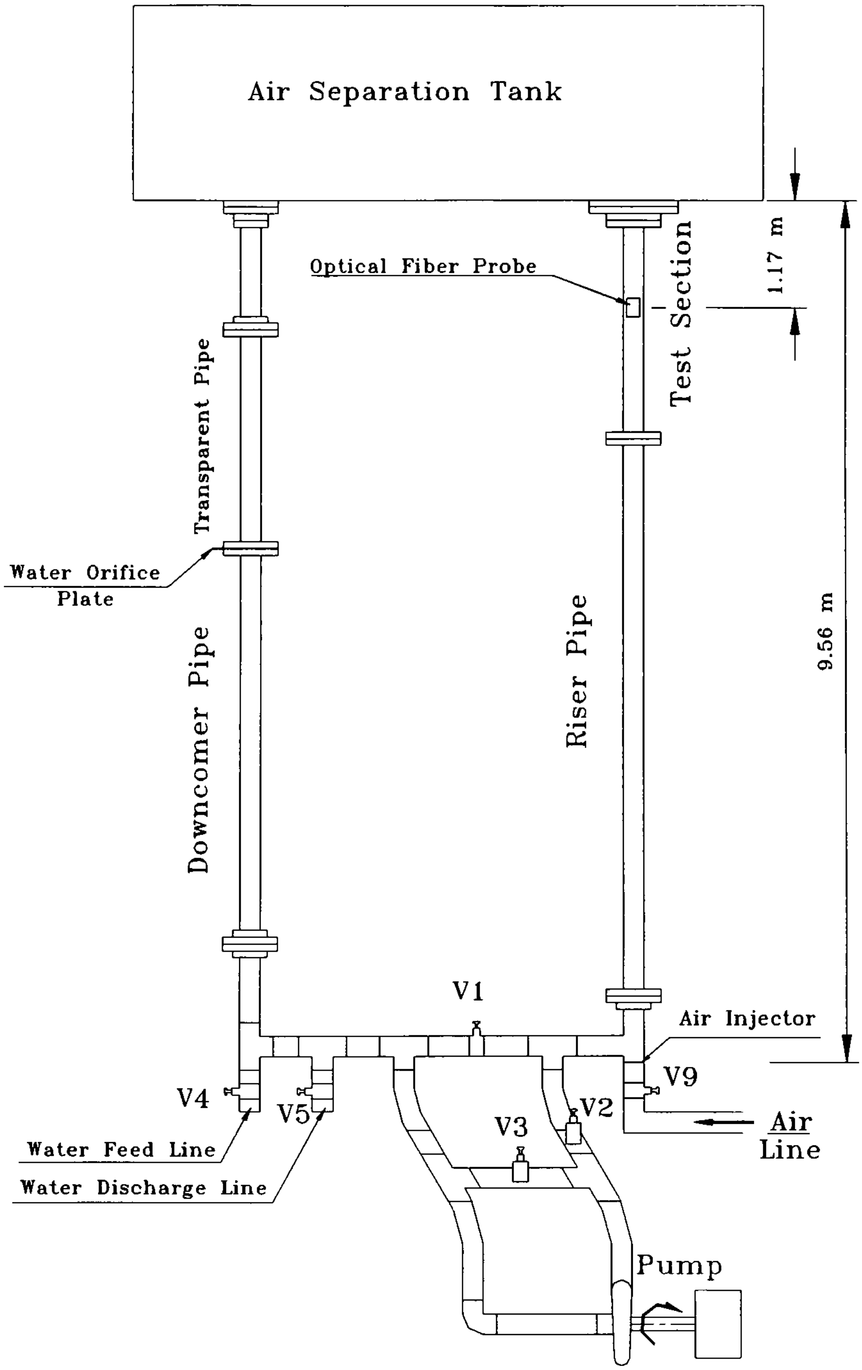

Figure 4.1 Schematic Diagram of the Test Loop

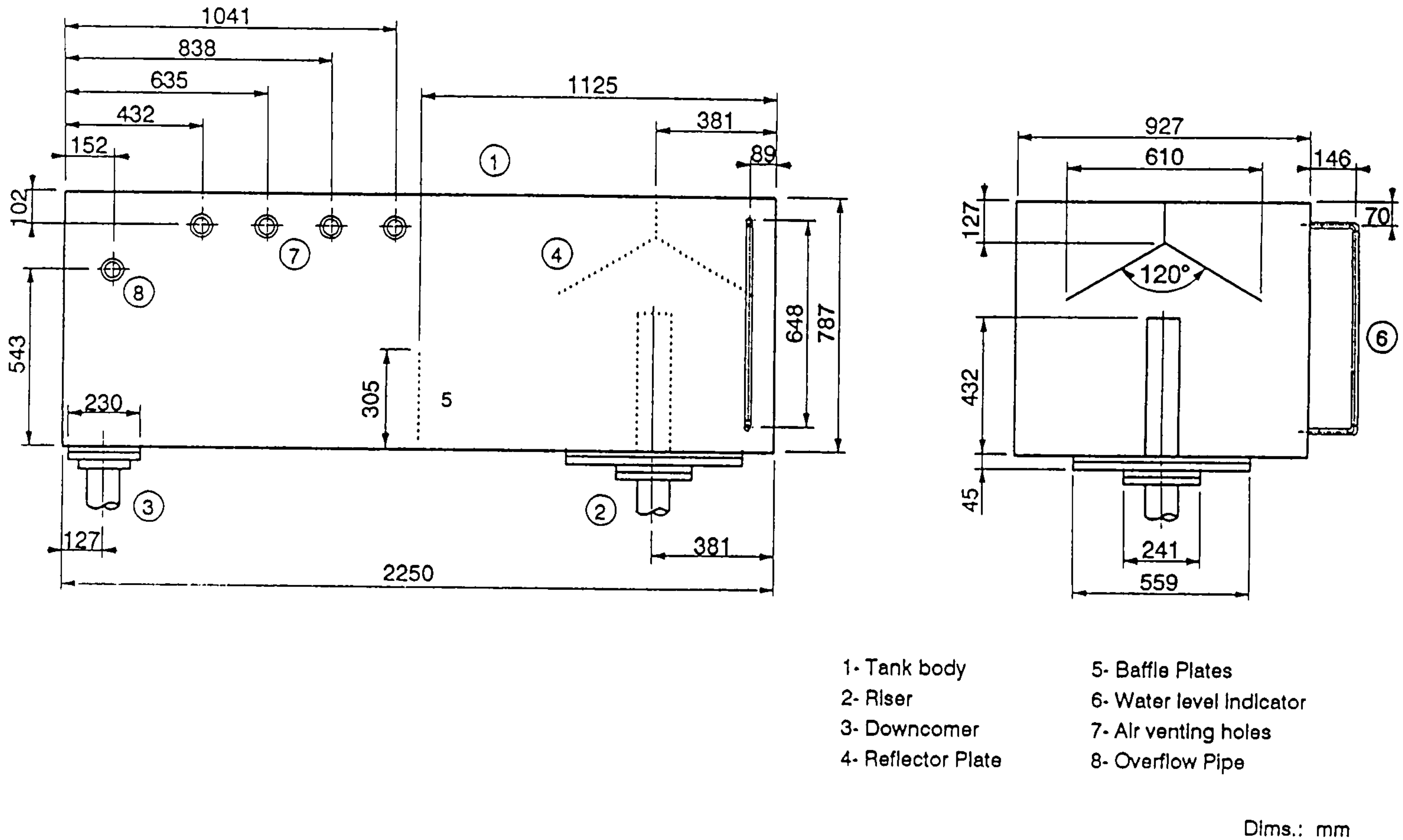

Figure 4.2 Schematic Diagram of Air Separation Tank

[Abdul-razzak 1995]

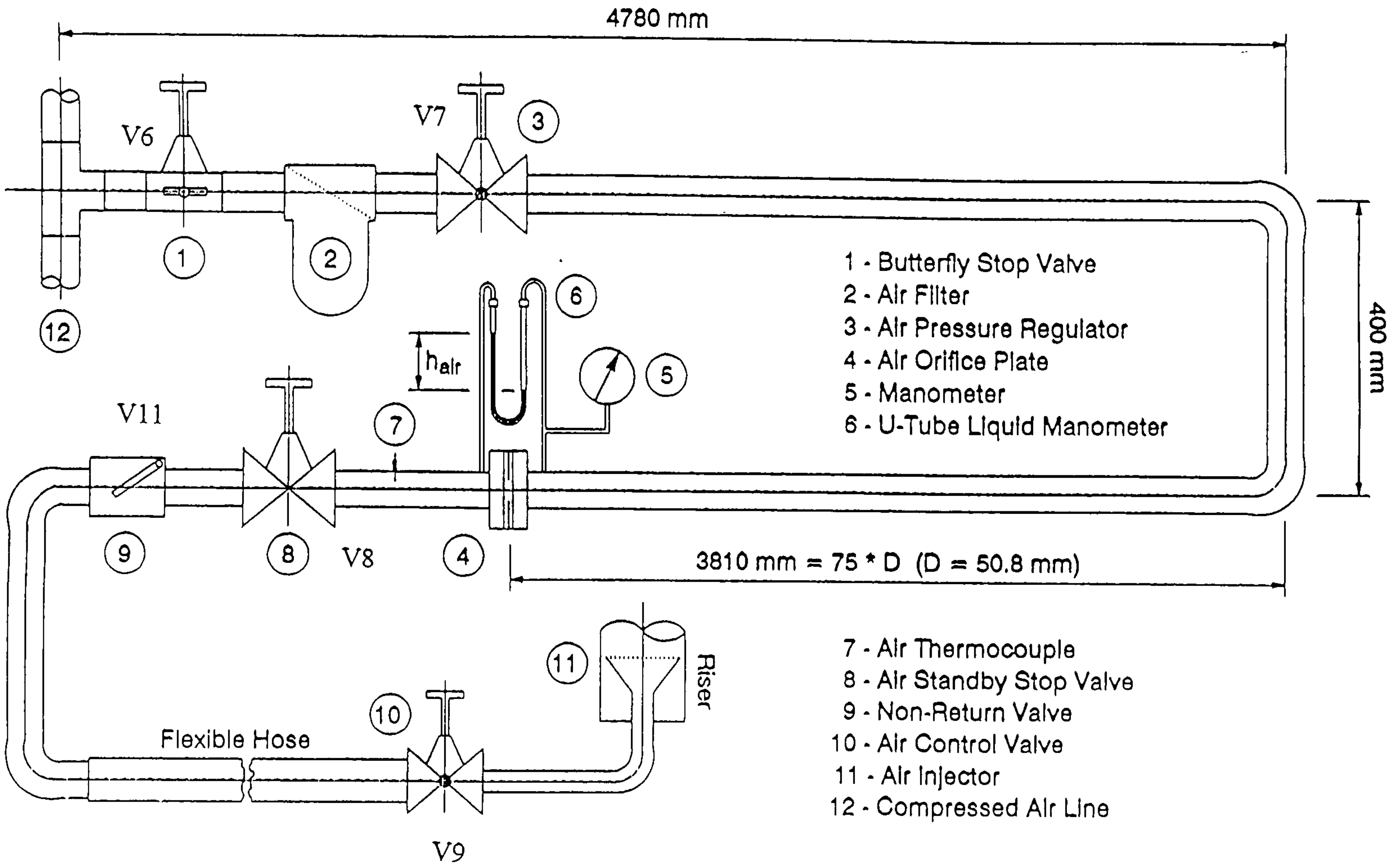

Figure 4.3 Schematic Diagram of Air Inlet Line

[Stankovic 1997]

4.2 Measurements and Instrumentation.

The main measurements for each test are the air and the water flow rates and the voltage output signals from the optical fiber probe which were used to calculate the local flow parameters, e.g. void fraction and interfacial area concentration. The air and water flow rates were measured by orifice plates which comply with ASME standards. Two calibrated water and mercury U-tube manometers were used to calibrate the pressure transducers used to measure the pressure drop across the air and water orifice plates respectively. A linear relation was obtained relating the pressure drop across the orifice plate and the voltage signals from the pressure transducers. The U-tube manometers were also used during the tests to confirm the pressure readings.

During each test the voltage measurements obtained from each pressure transducer were converted into the corresponding pressure drop value using the calibration curves. Volumetric flow rates are then calculated using the following equation:

$$\dot{V}_k = C * A_o \left[\frac{2 * \Delta P_{op}}{\rho_{k_{op}}} \right]^{1/2} \tag{4.1}$$

The subscript *k* denotes the appropriate phase, subscript *op* denotes that pressure drop across the respective orifice plate, ρ is the phase density at the orifice plate pressure and temperature, A_o denotes the orifice area and C is the flow coefficient.

The flow coefficient C depends on the flow Reynolds number and the orifice plate diameter ratio. According to ASME Report on Fluid Meters (1959), and the Daniel Industries Technical Data, its value for the water orifice plate is 0.65 to 0.66 for a diameter ratio of 0.6 and a 10 cm diameter pipe, and for the air orifice plate is 0.6 for a diameter of 0.2 and a 5 cm diameter pipe.

The superficial velocity j for each phase k is calculated as a function of the volumetric flow rate as follows:

$$j_k = \frac{\rho_{k_{op}} * \dot{V}_k}{\rho_{k_{TS}} * A_{TS}} \tag{4.2}$$

or directly as a function of the pressure drop using equation 4.1 as follows:

$$j_k = C * \left(\frac{\rho_{op}}{\rho_{TS}}\right)_k * \left(\frac{A_o}{A_{TS}}\right) * \left(\frac{2 * \Delta P_{op}}{\rho_{k_{op}}}\right)^{1/2} \tag{4.3}$$

where "ρ_{TS}" denotes the phase density corresponding to the pressure and temperature at the test section, and "A_{TS} " is the test section's cross-sectional area.

The local flow structure data were obtained using a Laser Dual Optical fiber probe with signal processing system, supplied by AECL (Atomic Energy of Canada Limited) at Chalk River. The probe measurements were carried out in the test section 1.17 m below the separation tank bottom (Figure 4.1).

The measurements of local parameters, including the radial profile of void fraction, interfacial area concentration, bubble velocity, bubble size and bubble frequency were taken at an axial position corresponds to L/D =42. The dual optical probe was radially traversed from r/R = 0 to 0.95.

The local parameters were measured using the optical dual-fiber probe shown in Figure 4.4. It consists of two identical fiber optic probes of 0.1 mm outer diameter. Their tips are 1.2 mm apart vertically and 1 mm horizontally. It was found that the proper vertical distance L_v between the two sensors is critical for analyzing the experimental data. The distance was dictated by possible bubble size, velocity, and the upper-limit of sampling frequency of the data-logging system. Accordingly, for the test conditions a 1.2 mm vertical distance was found to be appropriate. It is important to note that too small a distance results in inaccuracies in time duration measurements since it requires very high sampling frequencies. On the other hand, too large a distance increases the possibility of misinterpretation of signals since, multi-bubble contact may occur between two signals originating from the same bubble. During the present experiments, a sampling rate of 10 kHz per channel was used to ensure sufficient resolution in analyzing the high-speed, small bubbles. A sampling time of 125 seconds proved satisfactory for statistical analysis with detection of a sufficient number of bubbles for most of the flow conditions. The above configuration, sampling time and frequency were selected after preliminary tests carried out at AECL-Chalk River Laboratory and later at our laboratory.

As shown in Figure 3.3, the incident light is transmitted through one of the fibers and reaches the tip of the probe. The light is then refracted at the interface between the fiber, whose surface makes an angle of 45 degrees to the axis of the fiber optic, and the surrounding phase, depending on the refractive indices of the liquid and gas phases, and returns through the other fiber. The values of refractive index of liquids and gases are far different. Therefore, the time fraction of bubble existence can be determined by measuring the change in the amount of refractive light due to the difference of refractive index. As illustrated in Figure 4.5, the experimental data was obtained in the form of a voltage signal as a function of time from the front and rear sensors of the optical dual-fiber probe. The processing of these signals will be discussed in detail later in this chapter.

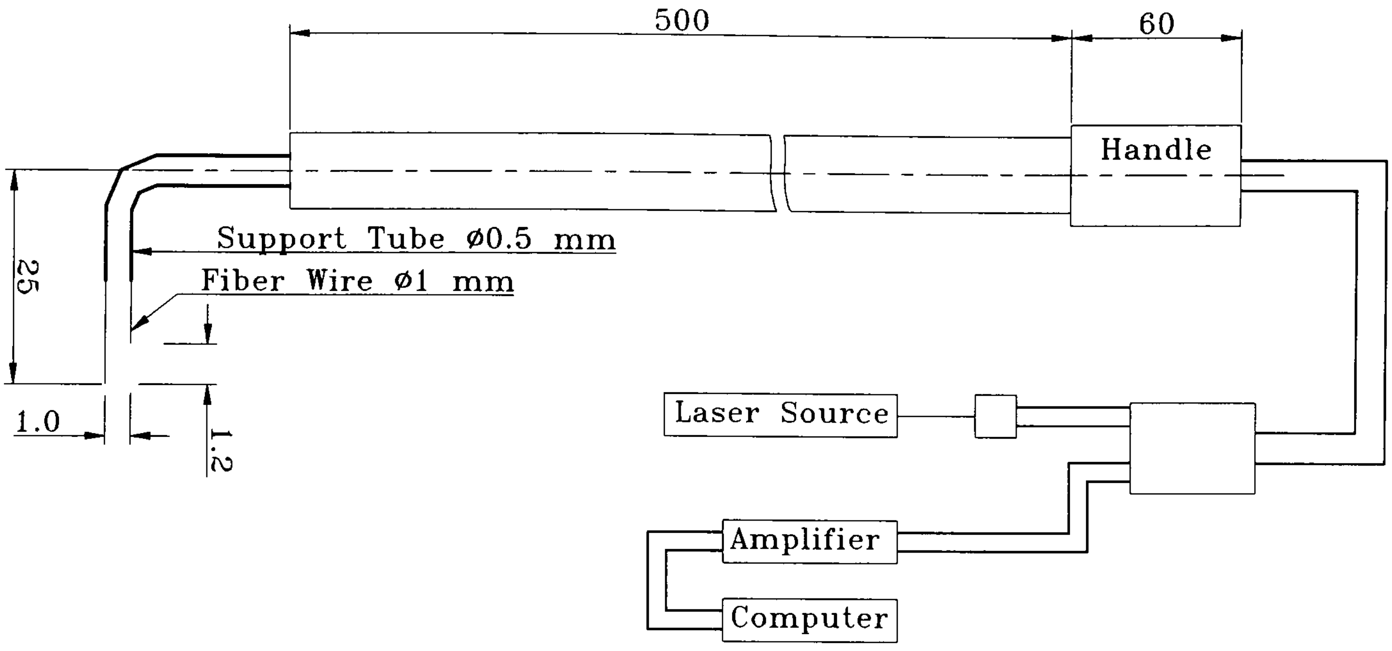

All dimensions are in mm

Figure 4.4 Optical Dual-Fiber Probe System

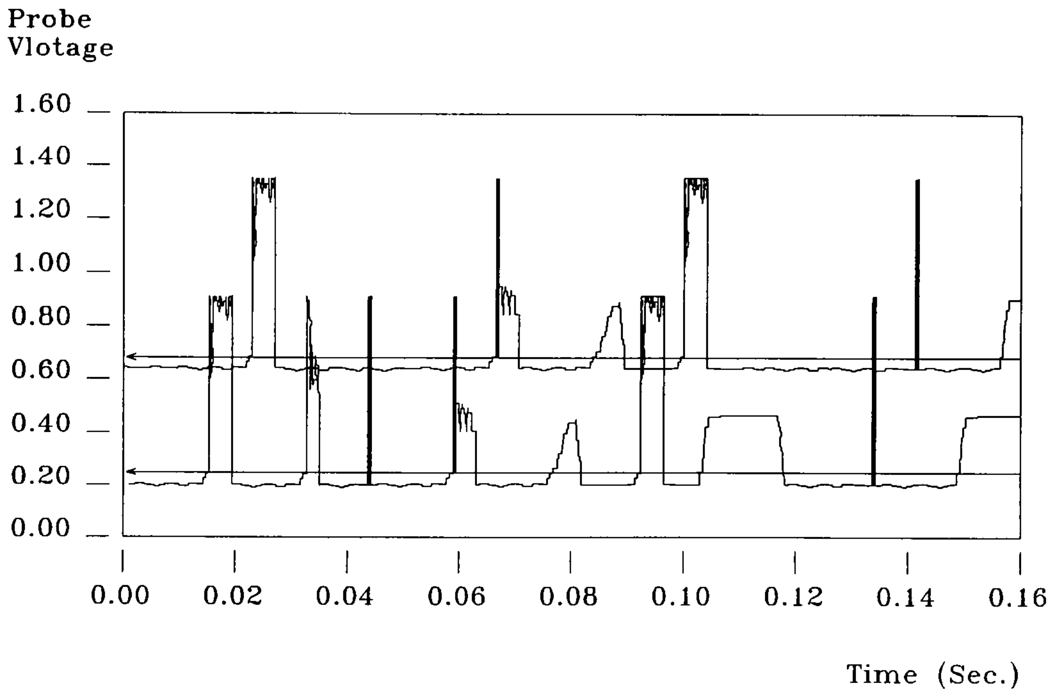

Figure 4.5 A Typical Output Signal of the Optical Dual-Fiber Probe

All measurements were acquired using a computer-based system. The signals obtained during the test included: the pressure drop across the two orifice plates, temperature of the air and water (or two-phase) and the voltage output from the local probe. These data were logged using a Pentium 150 personal computer with a BNC-2080 16 channel multifunction high speed analog/digital expansion board, and LabView software. The output data was processed using a Visual C++5 program, which will be discussed in detail in the following section.

4.3 Data Processing of The Probe Signals:

The probe output was obtained as two voltage signals from the front and rear probes as a function of time as shown in Figure 4.5. The change in voltage indicates a change in the phase in contact with probe. The threshold voltage representing the voltage above which the signal is considered to be in contact with the gas phase, has to be set prior to testing. As a gas interface contacts the front probe the voltage signal increases abruptly from $V_{f,min}$ to $V_{f,max}$, and then back to $V_{f,min}$ when the probe comes in contact with liquid. Another voltage signal for the rear probe may represent the same interfaces with $V_{r,max}$ and $V_{r,min}$ as shown by Figure 4.6. The increase and decrease identifies the individual phases and the time that they are in contact with the probe. Each increase and decrease can be considered as a complete bubble passing through the front or rear probe. Consequently, it is by simply counting the signal peaks that the number of bubbles N passing through this location during the sample time T could be obtained.

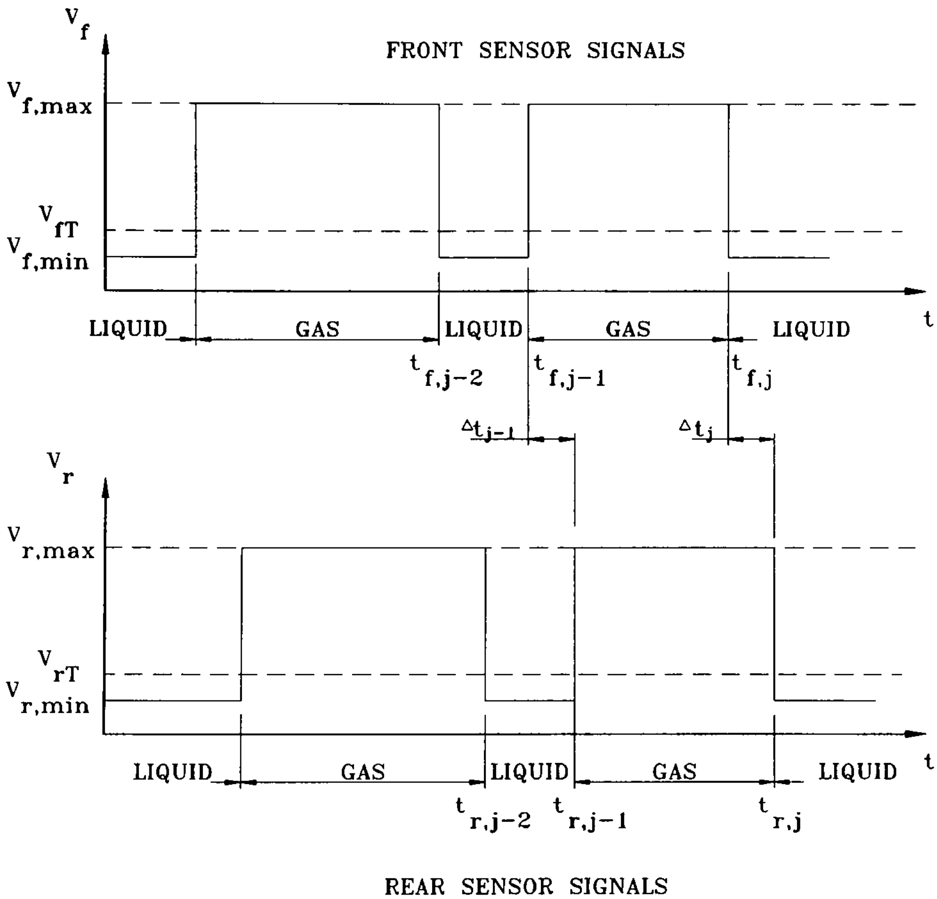

Figure 4.6 Schematic Diagram of Front and Rear Probe Signals

Ideally, all bubbles move vertically and hit the front probe along their center axis and then hit the rear probe. However, this is not the case in practice so miscounting was inevitable during the tests. This miscounting becomes apparent if a bubble is detected by only one of the probes, or if before a bubble penetrates the first probe, another bubble hits the second probe. Here, the time lag for the individual bubble is measured as a negative value which is physically unrealistic. Since the two signals detected by the front and rear probes do not always correspond to the same bubble and the residence time intervals of the gas and or liquid phases at the probes, the origin of the signal must be carefully identified to make sure it belongs to the same bubble. A successful bubble is one which hits the front probe and then the rear probe within a narrow region close to its center axis so that the signals are not disturbed by other bubbles. Failure to identify successful bubbles using these two conditions adversely affects the bubble velocity, diameter and IAC measurements. Validation of the data acquisition method for successful bubbles is justified using the following criteria, which are similar to that used by Revankar and Ishii (1992):

a) Upward moving bubbles hit the front probe before the rear one. Therefore, referring to Figure 4.6, the following conditions must be satisfied:

$$t_{rj} > t_{fj} \text{ and } t_{r(j-1)} > t_{f(j-1)} \quad \text{for } j=1,2,3\ldots, N_s \tag{4.4}$$

where f and r denote respectively the front and rear probes. $t_{(j-1)}$ is the time when the bubble first touches the front and rear probe and t_j is the time when the bubble leaves the probe tips. N_s is the number of successful bubbles, passing through the probe during the total sampling time T.

b) To ensure that the same bubble is being detected and that the measurements are being taken within an appropriate region around the bubble diameter, the two signal widths should be comparable. Hence the following condition should be also satisfied:

$$\left| (t_{fj} - t_{f(j-1)}) - (t_{rj} - t_{r(j-1)}) \right| \leq 0.3 * (t_{fj} - t_{f(j-1)}) \qquad \text{for } j=1,2,3\ldots,N_s \quad (4.5)$$

This condition will be briefly explained by the next geometrical analysis.

c) The final check is a physical limitation of the time difference between the front and rear probe signals. The following conditions should be satisfied:

$$\Delta t_{min} \leq t_{rj} - t_{fj} \leq \Delta t_{max} \qquad (4.6)$$

and,

$$\Delta t_{min} \leq t_{r(j-1)} - t_{f(j-1)} \leq \Delta t_{max} \qquad (4.7)$$

where Δt_{min} and Δt_{max} are the time limits corresponding to the possible maximum and minimum bubble velocities, respectively. Therefore, Δt_{min} and Δt_{max} should be determined by the combination of the vertical distance between the two probe tips L_v and the flow superficial velocities.

4.3.1 Measurements Geometrical Analysis

Bubble diameter is considered one of the more complicated parameters to be measured with a local probe. The main source of this complexity is that the measured distance is not always the diameter. To ensure an accurate measurement, condition 4.5 must be applied. The following Figure 4.7 shows how it can be implemented to ensure that the measured distance is within a region close to the bubble diameter.

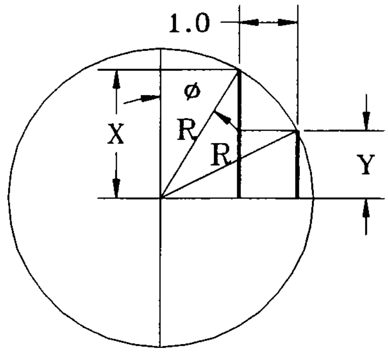

Figure 4.7 Schematic Diagram of Bubble Parameters Measurements

Considering an ideal case when a bubble is moving vertically and hits the probe, the front probe measures the distance X while the rear probe measures Y for a horizontal distance of 1 mm between the two probes. From the geometrical analysis of Figure 4.7, the following equations are obtained:

$$X = R * \text{Cos}(\Phi) \tag{4.8}$$

$$Y^2 = R^2 - (R * \text{Sin}(\Phi) + 1.0)^2 \tag{4.9}$$

where R denotes the bubble radius.

Considering equations (4.8) and (4.9), in order to satisfy the condition (4.5) the following condition must be satisfied:

$$|X - Y| \leq 0.3 * X \tag{4.10}$$

Substituting equations (4.8) and (4.9) into equation (4.10) results in the following equation:

$$1-\sqrt{\frac{1}{\mathrm{Cos}^2(\Phi)}-\frac{(\mathrm{R}*\mathrm{Sin}(\Phi)+1)^2}{\mathrm{R}^2*\mathrm{Cos}^2(\Phi)}}\leq 0.3 \tag{4.11}$$

For a given R, Equation (4.11) calculates the maximum Φ to satisfy this criteria. For a vertically moving-bubble with D_b= 3 mm, the maximum Φ corresponds to equation (4.11) is 2.767 degree which corresponds to $0.998 \leq X/R \leq 1$ and for a vertically-moving bubble with D_b= 6 mm, the maximum Φ is 26.64 degree which corresponds to $0.893 \leq X/R \leq 1$.

This analysis assumes a vertically-moving bubble, i.e. the angle between the vertical axes and the velocity vector is zero. However this is not always the case. Considering the angle (θ) between the velocity vector and the vertical axis, the projection distance between the front and rear probes will be $1.0/\mathrm{Cos}\ \theta$.

For a bubble moving with a certain angle (θ=20 degree) and D_b= 6 mm the corresponding Φ maximum is 24.625 degree which corresponds to $0.909 \leq X/R \leq 1$.

This geometrical analysis shows that to satisfy the condition 4.5 means that the measured distance is close enough to the actual bubble diameter. The 0.3 factor used in this condition was found to be accurate enough for the bubble diameter range of the current tests. However, it eliminates about 85 % of the bubbles and thus leads to more time for each test to reach acceptable results.

4.3.2 Local Void Fraction

By definition, local void fraction is the time fraction of the two phase flow occupied by gas measured at a specific location. Its time averaged value can be defined as the time that the probe is in contact with the gas phase during the total sample time T.

Accordingly, the time averaged local void fraction can be calculated as the number of voltage records higher than the threshold volt divided by the total number of sample records. Also it can be expressed in a form of Delta function δ(r,t), which equals one for each record higher than the threshold volt, or gas phase, and equals zero for records equal or less than that volt, liquid phase. It can be expressed in the following form:

$$\alpha(r) = \frac{1}{SN}\sum_{i=1}^{SN}\delta(r, t_i) \tag{4.12}$$

where SN denotes the sample number of records which was $1.25*10^6$ for the present tests and is given by:

$$SN = SR * T \tag{4.13}$$

where SR is the scan rate per second and T is the total sample time (10000 scan / sec and 125 sec respectively.

Time averaged local void fraction can be measured by the front or the rear probe. The values obtained by the two probes agreed to within ± 3 %.

4.3.3 Bubble Frequency

The local bubble frequency, f, is defined as the number of bubbles N passing through a specific point during the sample time T. It can be expressed as:

$$f = \frac{N}{T} \tag{4.14}$$

4.3.4 Local Bubble Velocity and its Spectrum.

Bubble velocity is determined using the signals from the two probes by measuring the time delay between the two "hits" of a bubble with the front and rear probes, $t_{fj-1} - t_{rj-1}$ (Figure 4.6). The previously mentioned procedure for distinguishing signals from the same bubble was applied and the velocity was calculated by knowledge of the time delay τ and the vertical distance between the tips of the two probes L_v.

$$U_b = \frac{L_v}{\tau} \tag{4.15}$$

The local time-averaged bubble velocity was measured with two different methods, direct average method and multichannel method.

Direct average method can be expressed as the average velocity of successful bubbles, and is expressed as follows:

$$U_b(r) = \frac{1}{N_S} \sum_{i=1}^{N_s} U_{bi}(r) \tag{4.16}$$

where $U_b(r)$ is the local time averaged bubble velocity, and N_s is the total number of successful bubbles.

The multichannel method was also applied for the present tests to evaluate results of the direct average method. The bubble delay time signals were processed as before to identify signals for the same bubbles. Then bubble velocities were proportionally transformed into equally spaced channels. The local bubble velocity, U_b (r), and the standard deviation of the bubble velocity spectrum, S(r), are given by the following formulas (Kataoka et al. 1985),

$$U_b(r) = \sum_{i=1}^{N_i} w_i U_{bi}(r) \tag{4.17}$$

$$S(r) = \left\{ \sum_{i=1}^{N_i} w_i \left[U_{bi}(r) - U_b(r) \right]^2 \right\}^{1/2} \tag{4.18}$$

where U_{bi} (r) is the instantaneous measured local bubble velocity in the *i*th channel, N_i is the number of channels, and w_i is the probability density of U_{bi} in this channel.

The results of these two methods were identical when long sampling times were used.

4.3.5 Bubble Size and its Distribution.

Knowledge of the local void fraction distribution across the pipe cross section does not completely identify the two-phase flow structure. It must also be combined with the bubble size distribution. The same void fraction may be due to either large number of small bubbles or a small number of large bubbles. The two cases differ from each other with regards to the other flow characteristics, such as interfacial area concentration and the thermal and momentum transfer coefficients.

The bubble diameter can be measured by calculating the bubble velocity as shown by equation 4.16, and combining this with the time required for this bubble to move completely through the front probe. The time is measured as the number of records for the bubble N_r divided by the sampling rate SR. The bubble diameter can then be expressed as:

$$D_{bi}(r) = \frac{N_r \; U_{bi}}{SR} \tag{4.19}$$

To obtain the local average bubble diameter two methods were used: the direct average method and Uga's statistical method.(Uga 1971)

(a) Direct Average method

For the direct average method, the local time-averaged bubble diameter is calculated by averaging the individually calculated bubble diameters over the number of successful bubbles as follows:

$$D_b(r) = \frac{1}{N_s} \sum_{i=1}^{N_s} D_{bi}(r) \tag{4.20}$$

Two assumptions were made when using this method. The first assumption is that bubbles were small (2.5-6 mm diameter) and nearly spherical. The second one is the assumption of unidirectionality, which was generally true when the measuring point was far from the wall (relative to bubble size), and using a very small probe tip (0.1 mm diameter) in comparison with the detected bubbles.

(b) Uga's Statistical method

The other method used to calculate the time-averaged local bubble diameter is the statistical method suggested by Uga (1971). In this method, single fiber optic probe is used to measure the penetration length of each bubble touching the probe to obtain the bubble diameter. The steps of this method can by summarized as follows:

1) The local time averaged bubble velocity, U_b, is used together with the signal of the front probe to calculate the penetration length X for each bubble passing through the probe
2) The resultant penetration lengths are then prepared in the form of a histogram versus its frequency of occurrence.
3) The histogram is then normalized by dividing each frequency by its penetration length. The normalized histogram is then plotted versus the penetration length as shown by Figure 4.8.
4) Using a curve fitting procedure, a smooth curve function g(x) is obtained the normalized frequency and the penetration curve.
5) A function relating the bubble size distribution with the time averaged bubble diameter is determined from the following relation:

$$F(x) = \frac{1}{2}[g(x) - x\frac{d\,g(x)}{d\,x}] \tag{4.21}$$

6) The time averaged local bubble diameter is the bubble diameter corresponds to the peak value of the F(x).

Bubble diameters results from Uga's statistical method were in good agreement to those results from direct averaged method.

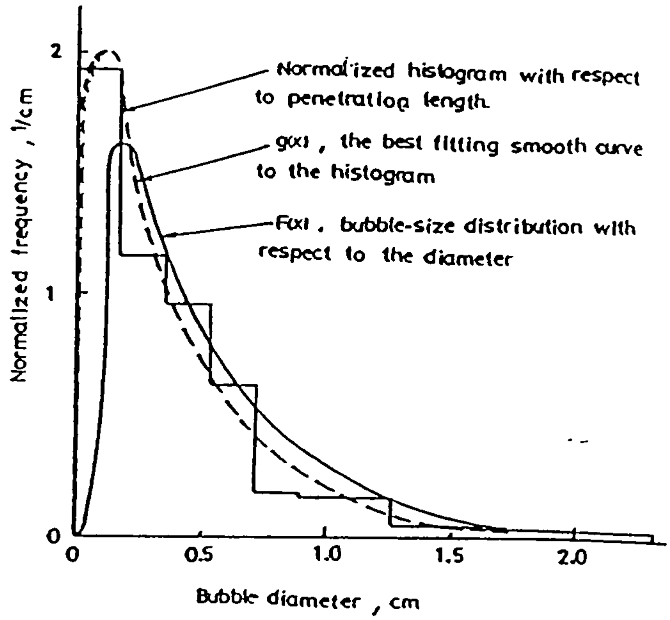

Figure 4.8 Schematic Diagram for Uga's Statistical Method Principles.

(Uga 1971)

4.3.6 Local Interfacial Area Concentration.

In the present work, two main methods were used to measure the local interfacial area concentration. These are described below:

(i) Bubble Diameter-Based Method :

In the bubble diameter-based method the local IAC is given as,

$$a_i(r) = \alpha(r)\frac{A_b}{V_b} \tag{4.22}$$

where $\alpha(r)$ is the local void fraction and A_b and V_b are the local mean bubble surface area and volume respectively, given by

$$A_b = \frac{1}{N}\sum_{i=1}^{N} A_{bi} \tag{4.23}$$

$$V_b = \frac{1}{N}\sum_{i=1}^{N} V_{bi} \tag{4.24}$$

where N is the total local number of bubbles at the sample time T.

The very simple approach for measuring local IAC was first reported by Akida and Yoshida (1974), assuming spherical bubbles for bubbly flow leads to:

$$a_i(r) = \frac{6\alpha(r)}{D_b(r)} \tag{4.25}$$

where $D_b(r)$ is the local bubble diameter.

In applying equation (4.25), the two methods for bubble diameter measurements, namely the direct average method and Uga's statistical method were used.

(ii) The Direct Method: (Kataoka et al. 1985)

The local IAC at any spatial location (r) was first reported by Ishii (1977) as:

$$a_i(r) = \frac{1}{T}\sum_{j=1}^{N}\frac{1}{\left|V_i \cdot n_i\right|_j} \qquad 1/m \tag{4.26}$$

where V_i, n_i are bubble interfacial velocity and the unit normal vector of the interface. The origin of equation (4.26) can be seen in the time-averaged conservation equation, i.e. equations (3.4) and (3.5).

The form of equation (4.26) suggested to many investigations the use of a double sensors probe to obtain the required velocity and interface direction. These include the early work of Herringe and Davis (1976), Veteau (1981) and Veteau and Charlot (1981).

Kataoka et al. (1985) suggested a modified method for the application of equation (4.26). Using statistical analysis to avoid the need for three-dimensional measurements, they suggested the following formula:

$$a_i = \left[\frac{1}{T}\sum_{j=1}^{N}\frac{1}{\left|V\right|_j}\right] * C \tag{4.27}$$

where C is a statistical factor.

By assuming that the angle α between the interfacial velocity and the vertical axial direction is random with an equal probability and the angle α varies in a range from zero to α_o, the statistical factor was found to be a function of α_o as follows:

$$C(\alpha_o) = \left\{1 - \cot(\frac{\alpha_o}{2})\ln\left[\cos(\frac{\alpha_o}{2})\right] - \tan(\frac{\alpha_o}{2})\ln\left[\sin(\frac{\alpha_o}{2})\right]\right\}^{-1} \tag{4.28}$$

Also α_o was related to the bubbles velocities in the form of:

$$\frac{\sin 2\alpha_o}{2\alpha_o} = \frac{1 - \dfrac{S^2(r)}{U_b^2(r)}}{1 + \dfrac{3S^2(r)}{U_b^2(r)}} \tag{4.29}$$

where S is the standard deviation of the bubble spectrum given by equation 4.18, and U_b is the mean bubble velocity given by equation 4.17.

The angle α_o is in the range of $0 \leq \alpha_o \leq \Pi/2$, so that the value of $C(\alpha_o)$ is in the range of $1 \leq C(\alpha_o) \leq 0.634$. The local IAC is then presented as:

$$a_i(r) = 4f\,[\,\sum_{j=1}^{N} \frac{1}{U_{zj}} / \sum_{j}\,]\, C(\alpha_o) \qquad 1/\mathrm{m} \tag{4.30}$$

where f is the bubble frequency and U_z is the vertical component of the bubble velocity which is measured by dual-fiber probes.

This method was successfully used by many investigators include Kataoka and Serizawa (1990) and Kocamustafaogullari and Wang (1991), to name a few.

In the present work, the results obtained by the method of Kataoka et al. (1985) were compared with those obtained using the bubble diameter-based methods.

4.3.7 Area Averaged Parameters.

Local time averaged parameters are measured and plotted as a function of the dimensionless distance (r/R). The area-averaged parameters can be obtained by integration of the corresponding radial profile of these local parameters,

$$<\varphi>\equiv \frac{1}{A} * \int_{0}^{R} \varphi(r) * 2\Pi r \, dr \tag{4.31}$$

where φ(r) is a function profile expressing any fitted group of results, and A is the test cross-sectional area.

The measured void fraction and the IAC profiles were fitted with smooth curves as a function of (r/R). The fitted profiles were then integrated using the following equation,

$$<\varphi>\equiv 2 * \int_{0}^{1} \varphi(r/R) * (r/R) \, d(r/R) \tag{4.32}$$

4.4 Experimental Procedure.

The experiments were carried out under bubbly flow conditions by varying the liquid and gas superficial velocities and the probe radial position. At each fixed gas superficial velocity, the liquid velocity was increased. For each set of gas and liquid superficial velocities, the fiber optic probe was traversed in the direction perpendicular to the tube vertical axis. Fifteen locations were selected through the pipe radius. The increment was 10 mm for $0 \leq r/R \leq 0.7$, and smaller increments were used for the remainder (r/R = 0.75, 0.8, 0.85, 0.87, 0.9, 0.92, and 0.95)

For each experimental condition the recorded data includes probe location and air and water superficial velocities. The output files for each run contain the scan condition for the probe tips. A typical experimental procedure is as follows:

1. Prepare experimental plan (j_l and j_g)
2. Check:
   a) Water level in the air separation tank;
   b) Position of each valve, leakage of pipes and connections if any;
   c) Electric cable connections.
3. Switch on all instruments and computer.
4. Check all signal readings and adjust it to zero if required.
5. Start injecting the air at a predetermined value and adjust water flow rate
6. Adjust the threshold value of the fiber optic signal
7. Set the data acquisition system and acquire data at a rate of 10 HZ for a 125 seconds period.
8. Obtain a complete set of data at fifteen radial locations by traversing the probe across the pipe radius.
9. At the completion of all measurements,
   a) Shut off the air supply;
   b) Turn off the pump in the case of forced circulation;
10. Check no flow instrument readings.

CHAPTER 5

EXPERIMENTAL RESULTS AND DISCUSSION

5.1 Introduction

Experimental results such as local distributions of void fraction, bubble velocity, bubble frequency, bubble diameter and interfacial area concentration for air-water, bubbly, cocurrent flow in a vertical 20 cm diameter pipe are presented in the following sections. Comparisons between present results and existing data and correlations are also presented. A complete list of the experimental results can be found in appendix A. The test conditions are presented by the following Table:

Pressure	1.0 Bar absolute (approximately)
Temperature	20-25 ^{0}C
Inlet air pressure at V9	28 PSI (193 Kpa) gauge
Water Mass Flux G_l	20-400 Kg/ m^2 s
Air Mass Flux G_g	0.031-0.078 Kg/ m^2 s
Superficial Liquid Velocity j_l	0.02, 0.06, 0.1, 0.2, 0.3 and 0.4 m/s
Superficial Liquid Velocity j_g	0.022, 0.033, 0.044 and 0.055 m/s
Void fraction	3.44 % - 12.7 %

Table 5.1: Test conditions

5.2 Local Void Fraction

To verify the present local void fraction measurements and ensure the repeatability of the measuring instruments, some void fraction profiles were obtained under similar conditions to those measured by Stankovic (1997) using the same facility with a single sensor probe. The results are compared in Figures 5.1 and 5.2. As shown, the present results are in excellent agreement with those obtained by Stankovic (1997).

Local void fraction profiles were obtained during the present tests under different flow conditions, i.e. gas and liquid superficial velocities. Selected groups of these profiles are shown in Figures 5.3 to 5.6. The profiles presented were obtained at constant superficial air velocities by varying the water superficial velocities. The profiles obtained at j_a=0.022, 0.033, 0.044 and 0.055 m/s are shown in Figures 5.3, 5.4, 5.5 and 5.6 respectively.

As shown, the local void fraction profiles are generally flat across the central part of the pipe and tend to be more parabolic with decreasing the liquid velocity at constant air velocity, i.e. with increasing void fraction. These observations are consistent with those of other researchers and in agreement with the results of Stankovic (1997).

The effect of pipe diameter on the local void fraction distribution in bubbly flow is examined by comparing the present profiles with the fully developed profiles obtained by Revankar and Ishii (1992) in a 5.08 cm diameter pipe under similar flow conditions. These comparisons are shown in Figures 5.7 to 5.9. As shown in Figure 5.7, the two profiles are in good agreement. Figures 5.8 and 5.9 show the saddle-type profiles obtained by Revankar and Ishii (1992) where the void fraction tends to peak near the wall and decreases to a flat profile in most of the core. As shown, the present data, obtained under the same air and water velocities in a large diameter (20 cm) pipe, did not show such a profile.

These results are consistent with those obtained by Stankovic (1997), who showed that the saddle-type profiles, which is common in bubbly flow in small diameter pipes, only appear in large diameter pipes under conditions of very low area-averaged void fraction $<\alpha> < 0.04$.

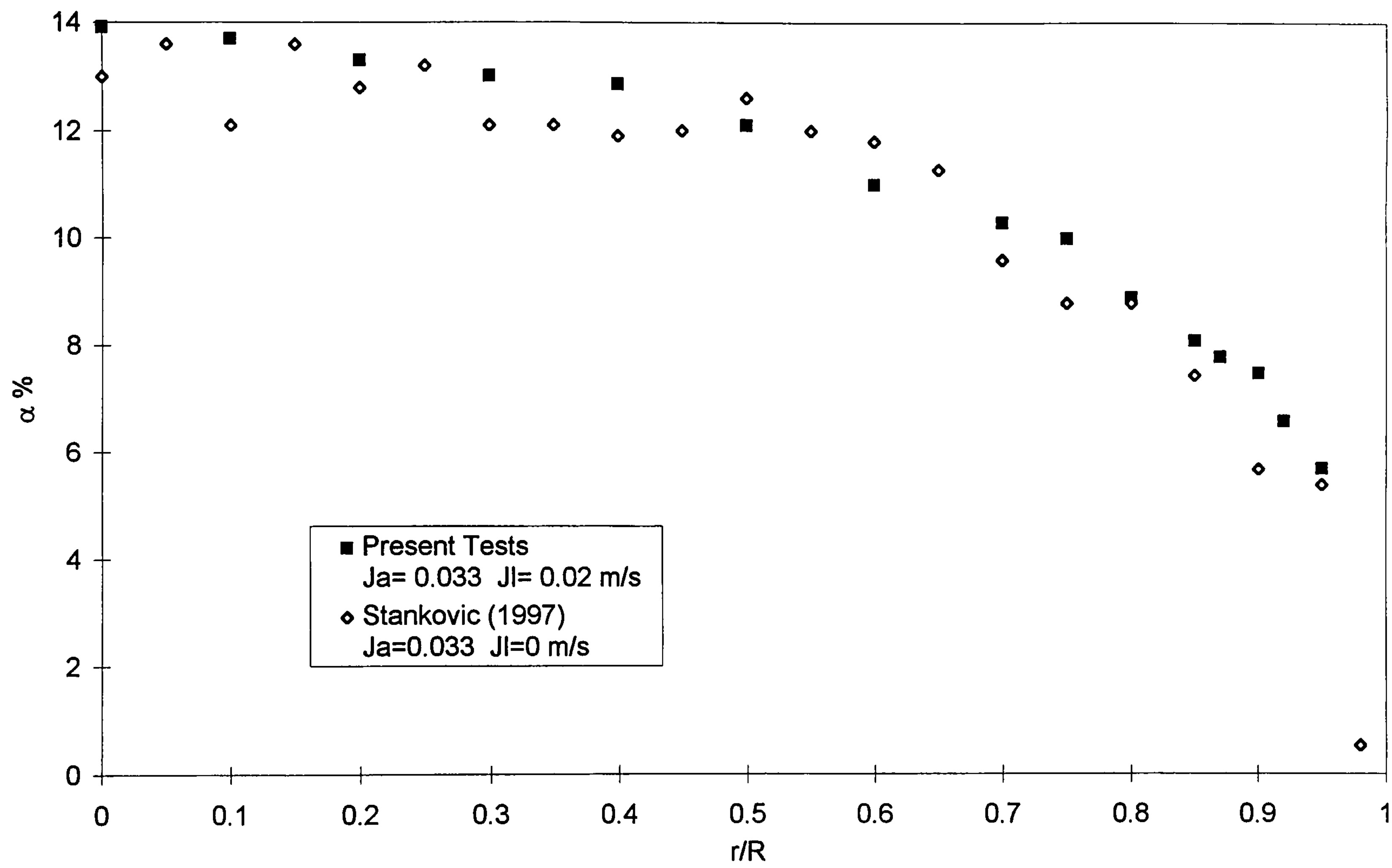

Figure 5.1: Comparison between Void Fraction Data of Present Work and Stankovic (1997) Data for D=20 cm

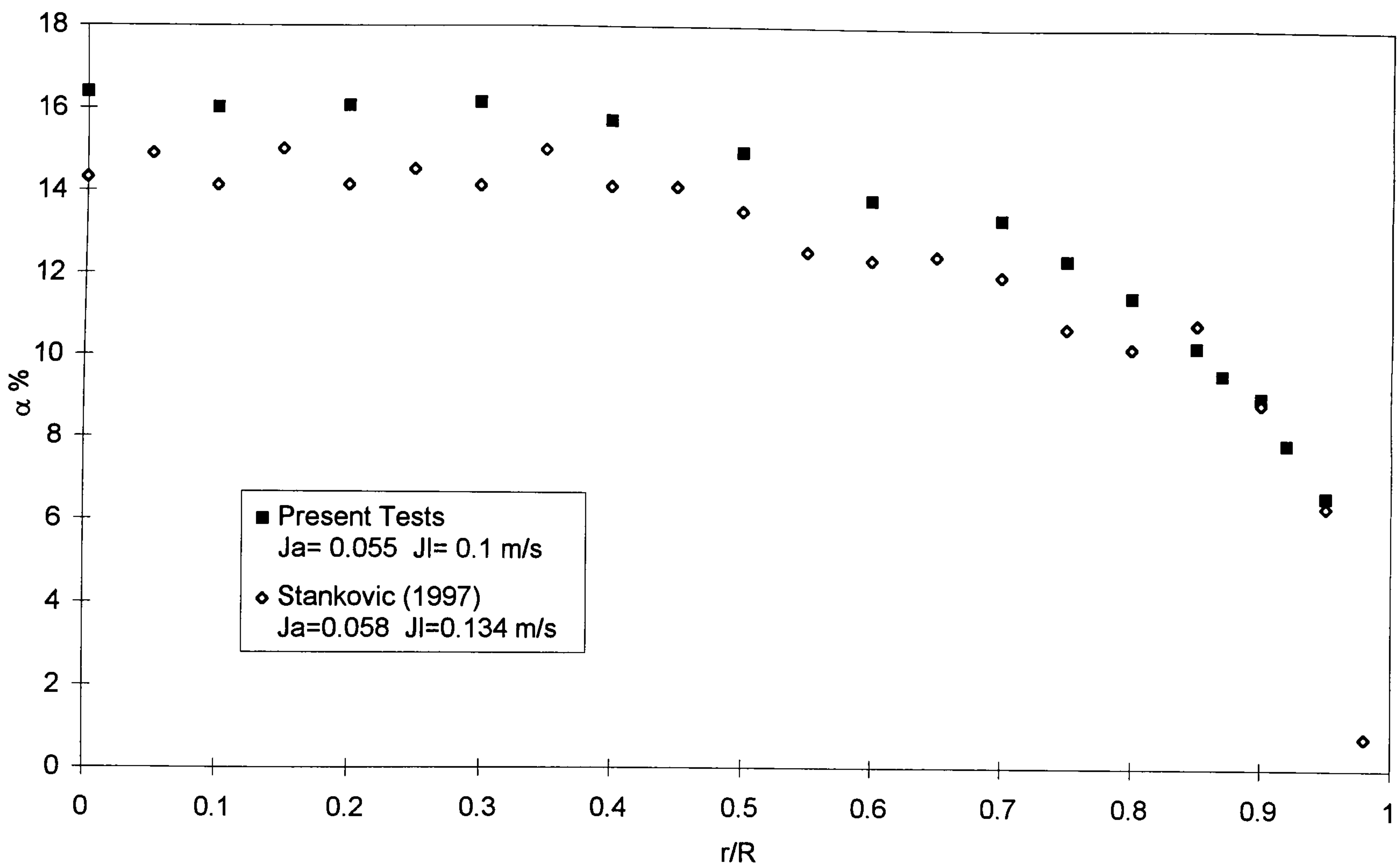

Figure 5.2: Comparison between Void Fraction Data of Present Work and Stankovic (1997) Data for D=20 cm

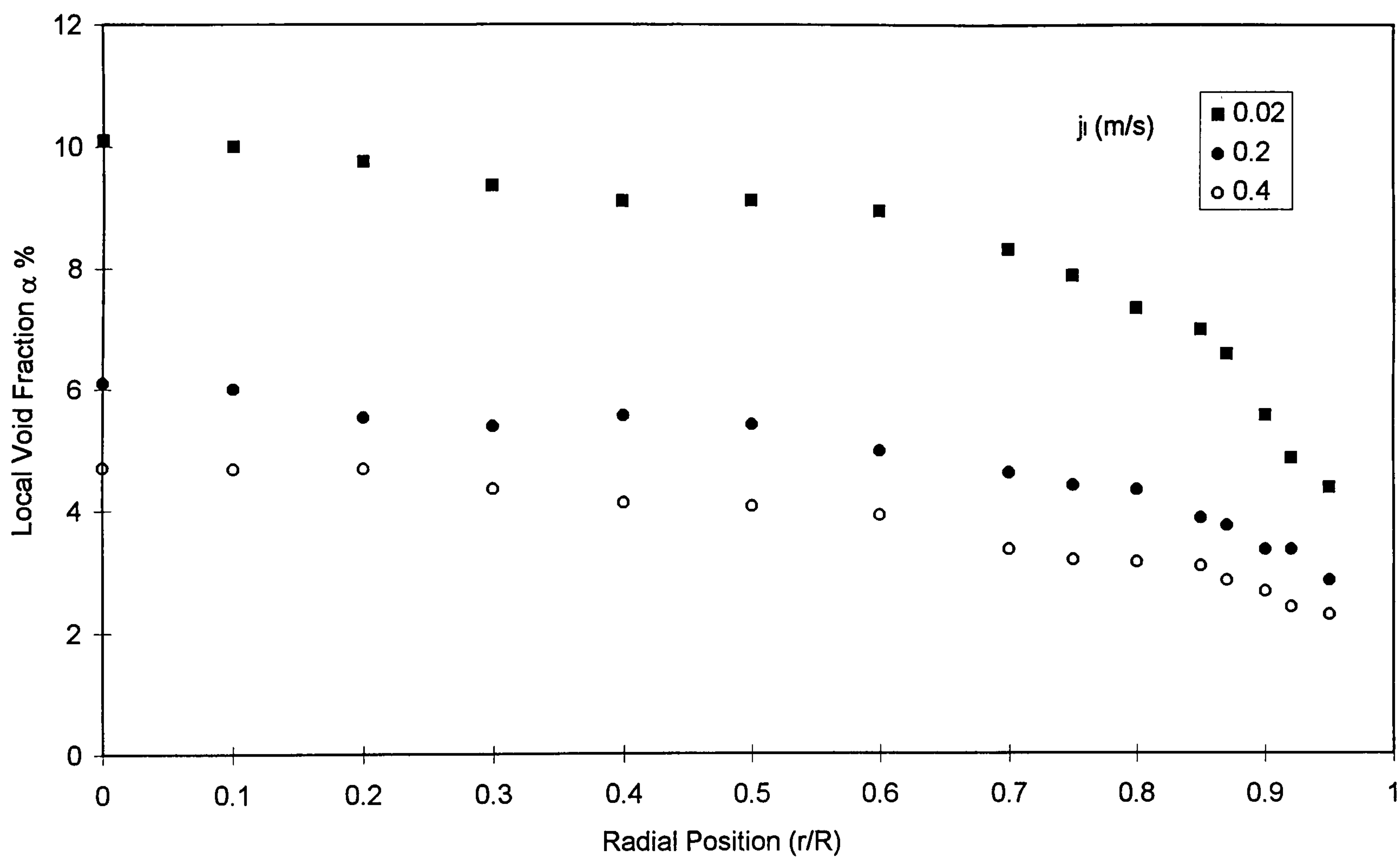

Figure 5.3: Radial Distribution of Void Fraction in 20 cm Diameter Pipe
at ja=0.022 m/s

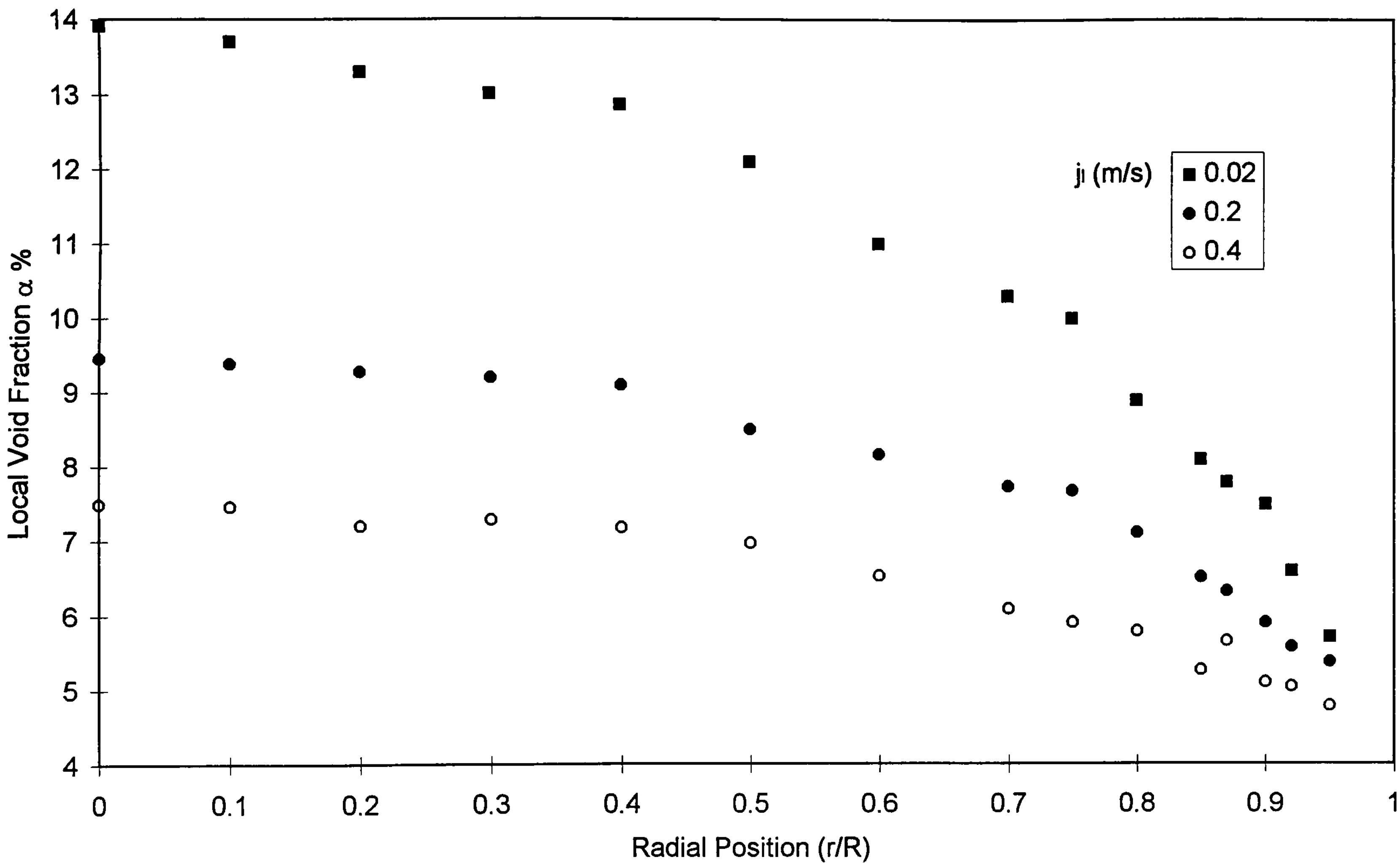

Figure 5.4: Radial Distribution of Void Fraction in 20 cm Diameter Pipe
at ja=0.033 m/s

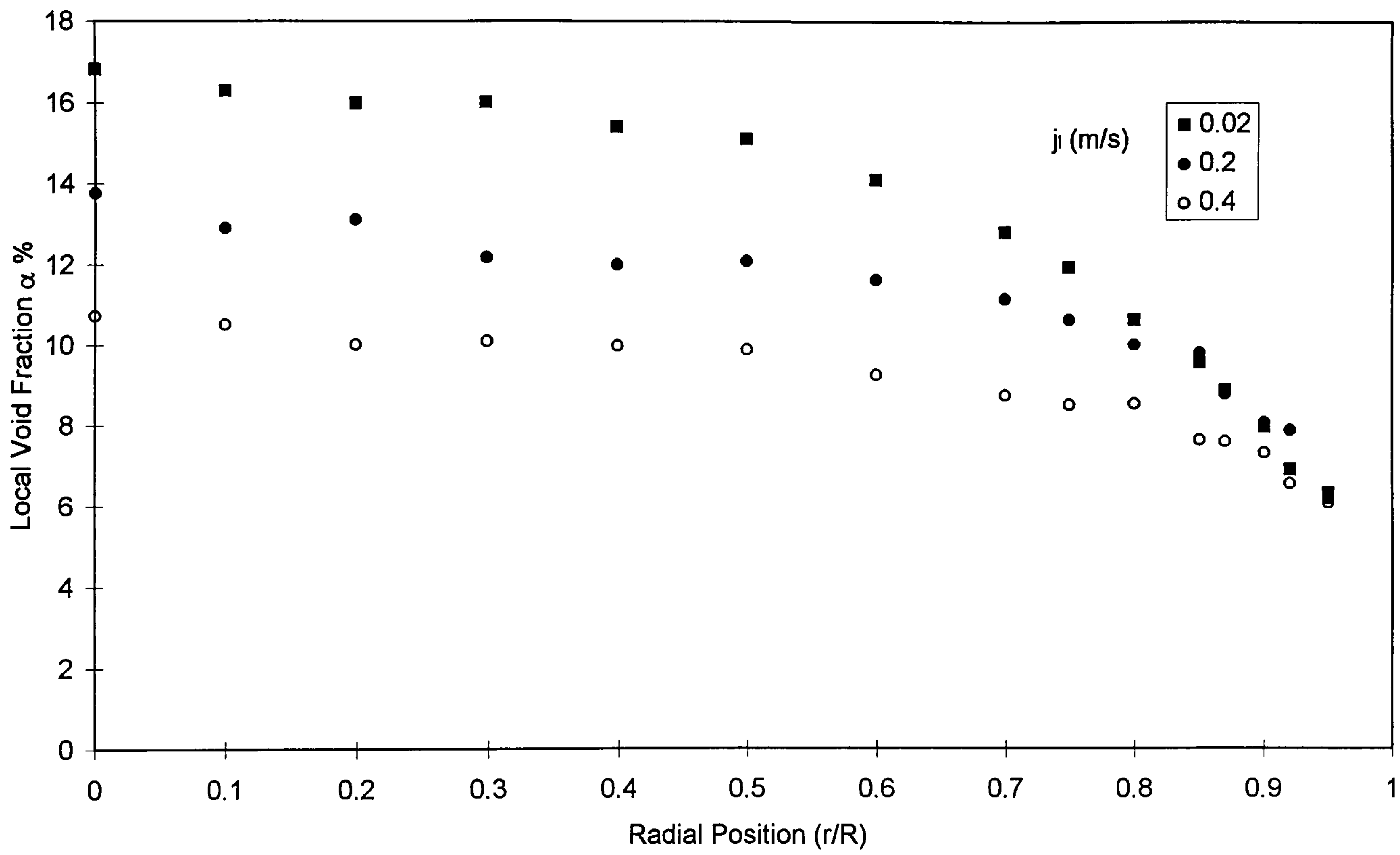

Figure 5.5: Radial Distribution of Void Fraction in 20 cm Diameter Pipe
at ja=0.044 m/s

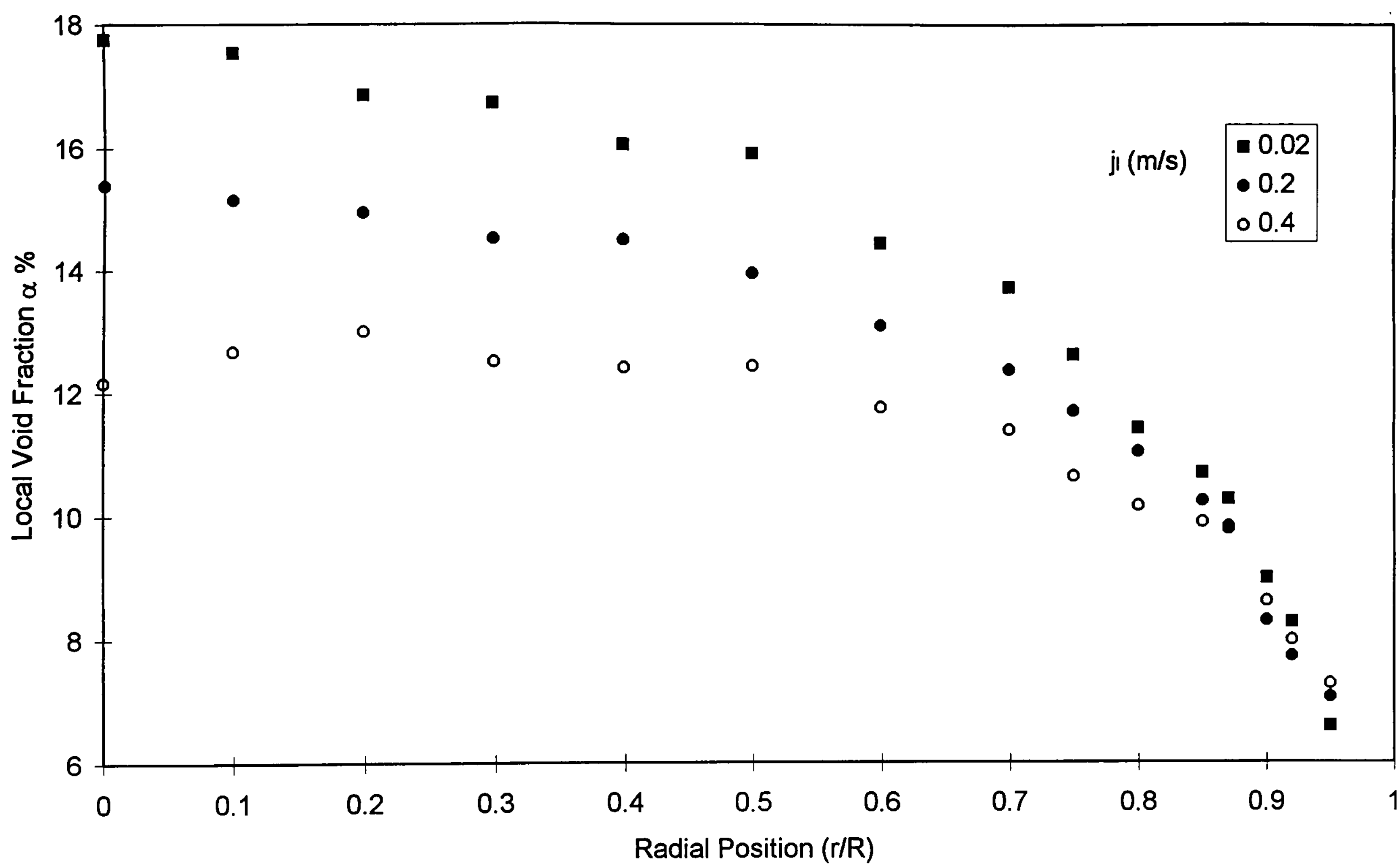

Figure 5.6: Radial Distribution of Void Fraction in 20 cm Diameter Pipe
at ja=0.055 m/s

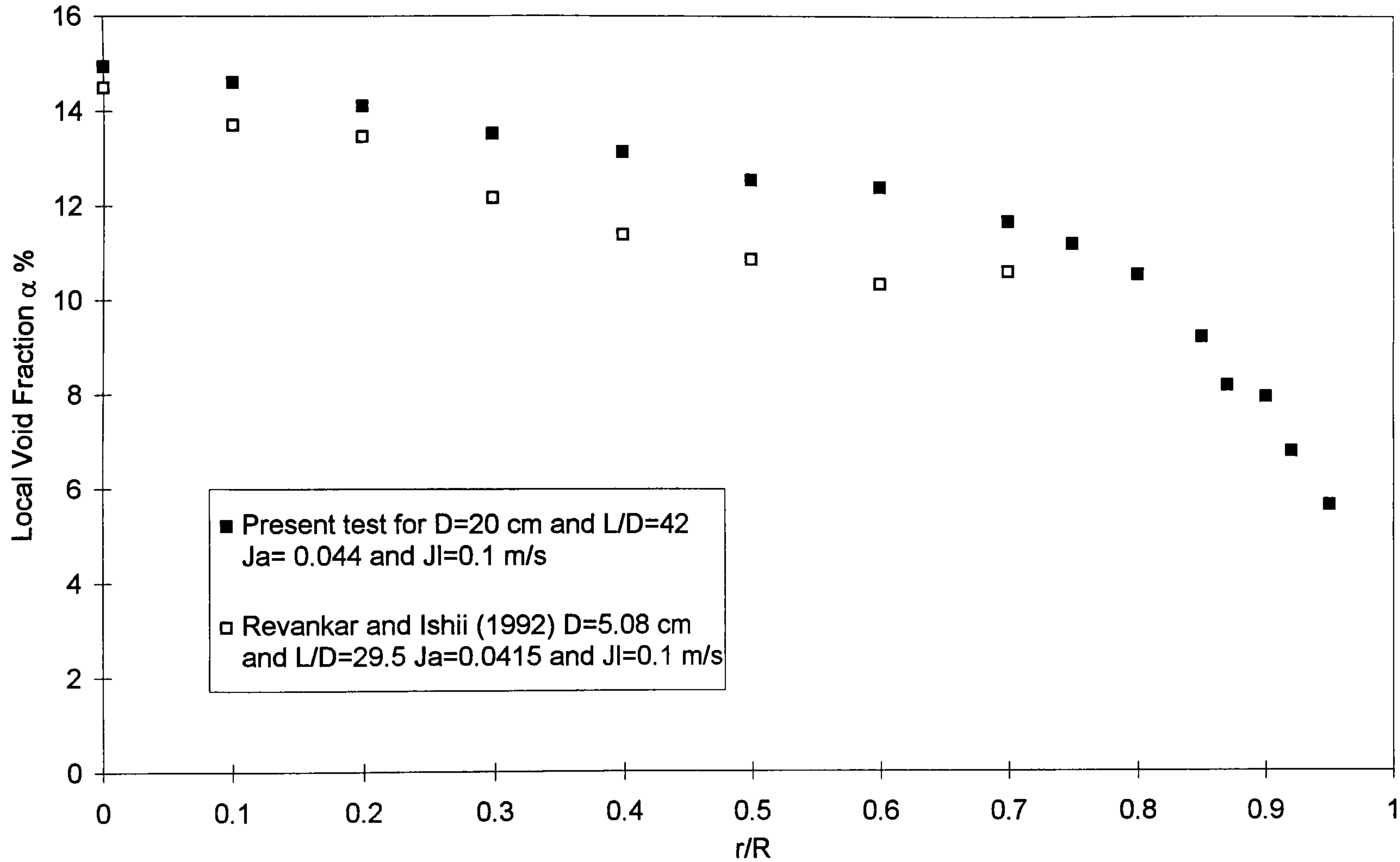

Figure 5.7: Comparison Between Void Fraction Data of Present Work and Revankar and Ishii (1992) Data

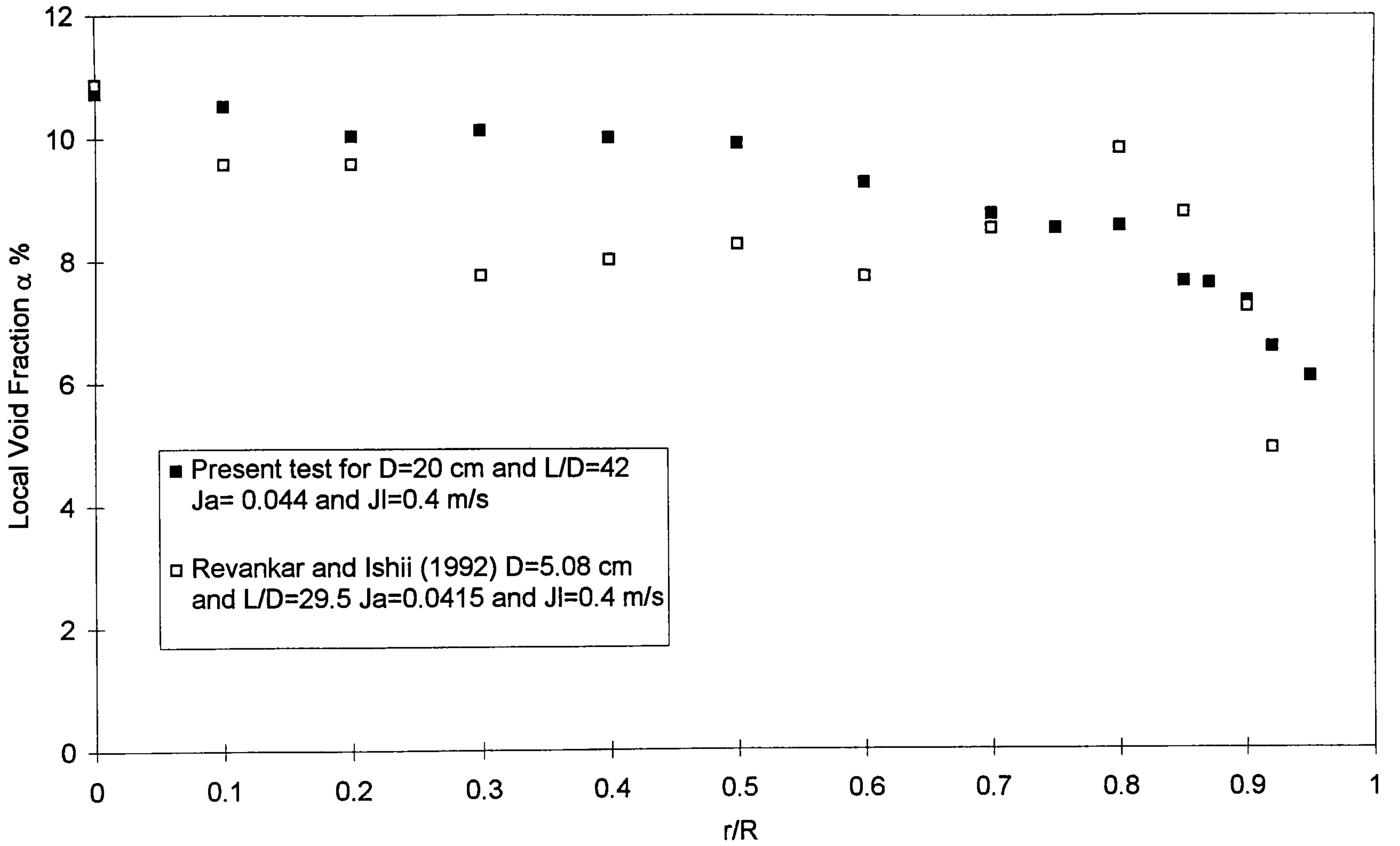

Figure 5.8: Comparison Between Void Fraction Data of Present Work and Revankar and Ishii (1992) Data

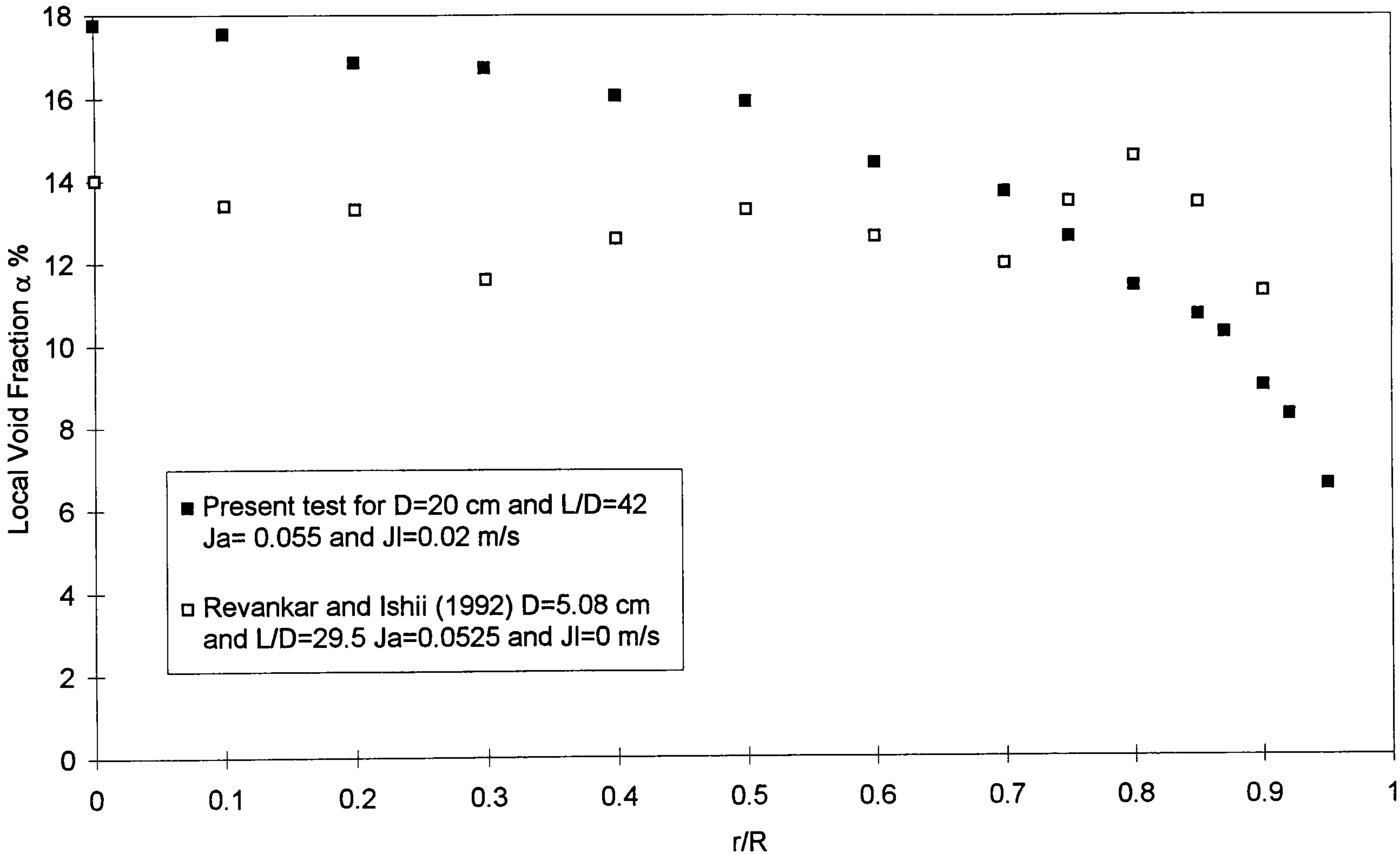

Figure 5.9: Comparison Between Void Fraction Data of Present Work and Revankar and Ishii (1992) Data

5.3 Bubble Velocity and Frequency

Radial bubble velocity distributions were obtained at different flow conditions. The distributions were obtained at constant superficial air velocities of 0.022, 0.033, 0.044 and 0.055 m/s by varying the water flow rate. Only sample results are shown in Figures 5.10 and 5.11. A complete listing of experimental results is given in Appendix A.

As shown, The local bubble velocity profiles are almost constant across the pipe cross section up to $r/R \approx 0.75$, then the bubble velocity decreases towards the wall due to increase of the shear stress near the wall. The profiles tend to be more parabolic with increasing the void fraction. The bubbles were observed to be rolling near the pipe wall particularly for low air superficial velocity flows.

As shown, Local bubble velocity increased with increasing air or water velocity. These observations are consistent with those of other researches for small diameter pipes e.g. Revakar and Ishii (1992).

The local bubble frequency was calculated for each test. Figures 5.12 and 5.13 show a sample of the experimental results. As shown, local bubble frequency profiles are parabolic with the peak at the pipe center. However, the slope of the profile increases as the pipe wall is approached. Local bubble frequency decreased with increase in water velocity at constant air velocity or decrease in air velocity at constant water velocity, i.e. decrease in void fraction.

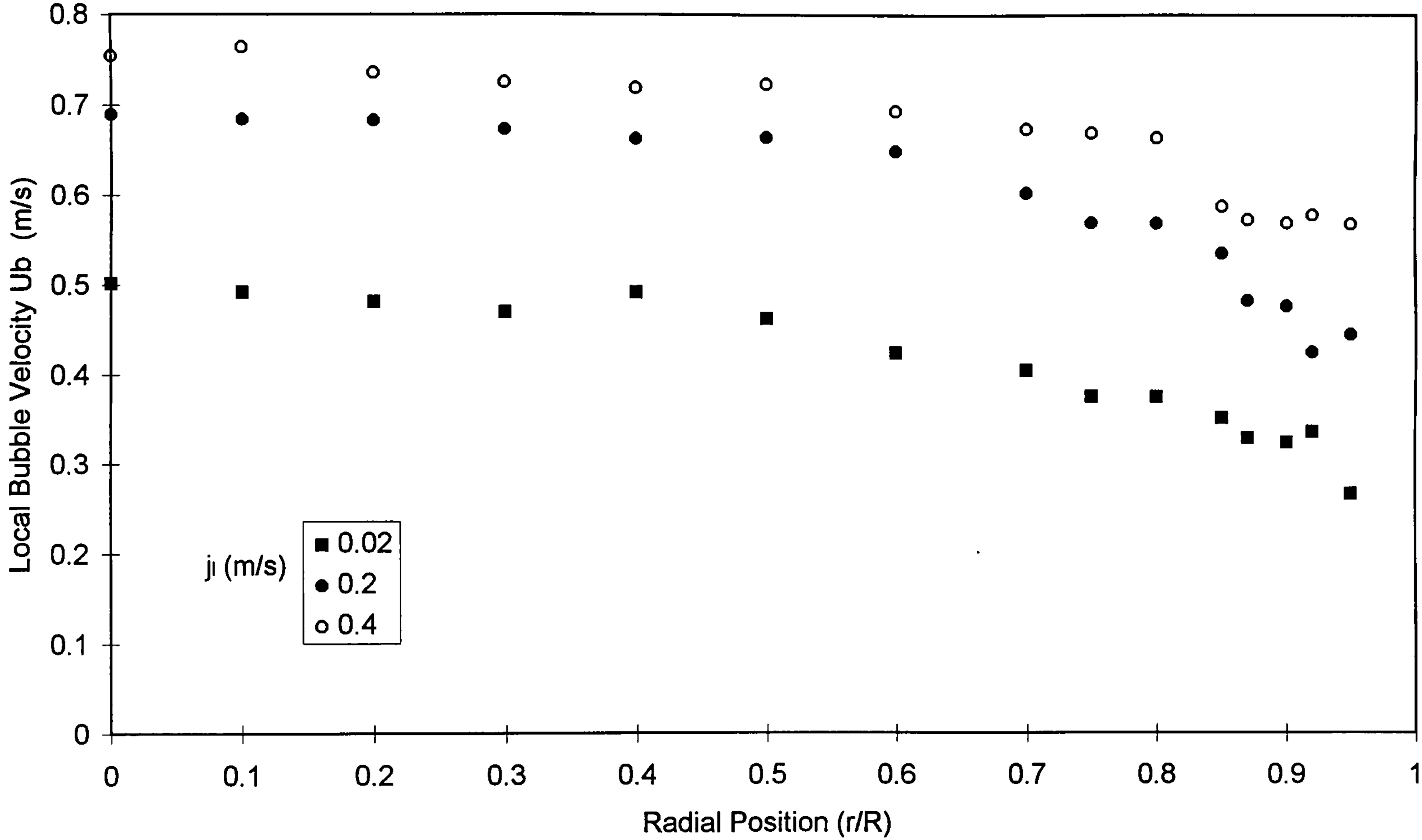

Figure 5.10: Bubble Velocity Distribution in 20 cm Diameter Pipe at ja=0.033 m/s

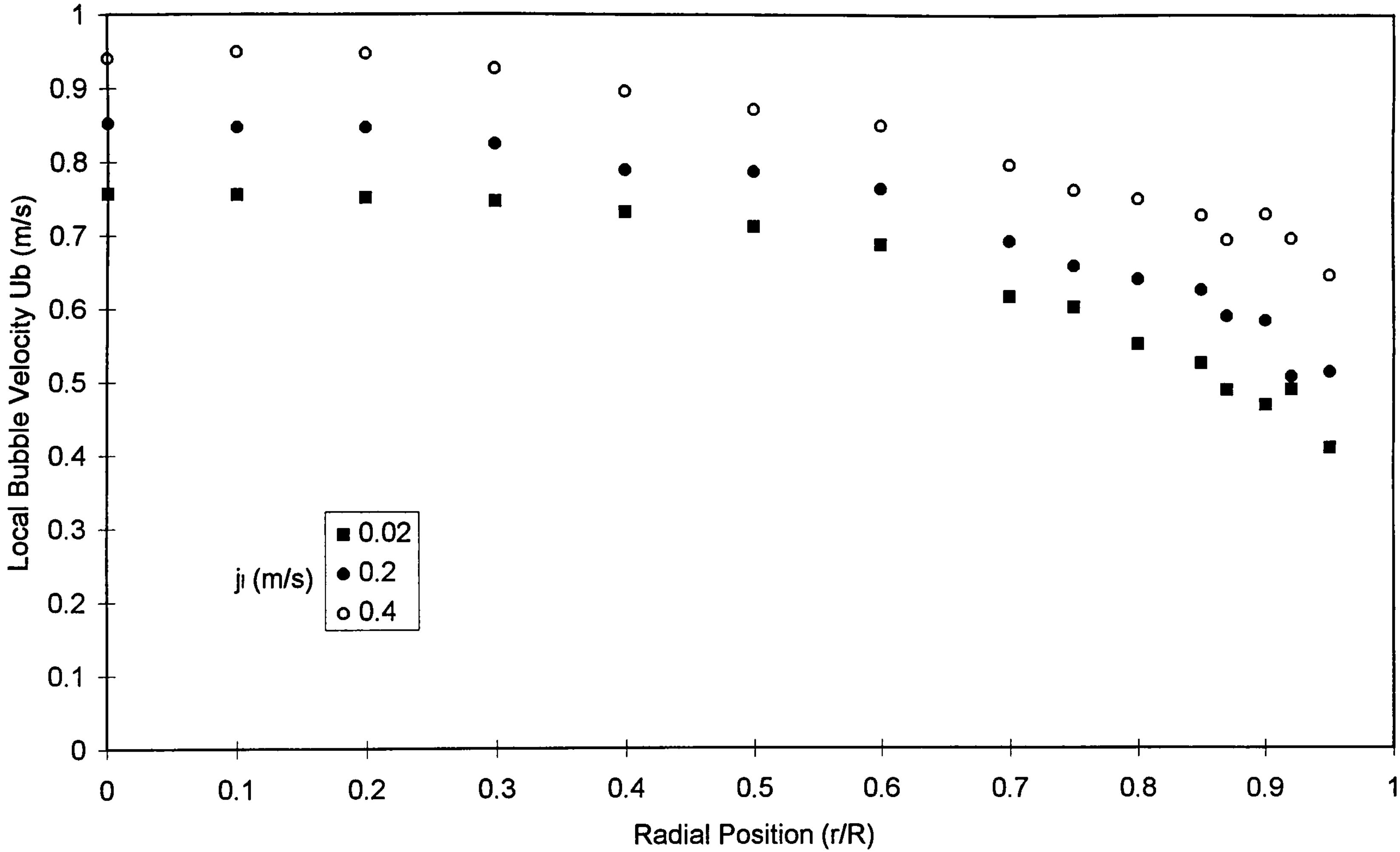

Figure 5.11: Bubble Velocity Distribution in 20 cm Diameter Pipe
at ja=0.044 m/s

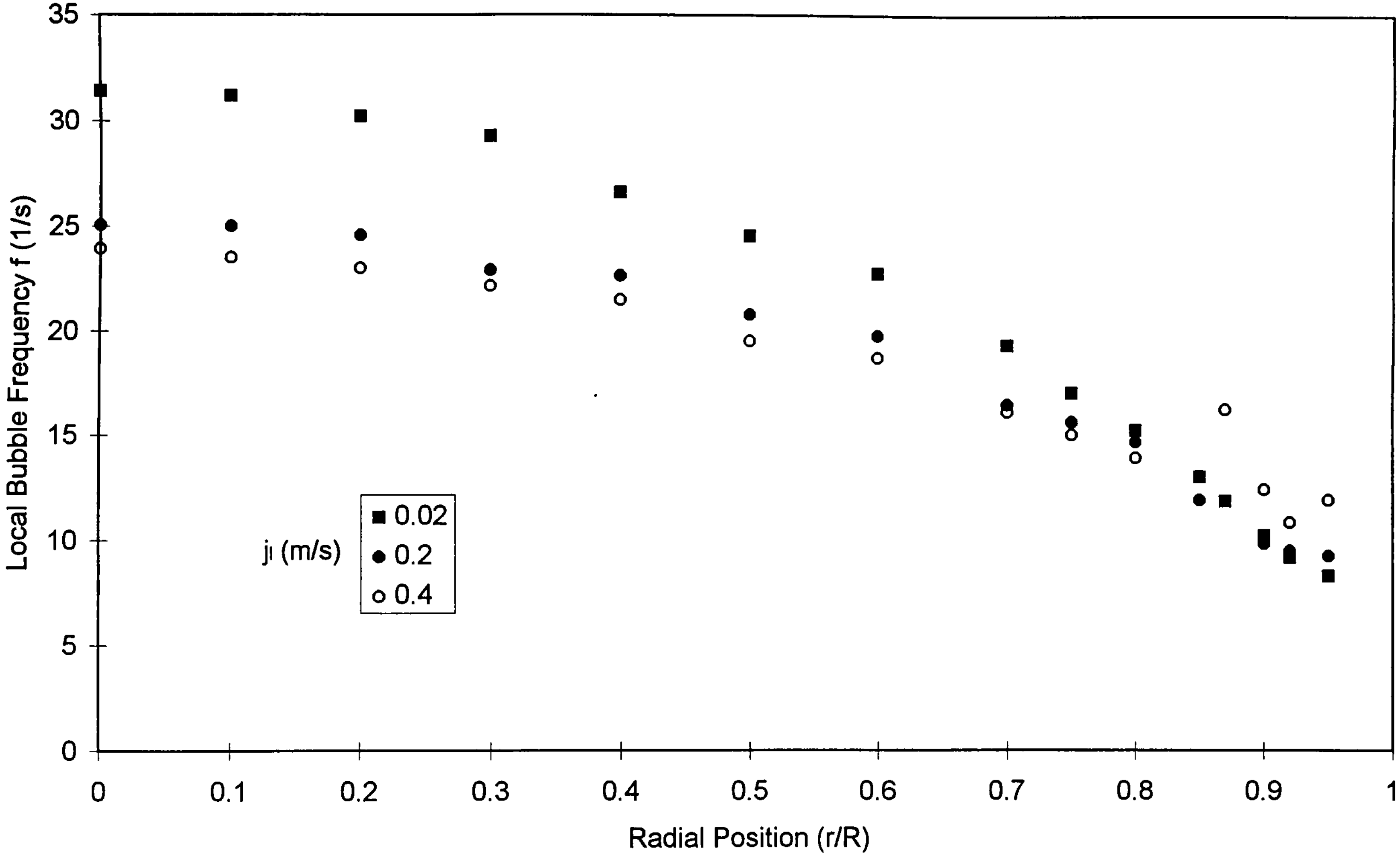

Figure 5.12: Bubble Frequency Distribution in 20 cm Diameter Pipe
at ja=0.033 m/s

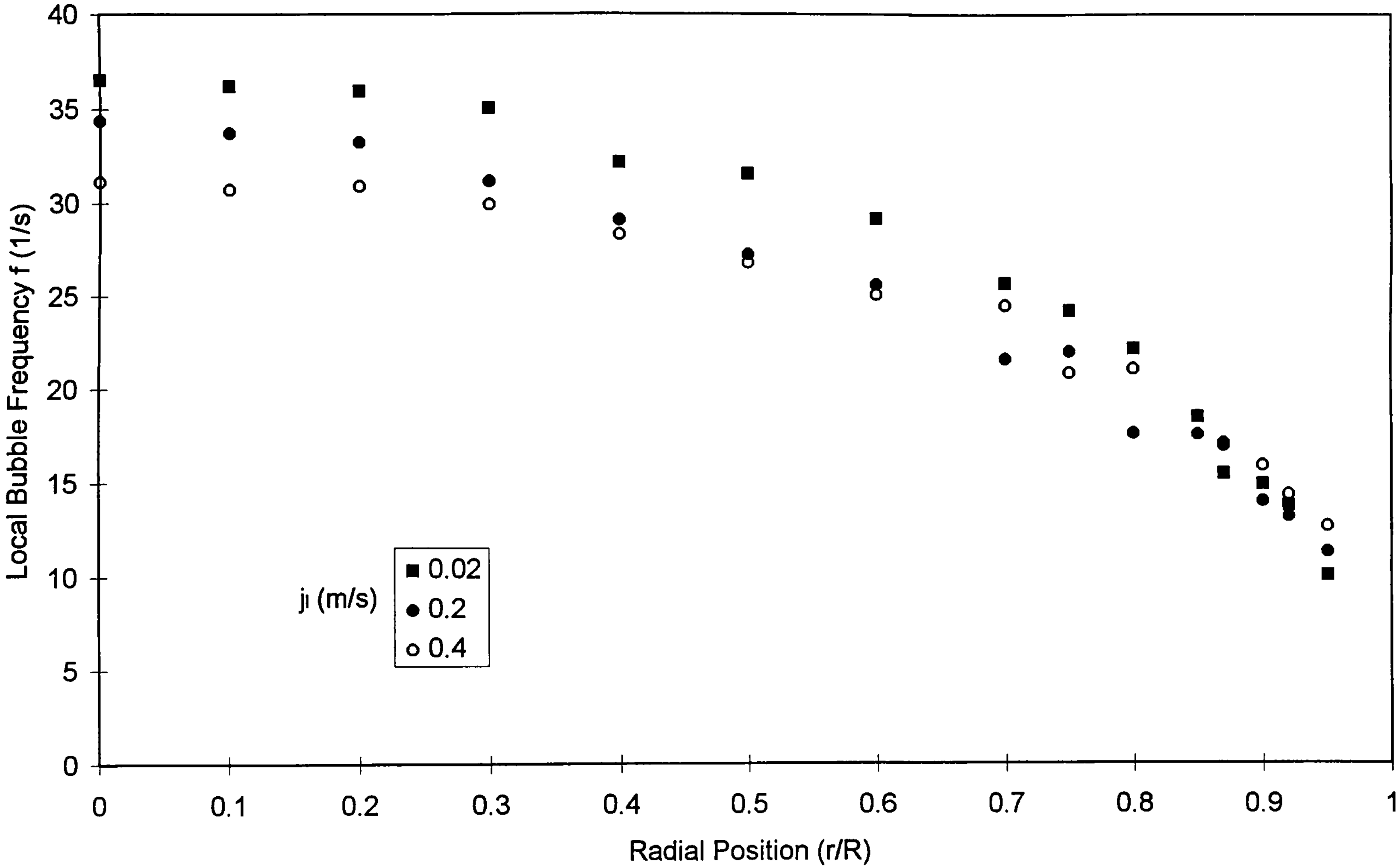

Figure 5.13: Bubble Frequency Distribution in 20 cm Diameter Pipe
at ja=0.044 m/s

5.4 Bubble Diameter

The Photographic measurement technique was used to verify the measurements. A high speed video camera was used in the tests under very low air flow rates. Diameters measured with both the direct average method and Uga's statistical method, described in section 4, were in good agreement with those measured with the photographic method.

The local bubble diameter profiles were obtained for each test using both methods, the direct average method and Uga's statistical method. Figures 5.14 and 5.15 show samples of the local bubble diameter profiles obtained using the average method. As shown, the local bubble diameter profiles are generally flat across the pipe cross section with higher values near the pipe wall. By comparing the two figures, it is evident that the local bubble diameter increased with increasing the void fraction with tendency to give a saddle distribution with high air flow rates.

The bubble diameter profiles were hardly affected by the change in water flow rate at a constant air flow rate. Unlike the bubble velocity or the void fraction, the local bubble diameter did not significantly change with 20 times increase in the water flow rate as shown in Figure 5.14.

The present observations are in good agreement to those of other researcher, e.g. Liu and Bankoff (1993), while the data reported by Revankar and Ishii (1992) showed a decrease in bubble diameter near the pipe wall. Also, Revankar and Ishii (1992) measured higher bubble diameters than the present work at similar flow conditions. It is important to note, however, that the work of Revankar and Ishii (1992) was carried out in a small diameter pipe (5.08 cm).

Figure 5.16 shows a comparison between local bubble diameters calculated with the average method and Uga's statistical method. As shown, the results obtained by the direct average method and those obtained using Uga's method are in good agreement.

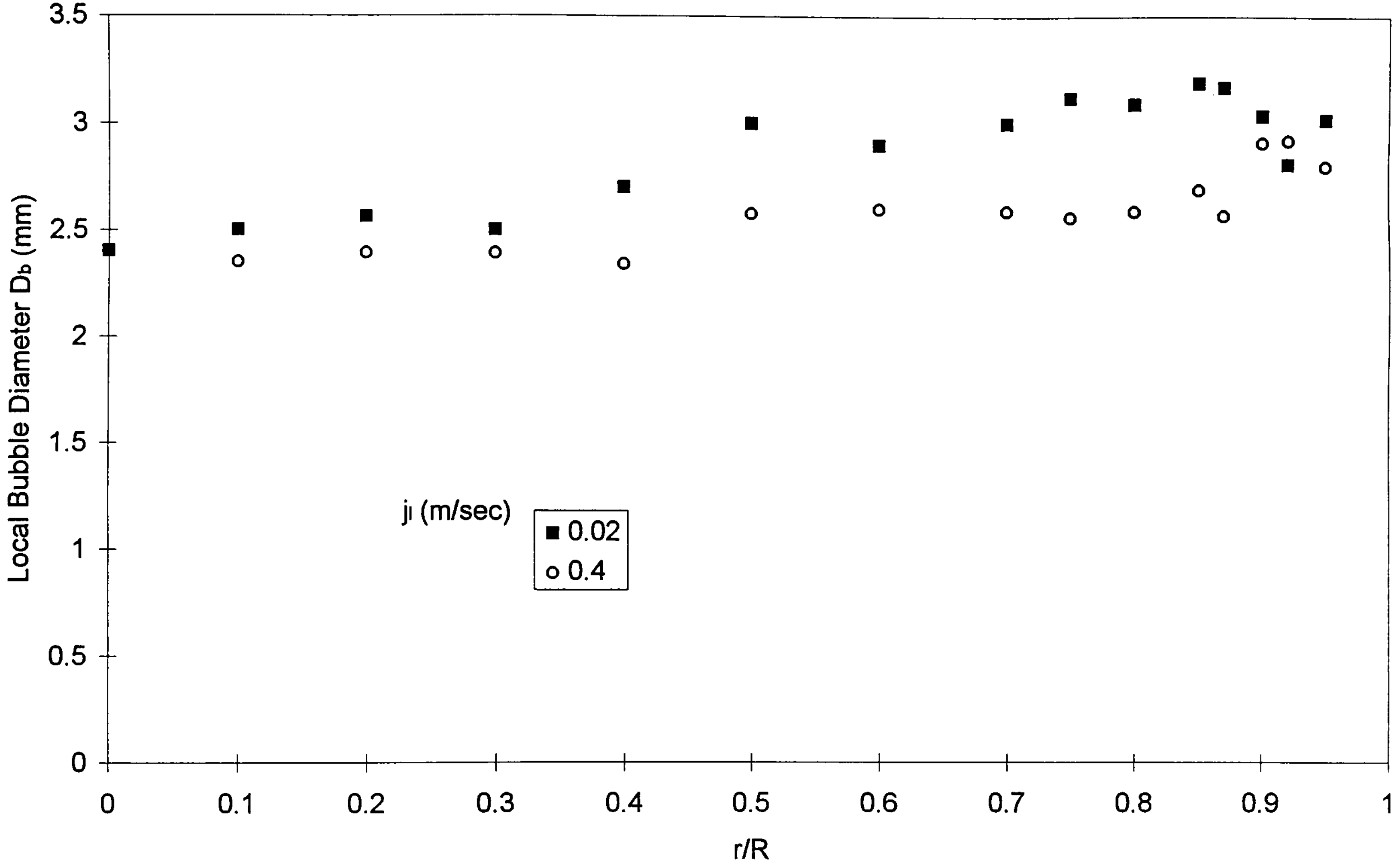

Figure 5.14: Bubble Diameter Distribution in 20 cm Diameter Pipe
at ja=0.022 m/s

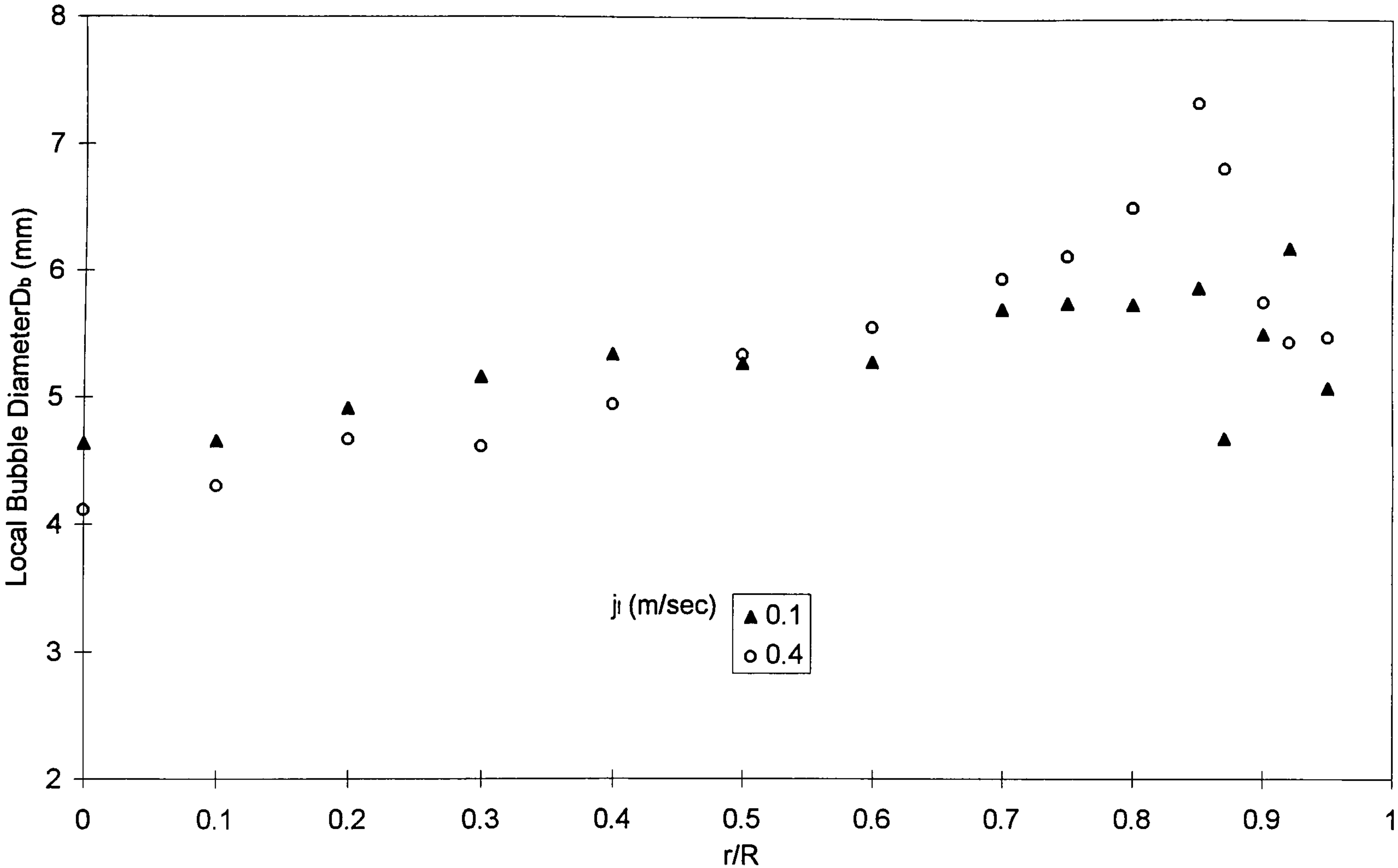

Figure 5.15: Bubble Diameter Distribution in 20 cm Diameter Pipe at ja=0.055 m/s

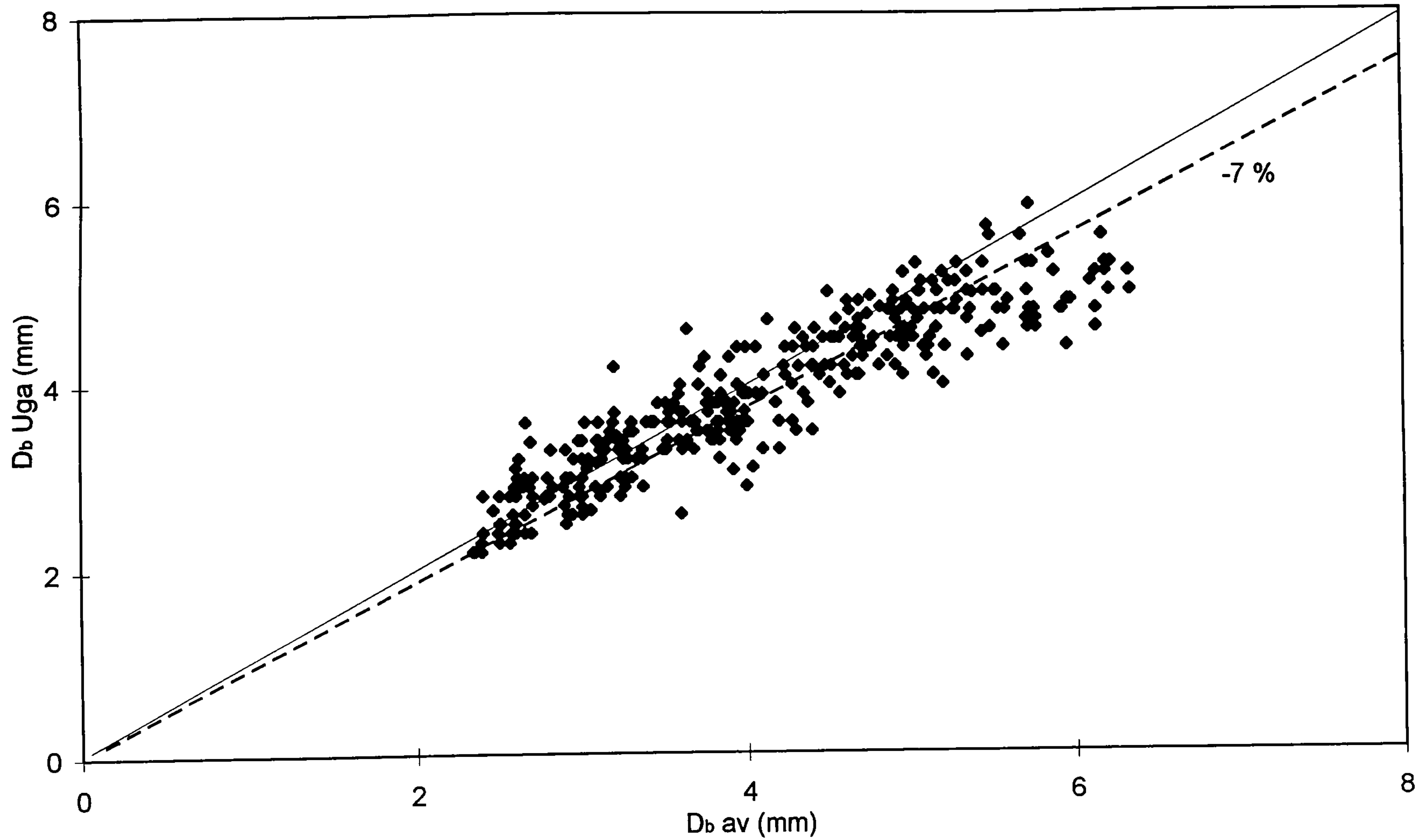

Figure 5.16: Comparison Between Bubble Diameter Measured by Direct Average Method and Uga's statistical Method in 20 cm Diameter Pipe

5.5 Interfacial Area Concentration (IAC).

The main objective of the present work is to provide further knowledge concerning the structure of bubbly two-phase flows in large-diameter vertical pipes, with particular reference to IAC. To achieve this objective, local IAC distribution profiles in a 20 cm diameter pipe were obtained using the bubble diameter-based methods and the method recommended by Kataoka et al (1985). The following sections present the present work results along with comparisons with results obtained in small diameter pipes and with the predictions of selected available correlations.

5.5.1 Comparing the Various Measuring Methods:

As shown earlier in section 5.4 and Figure 5.16, the bubble diameter obtained by the direct average method and Uga's statistical method were in good agreement. Accordingly, the same level of agreement will be achieved in using these two methods, in conjunction with the void fraction, to obtain the interfacial area concentration using equation (5.25).

In this section the bubble-diameter based methods, using Uga's method, is compared with the method recommended by Kataoka et al (1985). The results are shown in Figure 5.17. As shown, the two methods are in good agreement.

5.5.2 Local Interfacial Area Concentration (20 cm Diameter Pipe).

Local IAC profiles for air-water bubbly flows were obtained for each test condition proposed in Table 5.1. Only a selected group of the results at j_l= 0.02, 0.2 and 0.4 m/s and ja= 0.022, 0.033, 0.044 and 0.055 m/s is presented in the following Figures for clarity of presentation. A complete listing of experimental results of the three methods is given in Appendix A.

As described, results obtained using the three methods are similar so only those obtained using the direct method of Kataoka et al (1985) will be illustrated in the following Figures as the present results.

Figures 5.18 to 5.21 show the present local IAC profiles obtained using the method of Kataoka et al (1985). As shown, the IAC profiles are parabolic with lower values near the pipe wall. The local IAC values are higher and the profiles are more parabolic with increasing the void fraction. At higher gas flow rates the effect of varying the liquid flow rate upon the IAC value is less pronounced than its effect at low gas flow rates.

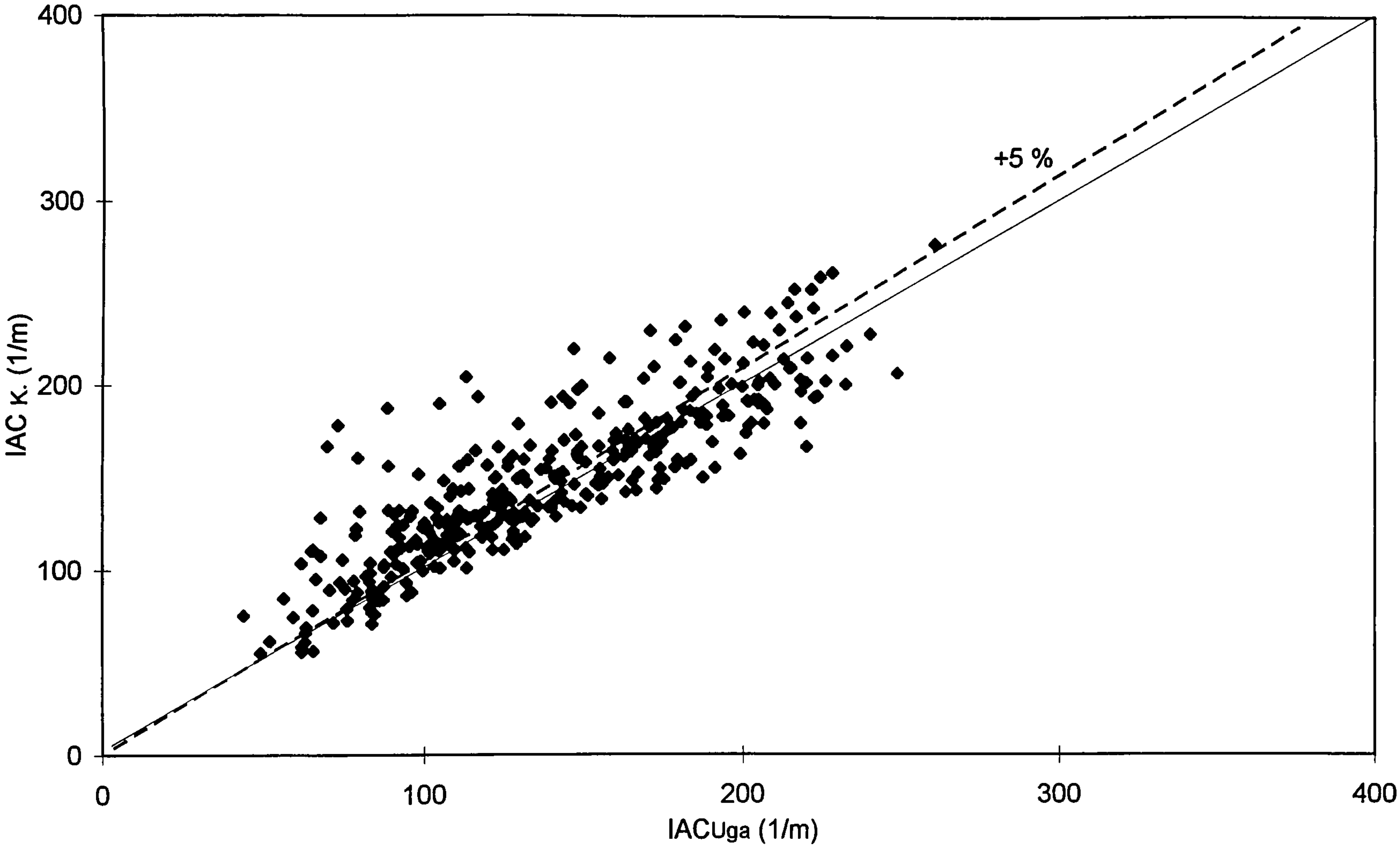

Figure 5.17: Comparison Between IAC Measured using Uga's bubble diameter Method and method of Kataoka et al. (1985) For 20 cm Diameter Pipe

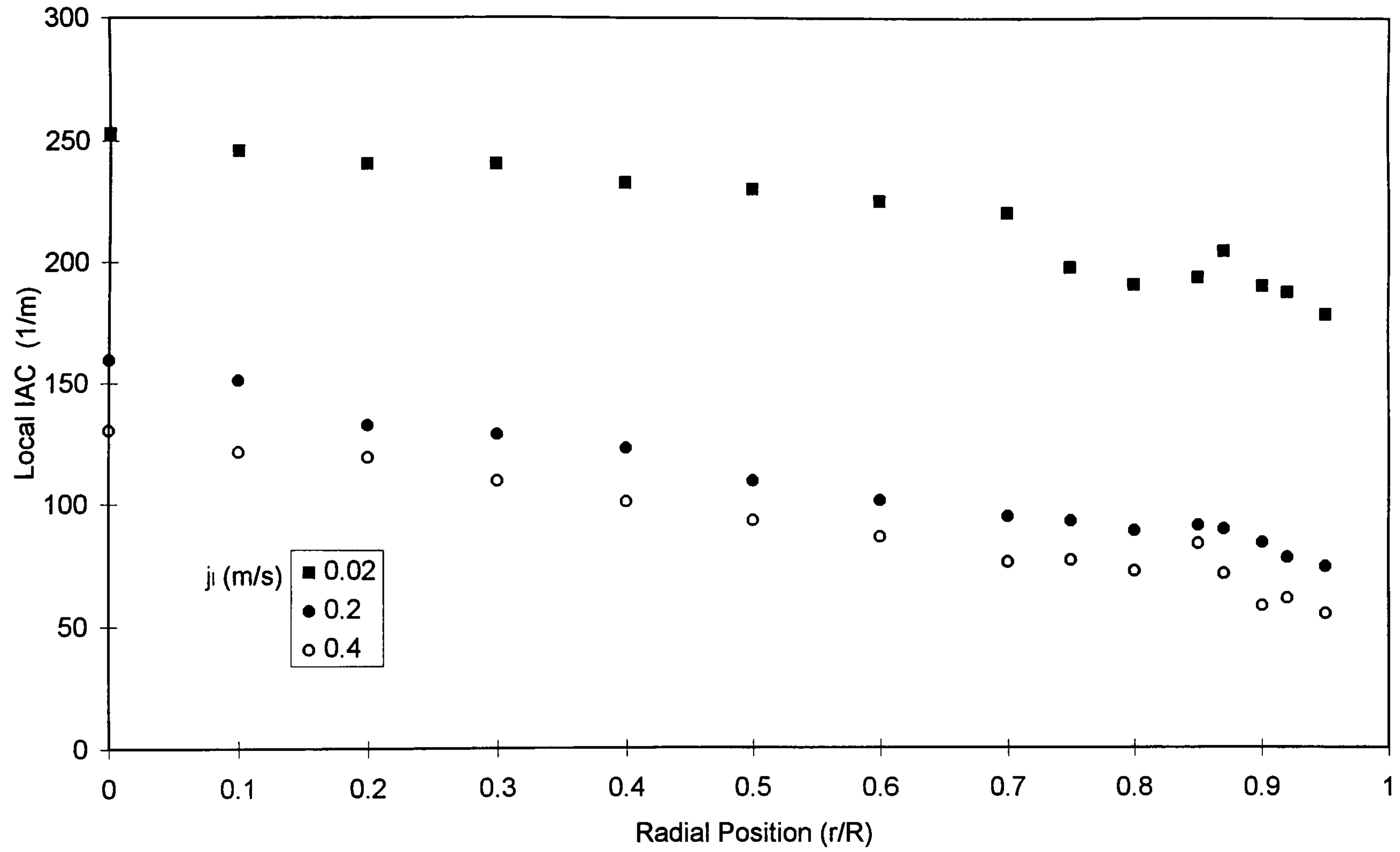

Figure 5.18: Local IAC Distribution Measured Using Method of **Kataoka et al. (1985)** in 20 cm Diameter Pipe at ja=0.022 m/s

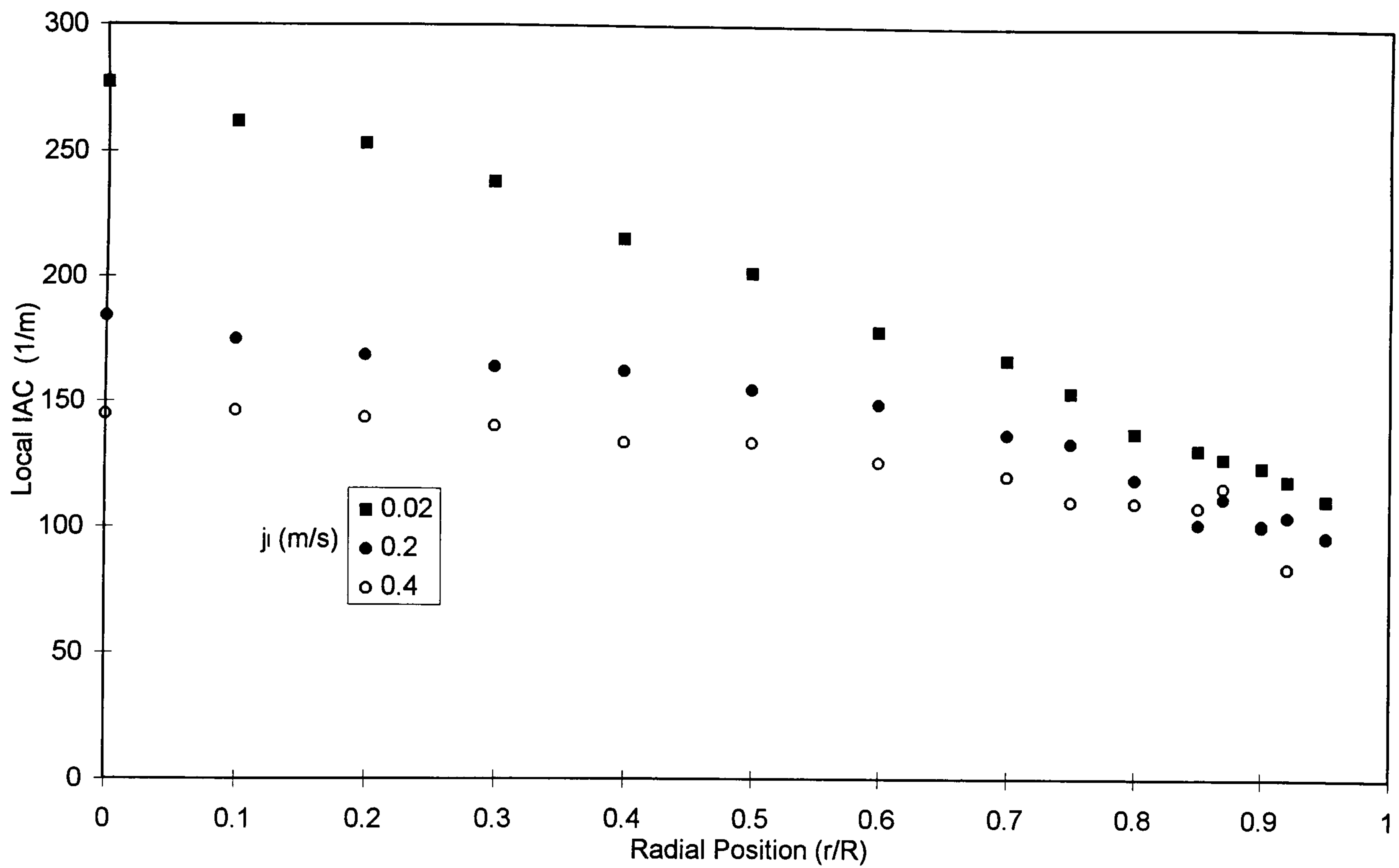

Figure 5.19: Local IAC Distribution Measured Using Method of **Kataoka et al. (1985)** in 20 cm Diameter Pipe at ja=0.033 m/s

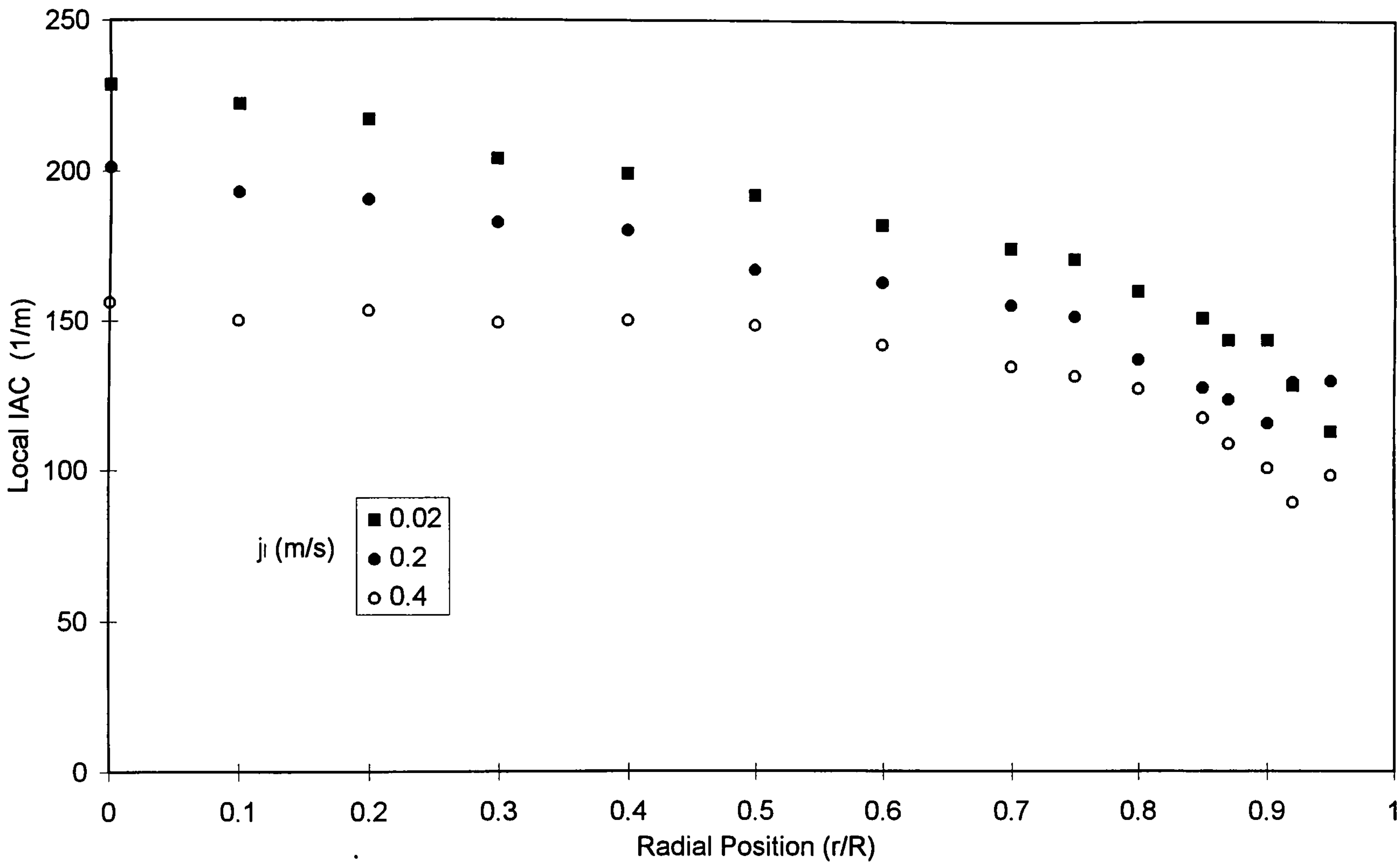

Figure 5.20: Local IAC Distribution Measured Using Method of **Kataoka et al (1985)** in 20 cm Diameter Pipe at ja=0.044 m/s

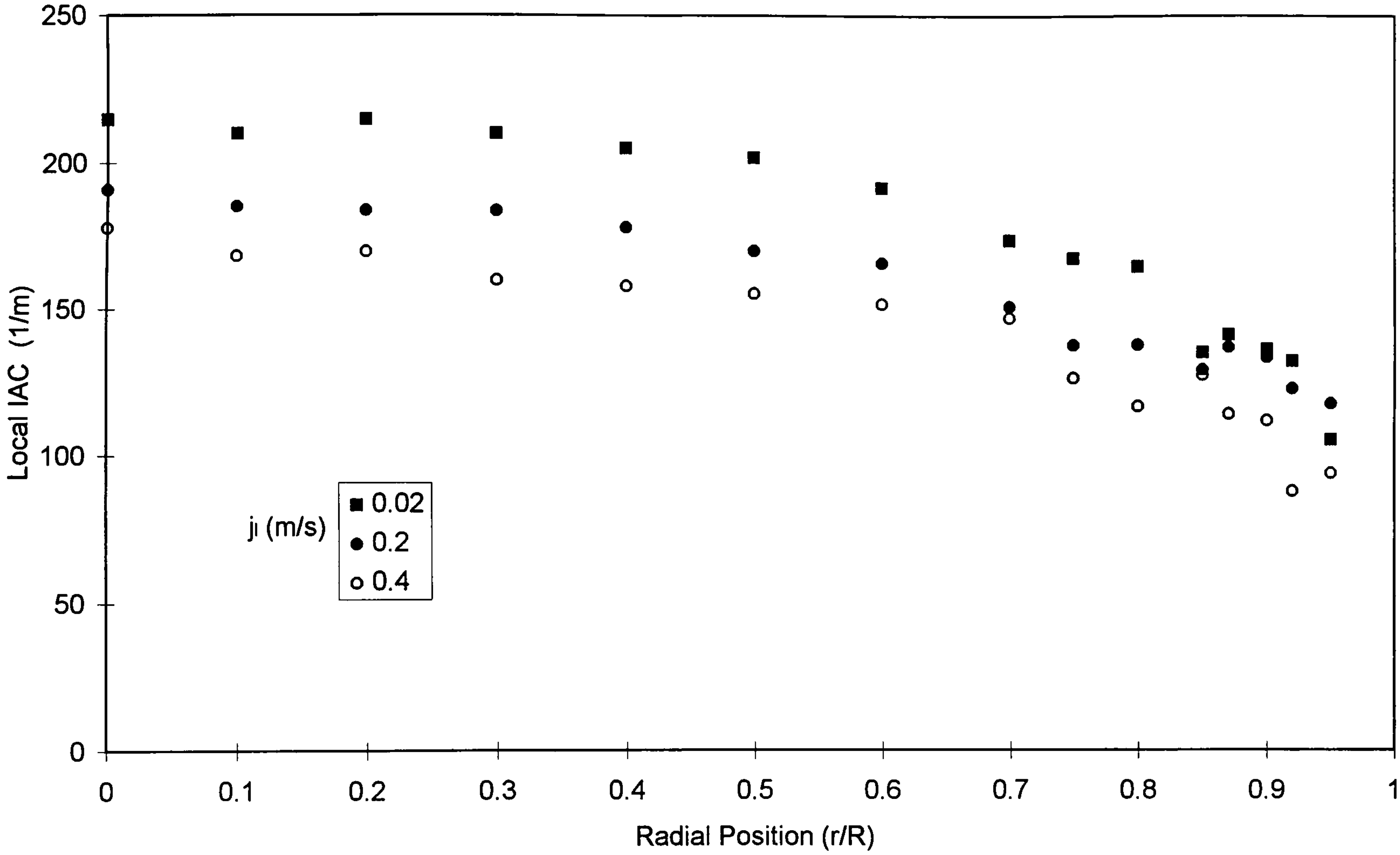

Figure 5.21: Local IAC Distribution Measured Using Method of **Kataoka et al (1985)** in 20 cm Diameter Pipe at ja=0.055 m/s

5.5.3 Comparison with Other Results:

As discussed earlier, the IAC data obtained using the method of Kataoka et al (1985) are in good agreement with those obtained using the bubble diameter with Uga's statistical method. The main advantage of the method of Kataoka et al. is its independence of bubble size, as it does not assume spherical bubbles, thus gives the method a wider applicability range. Data obtained using Kataoka's method will be denoted as present data and will be used to compare the present results with those of other researchers.

The present IAC data are compared with those of other researchers to check the applicability of previously obtained data using small diameter pipes to flows in large diameter pipes. Also, to check applicability of existing correlations, two correlations, which are applicable to available measurements, were used. The predictions of these correlations were compared with the present data under the same flow conditions.

Figures 5.22 to 5.24 show comparisons between the present local IAC profiles and those of Revankar and Ishii (1992) for small diameter pipe, 5.08 cm and L/D=29.5, at the same superficial velocities. As shown, the present data are higher than the data reported by Revankar and Ishii (1992) for small pipe diameter flows. As described earlier, the present data generally showed the same void fraction profiles and values and it also showed smaller local bubble diameters than those reported for small diameter pipes. As a result of the bubble diameter difference, the IAC measured in large diameter pipes are higher than the IAC in small diameter pipes under the same superficial velocity conditions.

Figures 5.23 and 5.24 show a saddle distribution for local IAC at low void fraction in small diameter pipes, which is not observed in the present work.

Available IAC correlations reflect data obtained for flows in small diameter pipes which are lower than the local data obtained for flows in large diameter pipe (20 cm). Area averaged IAC predicted using these correlations are lower than those measured for 20 cm diameter pipe. Figures 5.25 to 5.28 show comparisons between the present area-averaged results calculated by equation 4.32 and the predictions of the correlations of Tabie et al. (1989) and Akida and Yoshida (1974) applied to the same flow conditions.

As shown, although the predictions of the two correlations are in good agreement with each other, they underestimate the IAC measured in the present work. However, the agreement between the predictions of these correlations and the present data appears to improve with increasing the air flow rate. A complete list of area averaged data is listed in Appendix B.

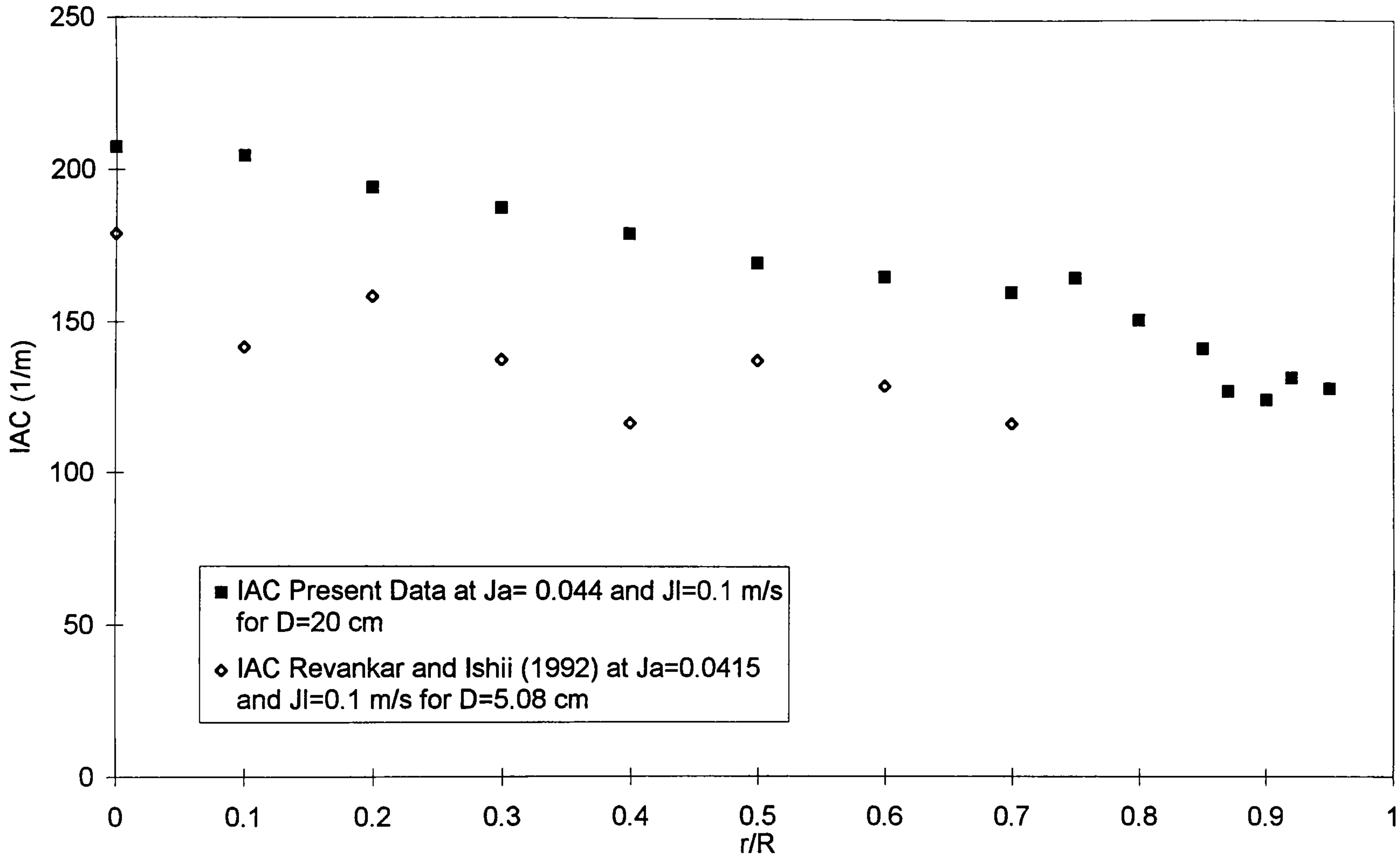

Figure 5.22: Comparison Between IAC From Present Work and Revankar and Ishii (1992)

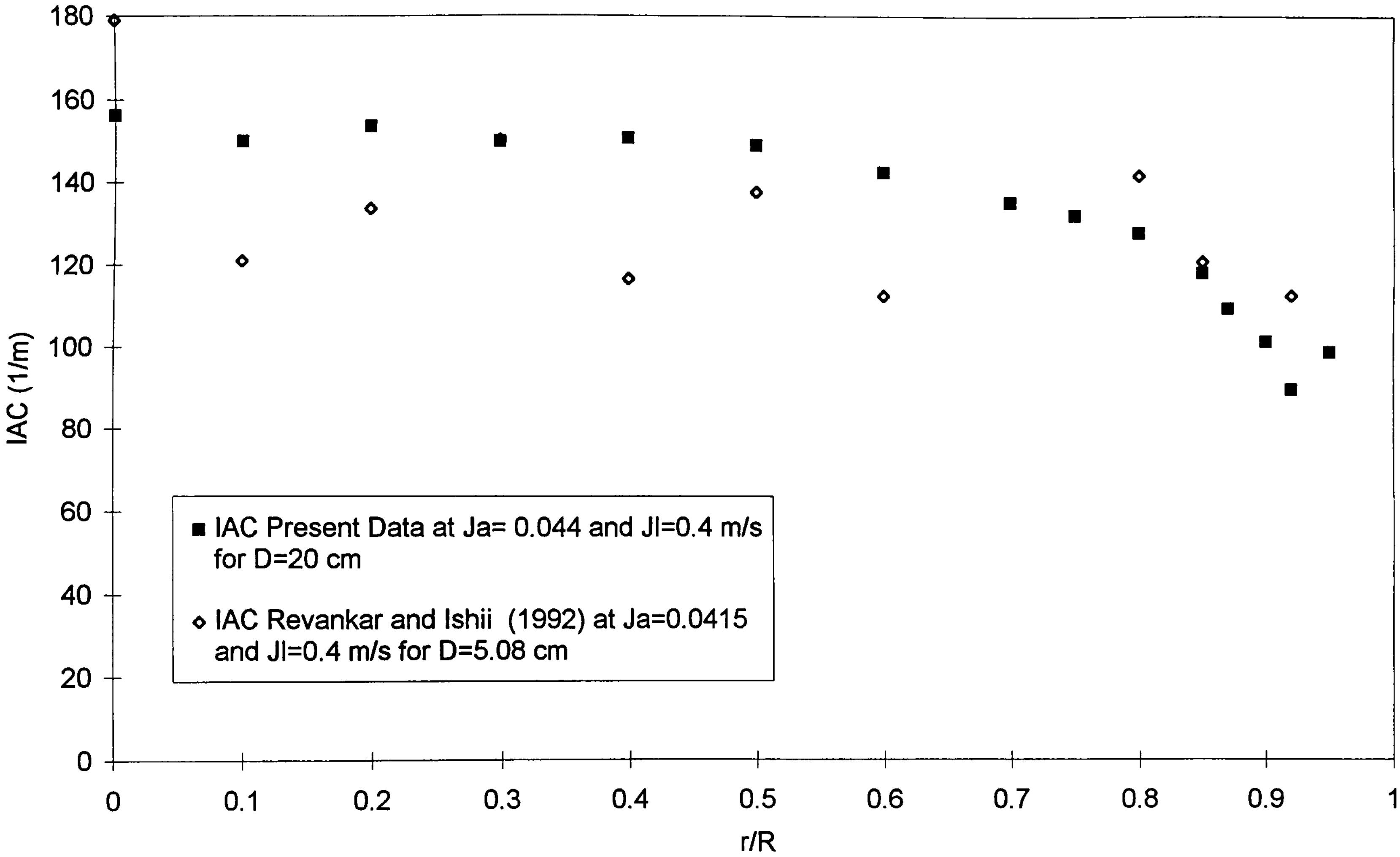

Figure 5.23: Comparison Between IAC From Present Work and Revankar and Ishii (1992)

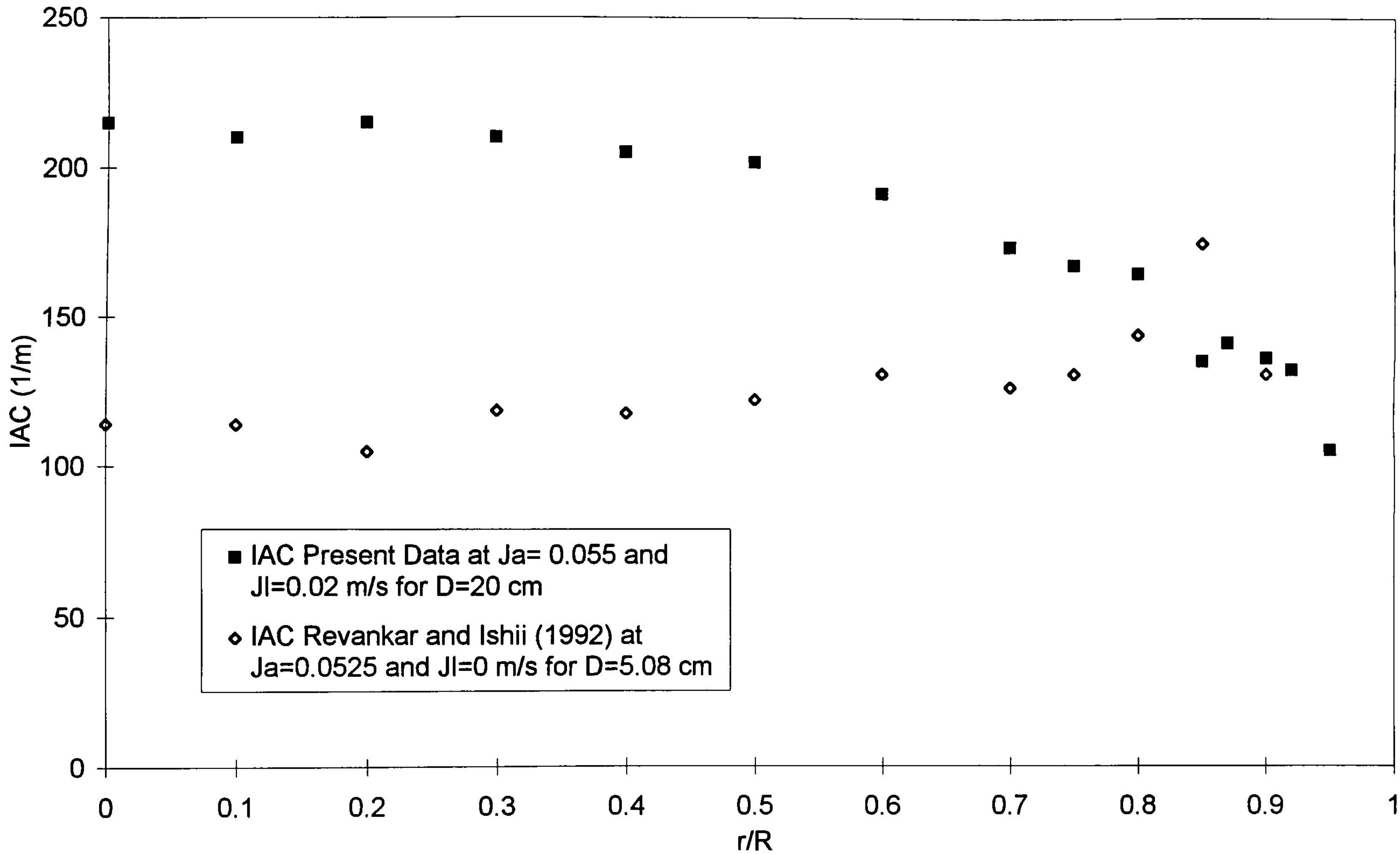

Figure 5.24: Comparison Between IAC From Present Work and Revankar and Ishii (1992)

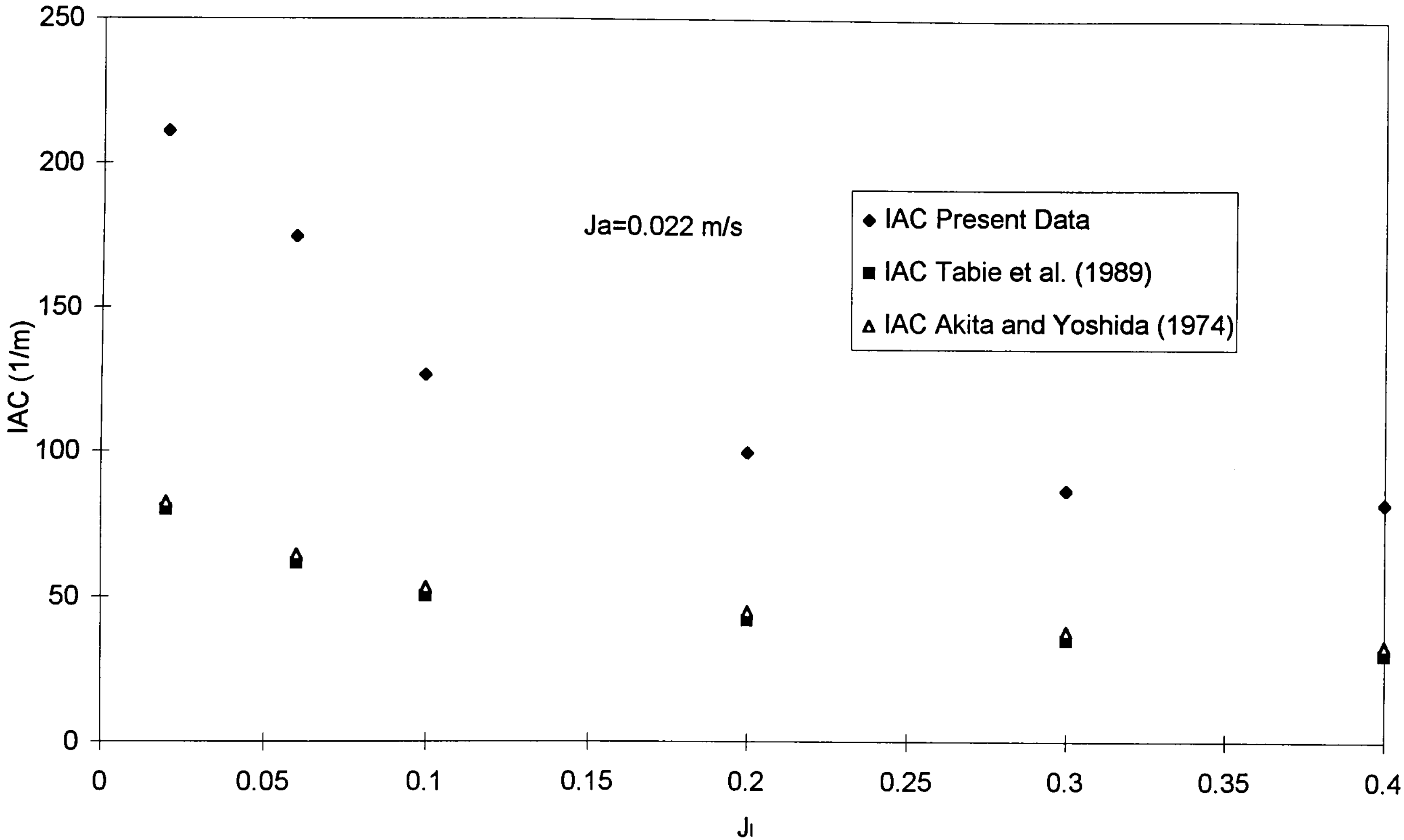

Figure 5.25: Comparison Between Area Averaged IAC Using Present Data and Correlations from Akita and Yoshida (1974) and Tabie et al. (1989) at ja=0.022

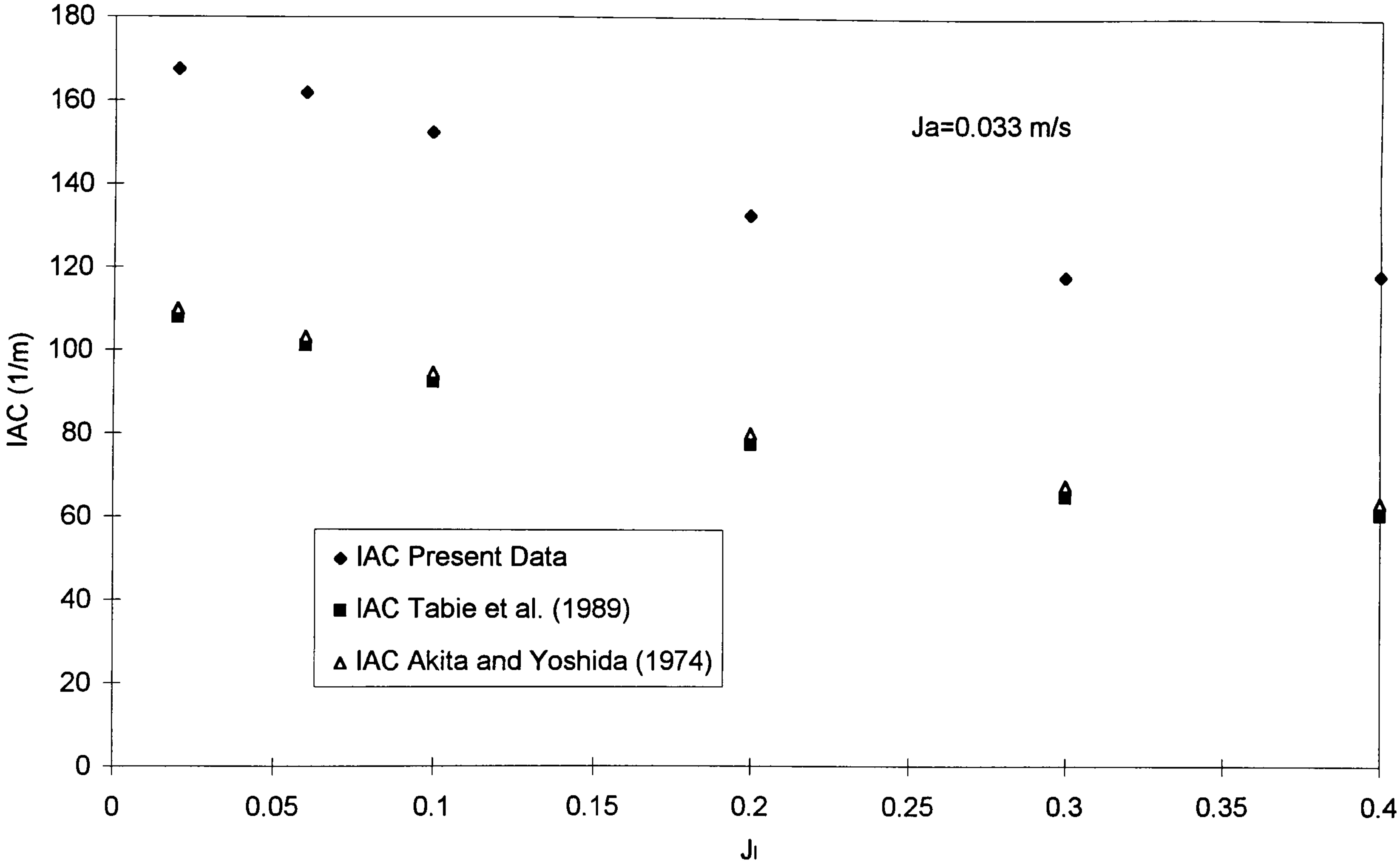

Figure 5.26: Comparison Between Area Averaged IAC Using Present Data and Correlations from Akita and Yoshida (1974) and Tabie et al. (1989) at ja=0.033 m/s

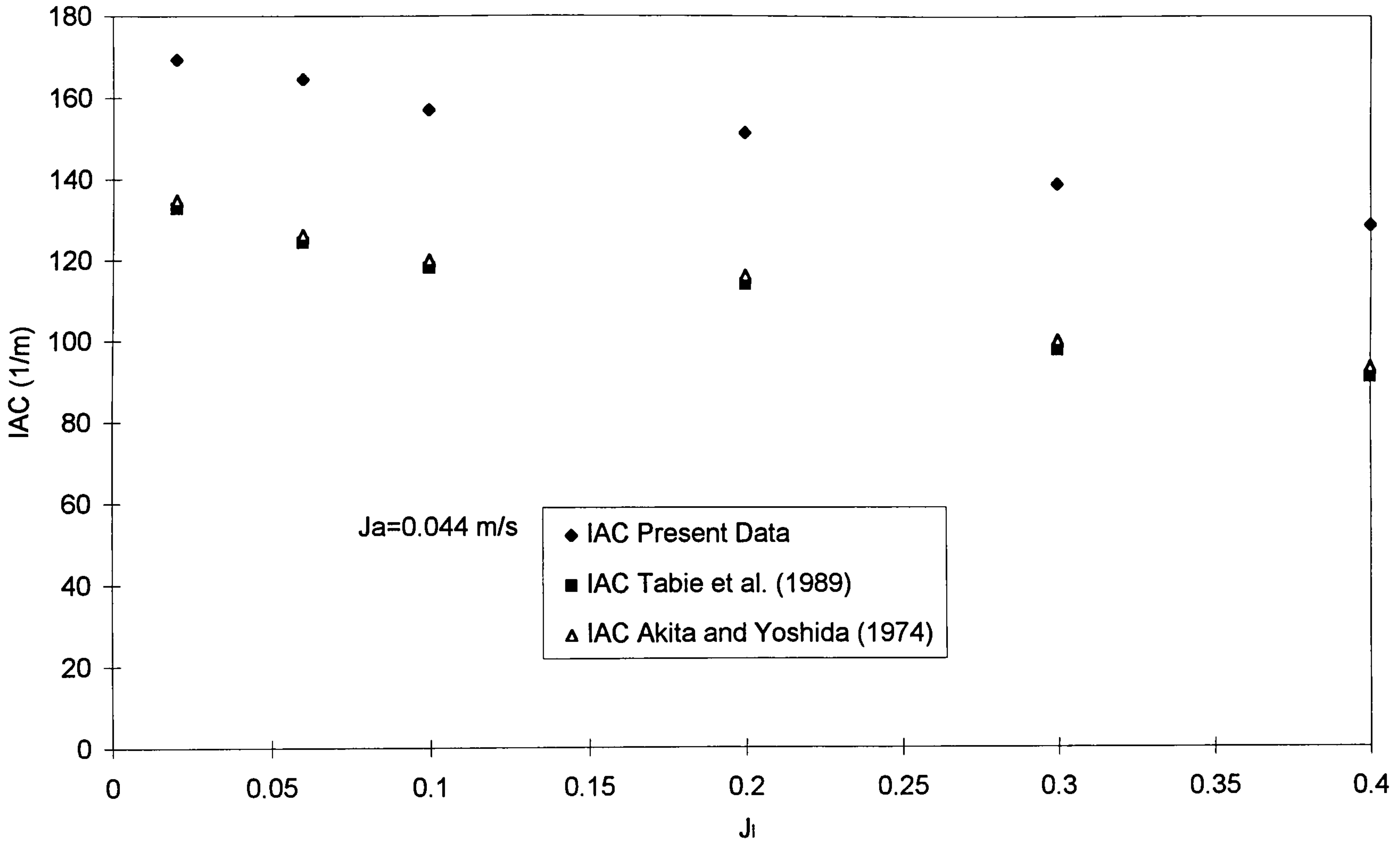

Figure 5.27: Comparison Between Area Averaged IAC Using Present Data and Correlations from Akita and Yoshida (1974) and Tabie et al. (1989) at ja=0.044 m/s

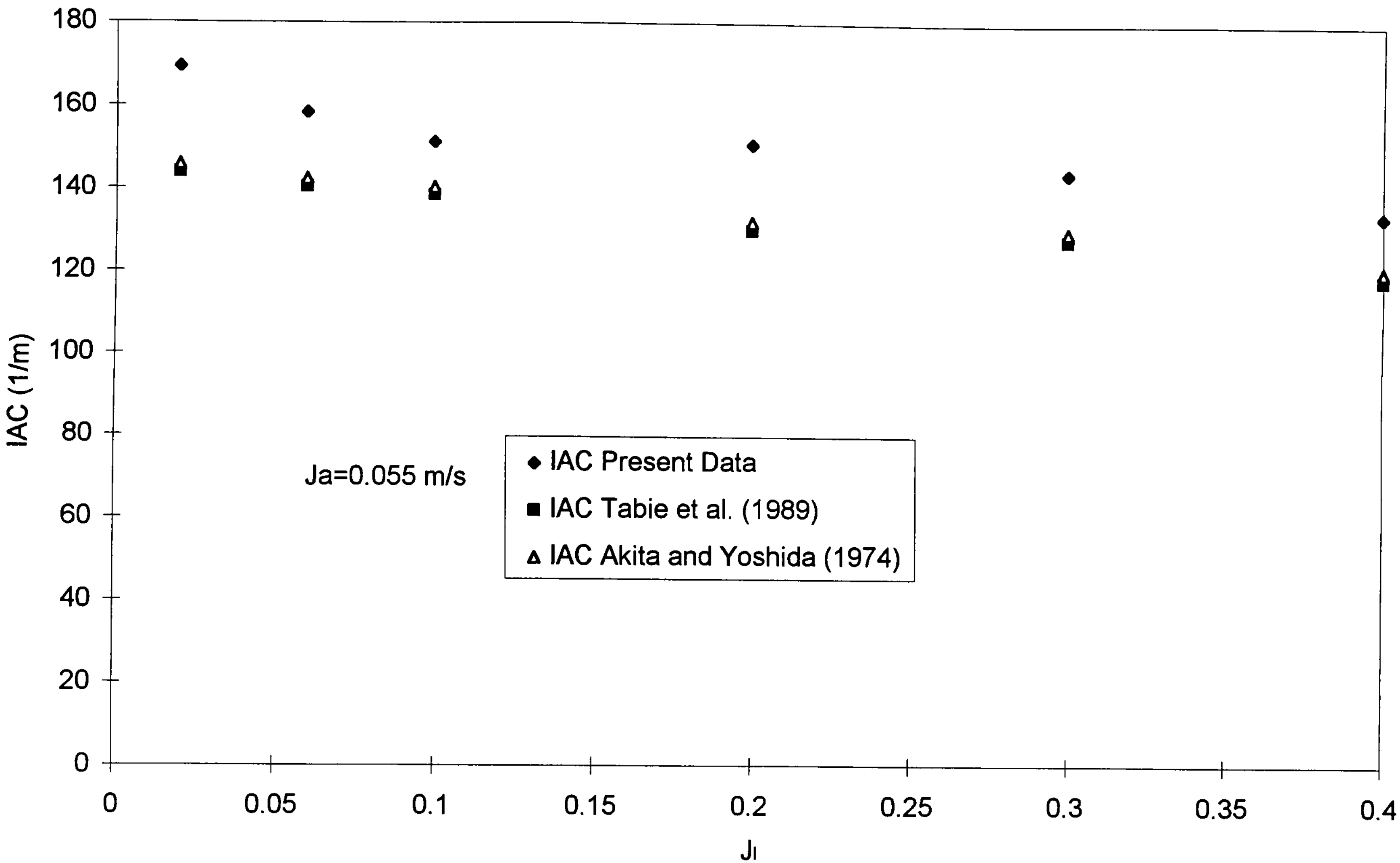

Figure 5.28: Comparison Between Area Averaged IAC Using Present Data and Correlations from Akita and Yoshida (1974) and Tabie et al. (1989) at ja=0.055 m/s

CHAPTER 6

CONCLUSION

6.1 Introduction

In order to study the two-phase bubbly flow structure and to measure the interfacial area concentration in large diameter pipes, the present work was performed. Air-water upward-cocurrent flow was investigated in a 20 cm inner-diameter pipe at a location with L/D = 42. Using a dual fiber optic probe, local flow parameters i.e. void fraction, bubble velocity, bubble frequency, bubble diameter and interfacial area concentration, were measured under a wide range of test conditions. The accuracy and response of the fiber optic probe along with the whole data acquisition system and the computer code were checked by photography using a high speed video camera.

Local distributions were plotted for each test and compared with selected existing data for small diameter pipes. The following is a summary of the results obtained in the present work:

6.2 Void Fraction, Bubble Frequency and Bubble Velocity.

Local void fraction ranging from 2.3 to 17.75 % and area-averaged void fraction ranging from 3.44 to 12.7 % were detected depending on the test conditions and radial position.

Increasing the water superficial velocity at constant gas flow rate decreases the void fraction, and the bubble frequency, while it increases the bubble velocity. Any change in gas or water flow rates significantly affect the core values of these three parameters and slightly affect the near-the-wall values. The same effects were observed by increasing the air velocity at constant water velocity.

The void fraction profiles are in good agreement with other profiles previously obtained under the same test conditions in small diameter pipes except for the saddle-type profile, which is frequently encountered in small diameter pipes under low area-averaged void fraction conditions.

6.3 Bubble Diameter.

The bubble diameter profiles were almost flat with a uniform distribution within the core region with increase in value near the wall. The two methods used to measure the bubble diameter, direct average method and Uga's statistical method, were in good agreement. The bubble diameter was generally insensitive to changing the flow rate, however, it increased with increasing the air velocity at constant water velocity.

The bubble diameters were generally smaller than those obtained in small diameter pipes under the same flow conditions.

6.4 Interfacial Area Concentration

Local IAC distribution profiles were obtained using bubble diameter-based method and the method of Kaoaoka et al. (1985). The profiles were parabolic with lower value near the wall.

Increasing the water flow rate under constant gas flow rate or decreasing gas flow rate under constant water flow rate, decreased the local IAC values with a more significant effect in the core zone.

The present work showed higher IAC values in large diameter pipes as compared with data obtained under the same flow conditions in small diameter pipes. Also, it showed higher area-averaged IAC than those predicted by applying the selected correlations. The agreement with available small-diameter pipe data and correlations improved at high gas and liquid flow rates.

6.5 Recommendations For Future Work.

As a continuation of this two-phase flow parameters investigation, the following topics are recommended for future studies:

I. Obtain a more comprehensive data base suitable for the development of design correlations for bubbly flow in large diameter pipes.

II. Study the applicability of the method of Kataoka et al. Measuring the IAC with higher gas flow rates, or churn flow regime.

III. Study the effect of temperature change on IAC for large diameter pipes.

REFRENCES

Abdul-Razzak, A., Nada, S. M. and Shoukri, M. (1995). Two-Phase Flow Regimes And Void Fraction-Quality Relation In Large Vertical Pipes. *Interim Report,* McMaster University.

Akita, K., and Yoshida, F. (1974). Bubble Size, Interfacial Area, and Liquid-Phase Mass transfer Coefficient In bubble Columns. *Ind. Eng. Chem., Process Des. Develop.,* 13(1), pp. 84-91.

Calderbank, P. H. (1958). Physical Rate Processes In Industrial Fermentation I- The Interfacial Area In Gas-Liquid Contacting With Mechanical Agitation. *Trans. Inst. Chem. Eng.*, 36, pp. 443-463.

Carey, V. P. (1992). Liquid-Vapour Phase-Change Phenomena.

Chan, A. M. (Mar. 1977). Transient Void Fraction Measurements In Rod Bundle Geometries. *OECD / CNSI Specialist Meeting.*

Dejesus, J. M. And Kawaji, M. (1990). Investigation Of Interfacial Area and Void Fraction in Upward, Cocurrent Gas-Liquid Flow. *The Canadian Journal Of Chemical Engineering*, 68, pp. 904-912.

Delhaye, J. M. (1981). Two-Phase Flow And Heat Transfer In Power And Process Industries. *Hemisphere Publishing Corporation.*

Delhaye, J. M. and Cognet, G. (1984). Measuring Techniques In Gas-Liquid Two-Phase Flows.

Dillon, G. B. And Harris, I. J. (1966). The Determination Of Mass Transfer Coefficients And Interfacial Areas in Gas-Liquid Contacting Systems. *The Canadian Journal Of Chemical Engineering*, pp. 307-312.

Herringe, R. A. and Davis, M. R. (1976). Structure Development Of Gas-Liquid Mixture Flows. *J. Fluid Mech.* 73(1), pp. 97-123.

Hinata, S., Sakurai, M., Nakazawa, M., Venart, J., Sousa, A. and Zhou, B. (1991). Miniature Optical Fiber Sensor Used To Measure Local Void Fractions. *Heat Transfer-Japanese Research.* 20(5) pp. 429-440.

Ishii, M. (1977). One-Dimensional Drift-Flux Model and Constitutive Equations For Relative Motion Between Phases in Various Two-Phase Flow Regimes. *Anl-77-47.*

Ishii, M. and Mishima, K. (1980). Study Of Two-Fluid Model And Interfacial Area. *Nurec/Cr-1873-Anl-80-111.*

Ishii, M. and Mishima, K. (1994). Two-Fluid Model And Hydrodynamics Constitutive Relations. *Nuclear Eng. And design,* 82, pp. 107-126.

Kasturi, G. and Stepanek J. B. (1974). Two-Phase Flow-III. Interfacial Area In CoCurrent Gas-Liquid Flow. *Chemical Engineering Science,* 29, pp. 713-719.

Kataoka, I., Ishii, M. and Serizawa, A. (1985). Local Formulation And Measurements Of Interfacial Area Concentration In Two-Phase Flow. *Int. J. Multiphase Flow* 12(4), pp. 505-529.

Kataoka, I., and Ishii, M. (1987). Drift Flux Model For Large Diameter Pipe And New Correlation For Pool Void Fraction. *Int. J. Heat Transfer.* 30(9), pp. 1927-1987.

Kataoka, I. and Serizawa, A. (1990). Interfacial Area Concentration In Bubbly Flow. *Nuclear Eng. And Design,* 120, pp. 163-180.

Kawaji, M. Pressure Drop And Void Fraction And Two-Phase Flow Modelling-II. *Chem. Eng. Dept. Univ. of Toronto, Short course lecture notes.*

Kelly, J. E. and Kazimi, M. S. (1982). Interfacial Exchange Relations For Two-Fluid Vapor-Liquid Flow: A Simplified Regime-Map Approach. *Nuclear Science and Engineering.* 81, pp. 305-318.

Kocamustafaogullari, G. and Wang, Z. (1991). An Experimental Study On Local Interfacial Parameters In A Horizontal Bubbly Two-Phase Flow. *Int. J. Multiphase Flow.* 17(5) pp. 553-572.

Kocamustafaogullari, G., Huang, W. D. and Razi, J. (1994). Measurement And Modeling Of Average Void Fraction, Bubble Size, And Interfacial Area. *Nuclear Eng. And Design.* 148 pp. 437-453.

Landau, J., Boyle, J., Gomaa, H. G. and Al-Taweel, M. (1977). Comparison Of Methods For Measuring Interfacial Areas In Gas-Liquid Dispersions. *The Canadian Journal Of Chemical Eng.* 55, pp. 13-18.

Leung, W. H., Revankar, S. T., Ishii, Y., and Ishii, M. (1995). Axial Development Of Interfacial Area And Void Concentration Profiles Measured By Double-Sensor Probe Method. *Int. J. Heat Mass Transfer* 38(3), pp. 445-453.

Liu, T. J. and bankoff, S. G. (1993). Structure Of Air-Water Bubbly Flow In A Vertical Pipe I. Liquid Mean velocity And Turbulence Measurements. *Int. J. Heat Mass Transfer* 36(4), pp. 1049-1060.

Liu, T. J. and bankoff, S. G. (1993). Structure Of Air-Water Bubbly Flow In A Vertical Pipe II. Void Fraction, Bubble Velocity and Bubble Size Distribution. *Int. J. Heat Mass Transfer* 36(4), pp. 1061-1072.

Liu, T. T. (1989). Experimental Investigation Of Turbulence Structure In Two-Phase Bubbly Flow. *Ph.D. Thesis McMaster University.*

Moffat, R. J. (1988). Describing The Uncertainties In Experimental Results. *Experimental Thermal and Fluid Science,* 1, pp. 3-17.

Revankar, S. T. and Ishii, M. (1992). Local Interfacial Area Measurement In Bubbly Flow. *Int. J. Heat Mass Transfer* 35(4), pp. 913-925.

Rinne, A. and Loth, R. (1996). Development Of Local two-Phase Flow Parameters For Vertical Bubbly Flow In A Pipe With Sudden Expansion. *Experimental Thermal and Fluid Science Inc.* 13, pp. 152-166.

Serizawa, A., Kataoka, I. and Michiyoshi, I. (1975). Turbulence Structure Of Air-Water Bubbly Flow-I. Measuring Techniques. *Int. J. Multiphase Flow* 2, pp. 221-233.

Serizawa, A., Kataoka, I. and Michiyoshi, I. (1975). Turbulence Structure Of Air-Water Bubbly Flow-II. Local Properties. *Int. J. Multiphase Flow* 2, pp. 235-246.

Sharma, M. M. and Danckwerts, P. V. (1970). Chemical Methods Of Measuring Interfacial Area And Mass Transfer Coefficient In Two-Fluid Systems. *British Chemical Engineering* 15(4), pp. 522-527.

Shilimkan, R. V. and Stepanek, J. B. (1977). Interfacial Area In CoCurrent Gas-Liquid Upward Flow In Tubes Of Various Size. *Chemical Eng. Science* 32, pp. 149-154.

Shoukri, M. (1994a). Introduction To Two-Phase Flow. *Lecture Notes.* McMaster University.

Shoukri, M. (1994b). Two-Phase Flow Modelling I- Fundamentals. *Lecture Notes.* McMaster University.

Shoukri, M. (1994c). Two-Phase Flow Modelling III- Application Of The Two-Fluid model. *Lecture Notes.* McMaster University.

Sridharan, K. and Sharma, M. M. (1976). New systems And Methods For The Measurement Of Effective Interfacial Area And Mass Transfer Coefficients in Gas-Liquid Contactors. *Chemical Eng. Science* 31, pp. 767-774.

Stankovic, Branko (1997). An Experimental Study On The Local Void Fraction Measurements In Large-Diameter Vertical Pipes Using Optical Fiber Probes.. *M.Eng Thesis McMaster University.*

Stegeman, D., Knop, P. A., Wijnands, J. G. and Westerterp, K. R. (1996). Interfacial Area And Gas Holdup In A Column Reactor At Elevated Pressures. *Ind. Eng. Chem. Res.* 36, pp. 3842-3847.

Sun, G. (1997). An Experimental Study On Structure Of Air-Water Bubbly Flow In A Large Diameter Pipe. *Internal Report.* McMaster University.

Tabei, K., Hasatani, M. and Kuroda, M. (1989). Effective Gas-Liquid Interfacial area In A Mobile-Bed Contactor. *Int. Chemical Engineering,* 29(4), pp. 679-688.

Taitel, Y., Bornea, D. and Dukler, A. E. (1980). Modelling Flow Pattern Transitions For Steady Upward Gas-Liquid Flow In Vertical Tubes. *AICHE Journal,* 26(3), pp. 345-354.

Tomida, T., Yusa, F. and Okazaki, T. (1978). Effective Interfacial Area And Liquid-Side Mass Transfer coefficient In The Upward Two-Phase Flow of Gas-Liquid Mixture. *Chemical Eng. J.* 16, pp. 81-88.

Uga, T. (1972). Determination Of Bubble-Size Distribution In A Boiling Water Reactor. *Nuclear Eng. And Design.* 22, pp. 252-261.

Watson, A. P., Cormack, D. E. and Charles M. E. (1979). A Preliminary Study Of Interfacial Areas In Vertical CoCurrent, Two-Phase Upflow. *The Canadian Journal Of Chemical Engineering.* 57 pp. 16-23.

Zeitoun, O., Shoukri, M. and Chatoorgoon, V. (1994). Measurement Of Interfacial Area Concentration In Subcooled Liquid-Vapour Flow. *Nuclear Engineering and Design.* 152 pp. 243-255.

Zeitoun, O., Shoukri, M. and Chatoorgoon, V. (1995). Interfacial Heat Transfer Between Steam Bubbles And Subcooled Water In Vertical Upward Flow. *J. Heat Transfer.* 117 pp. 402-407.

Appendix A

Local Experimental Results For 20 cm Diameter Pipe

Jl (m/s)	r/R	α %	no of S.B.	Uav(m/s)	Dav(mm)	IACav(1/m)	NOB	freq.(1/s)	IAC k (1/m)	Duga (mm)	IAC UGA
0.02	0	10.1	200	0.501	2.4	252.5	2880	23.10	252.79	2.8	216.43
	0.1	10	215	0.492	2.5	240	2882	23.10	245.7	2.8	214.29
	0.2	9.75	183	0.481	2.56	228.51	2781	22.30	240.2	2.8	208.93
	0.3	9.36	231	0.47	2.5	224.64	2785	22.28	240.28	2.8	200.57
	0.4	9.1	183	0.492	2.7	202.2	2485	19.88	232.54	3	182.00
	0.5	9.12	208	0.463	3	182.4	2366	18.94	230.01	3.2	171.00
	0.6	8.95	134	0.425	2.9	185.17	2072	16.61	225.235	3	179.00
	0.7	8.32	123	0.4057	3	166.4	1874	15.00	220.33	3.4	146.82
	0.75	7.89	162	0.377	3.12	151.73	1842	14.76	198.12	3.2	147.94
	0.8	7.35	137	0.376	3.09	142.7	1748	14.02	190.99	3.16	139.56
	0.85	7	90	0.353	3.19	131.66	1480	11.87	193.89	3.6	116.67
	0.87	6.6	87	0.33	3.17	124.9	1400	11.20	204.72	3.5	113.14
	0.9	5.59	117	0.325	3.038	110.4	1480	11.86	190.35	3.2	104.81
	0.92	4.88	90	0.337	2.81	104.2	1179	9.43	187.56	3.3	88.73
	0.95	4.4	69	0.267	3.02	87.41	1029	8.25	178.42	3.6	73.33
0.06	0	7.92	188	0.51	2.5	190.08	2726	21.86	222.62	2.3	206.61
	0.1	7.65	150	0.523	2.51	182.87	2622	21.00	213.65	2.5	183.60
	0.2	7.6	139	0.512	2.46	185.37	2537	20.30	210.63	2.65	172.08
	0.3	7.9	109	0.527	2.65	178.87	2232	17.86	215.19	3	158.00
	0.4	7.46	133	0.533	2.61	171.49	2073	16.59	200.12	3	149.20
	0.5	7.4	134	0.493	2.6	170.77	2059	16.48	194.27	3.1	143.23
	0.6	6.9	109	0.497	2.62	158.02	1779	14.23	179.51	3.2	129.38
	0.7	6.77	109	0.473	2.9	140.07	1523	12.19	166.84	3.3	123.09
	0.75	6.28	124	0.442	3.155	119.43	1486	11.61	156.55	3.4	110.82
	0.8	5.48	136	0.401	2.68	122.69	1497	11.98	160	2.9	113.38
	0.85	5.4	109	0.39	3.05	106.23	1252	10.03	150.65	2.65	122.26
	0.87	5.4	88	0.397	3.14	103.18	1223	9.79	152.19	3.3	98.18
	0.9	4.74	72	0.339	3.25	87.51	1057	8.46	156.35	3.2	88.88
	0.92	3.97	83	0.32	2.98	79.93	1124	8.99	166.89	3.4	70.06
	0.95	3.97	54	0.28	2.93	81.30	878	7.03	160.96	3	79.40

Test Results for ja=0.022 m/s

Jl (m/s)	r/R	α %	no of S.B.	Uav(m/s)	Dav(mm)	IACav(1/m)	NOB	freq.(1/s)	IAC k (1/m)	Duga (mm)	IAC UGA
0.1	0	6.79	150	0.593	2.6	156.69	2219	17.76	190.69	2.8	145.50
	0.1	6.7	333	0.591	2.7	148.89	2163	17.31	170.67	2.8	143.57
	0.2	6.8	205	0.599	2.95	138.31	2096	16.80	161.9	3.2	127.50
	0.3	6.78	149	0.592	3.09	131.65	2027	16.22	156.99	3.4	119.65
	0.4	6.55	102	0.573	3	131.00	1796	14.37	160.18	3	131.00
	0.5	6.12	98	0.561	3.27	112.29	1653	13.24	143.08	3.3	111.27
	0.6	5.66	132	0.526	3.23	105.14	1576	12.61	127.98	3	113.20
	0.7	5.5	133	0.534	3.49	94.56	1380	11.07	125.94	3.3	100.00
	0.75	5.13	112	0.531	3.37	91.34	1260	10.08	132.39	3.2	96.19
	0.8	4.98	116	0.517	3.51	85.13	1282	10.27	119.15	3.8	78.63
	0.85	4.52	103	0.468	3.6	75.33	1112	8.92	107.79	4	67.80
	0.87	4.33	90	0.453	3.72	69.84	951	7.61	103.57	4.2	61.86
	0.9	3.93	87	0.447	3.84	61.41	899	7.19	110.91	3.6	65.50
	0.92	3.68	69	0.428	3.59	61.50	806	6.46	110.45	3.4	64.94
	0.95	3.22	55	0.404	4.06	47.59	663	5.31	75.52	4.4	43.91
0.2	0	6.1	125	0.617	2.64	138.64	1990	15.97	159.45	2.9	126.21
	0.1	6	128	0.615	2.77	129.96	1984	15.91	150.9	2.77	129.96
	0.2	5.53	135	0.614	2.66	124.74	1875	15.01	132.66	3.6	92.17
	0.3	5.4	131	0.606	2.69	120.45	1791	14.33	129.24	3.39	95.58
	0.4	5.58	119	0.588	3	111.60	1720	13.76	123.49	2.8	119.57
	0.5	5.44	113	0.577	3.3	98.91	1617	12.94	109.98	3.6	90.67
	0.6	5	112	0.567	3.2	93.75	1400	11.22	101.79	3.43	87.46
	0.7	4.64	139	0.56	3.2	87.00	1236	9.91	95.24	4.2	66.29
	0.75	4.43	112	0.556	3.1	85.74	1230	9.86	93.4	3.6	73.83
	0.8	4.36	126	0.537	3.2	81.75	1139	9.13	89.3	3.7	70.70
	0.85	3.9	85	0.49	3	78.00	1093	8.78	91.512	2.68	87.31
	0.87	3.77	65	0.47	3.3	68.55	1016	8.13	90.11	3	75.40
	0.9	3.38	76	0.443	3.42	59.30	821	6.57	84.65	3.6	56.33
	0.92	3.38	54	0.484	4.04	50.20	750	6.00	78.281	3.1	65.42
	0.95	2.87	53	0.385	4	43.05	686	5.50	74.72	2.9	59.38

Test Results for ja=0.022 m/s

Jl (m/s)	r/R	α %	no of S.B.	Uav(m/s)	Dav(mm)	IACav(1/m)	NOB	freq.(1/s)	IAC k (1/m)	Duga (mm)	IAC UGA
0.3	0	5.22	250	0.6445	2.59	120.93	1909	15.34	140.40	2.9	108.00
	0.1	5.09	104	0.654	2.49	122.65	1859	14.91	129.90	2.4	127.25
	0.2	5.04	94	0.647	2.5	120.96	1804	14.44	118.20	2.5	120.96
	0.3	4.85	108	0.63	2.6	111.92	1763	14.14	111.22	2.4	121.25
	0.4	4.99	93	0.597	2.65	112.98	1686	13.49	111.20	2.4	124.75
	0.5	4.48	347	0.59	2.7	99.56	1518	12.15	100.00	2.7	99.56
	0.6	4.41	111	0.582	3.03	87.33	1387	11.10	87.23	3.1	85.35
	0.7	3.9	85	0.58	2.78	84.17	1192	9.55	88.98	2.8	83.57
	0.75	3.67	132	0.571	2.88	76.46	1108	8.88	79.36	2.9	75.93
	0.8	3.57	137	0.557	2.89	74.12	1140	9.12	88.29	2.7	79.33
	0.85	3.48	98	0.556	2.9	72.00	1035	8.28	86.22	2.5	83.52
	0.87	3.16	75	0.539	3.26	58.16	905	7.25	66.10	3	63.20
	0.9	3.06	79	0.518	3.37	54.48	821	6.57	69.00	2.9	63.31
	0.92	2.73	97	0.444	3	54.60	911	7.29	61.09	2.6	63.00
	0.95	2.69	61	0.446	3.6	44.83	693	5.55	55.79	2.6	62.08
0.4	0	4.7	90	0.67	2.4	117.50	1815	14.53	130.34	2.4	117.50
	0.1	4.68	99	0.701	2.35	119.49	1756	14.05	121.51	2.2	127.64
	0.2	4.69	102	0.685	2.39	117.74	1766	14.15	119.327	2.2	127.91
	0.3	4.37	141	0.693	2.39	109.71	1707	13.66	110.03	2.3	114.00
	0.4	4.15	90	0.659	2.34	106.41	1576	12.61	101.4	2.2	113.18
	0.5	4.09	73	0.642	2.58	95.12	1507	12.07	93.62	2.6	94.38
	0.6	3.94	80	0.65	2.6	90.92	1330	10.64	86.65	2.5	94.56
	0.7	3.38	93	0.651	2.59	78.30	1184	9.49	76.43	2.4	84.50
	0.75	3.21	122	0.627	2.56	75.23	1108	8.88	77.33	2.3	83.74
	0.8	3.17	80	0.571	2.59	73.44	1089	8.71	72.76	2.5	76.08
	0.85	3.11	90	0.572	2.69	69.37	1005	8.06	84.05	2.4	77.75
	0.87	2.87	108	0.573	2.57	67.00	1030	8.24	71.756	2.4	71.75
	0.9	2.69	97	0.57	2.91	55.46	905	7.24	58.55	2.6	62.08
	0.92	2.43	113	0.547	2.92	49.93	832	6.67	61.58	2.8	52.07
	0.95	2.3	96	0.576	2.8	49.29	785	6.30	55.14	2.8	49.29

Test Results for ja=0.022 m/s

Jl (m/s)	r/R	α %	no of S. B	Uav(m/s)	Dav(mm)	IACav(1/m)	NOB	freq.(1/s)	IAC k (1/m)	Duga (mm)	IAC UGA
0.02	0	13.91	279	0.611	3.25	256.80	3925	31.41	277.25	3.2	260.81
	0.1	13.7	297	0.628	3.39	242.48	3899	31.20	261.84	3.6	228.33
	0.2	13.3	364	0.596	3.43	232.65	3775	30.20	252.95	3.6	221.67
	0.3	13.01	295	0.591	3.54	220.51	3644	29.25	237.94	3.6	216.83
	0.4	12.86	310	0.579	3.71	207.98	3319	26.56	215.46	3.5	220.46
	0.5	12.1	283	0.56	3.68	197.28	3067	24.54	202.24	3.3	220.00
	0.6	11	184	0.505	3.7	178.38	2843	22.77	179.03	3.5	188.57
	0.7	10.3	174	0.494	3.95	156.46	2416	19.34	167.65	4	154.50
	0.75	10	169	0.52	4	150.00	2133	17.07	154.58	4.4	136.36
	0.8	8.9	160	0.524	3.95	135.19	1913	15.31	138.43	4.4	121.36
	0.85	8.1	119	0.442	3.76	129.26	1630	13.06	131.65	3.8	127.89
	0.87	7.8	83	0.434	3.85	121.56	1487	11.94	128.35	4.1	114.15
	0.9	7.5	106	0.358	3.91	115.09	1282	10.28	124.96	3.7	121.62
	0.92	6.6	87	0.374	3.77	105.04	1155	9.25	119.4	3.7	107.03
	0.95	5.71	58	0.348	3.88	88.30	1045	8.36	111.85	3.7	92.59
0.06	0	12.72	349	0.643	3.1	246.19	3881	31.18	259.56	3.4	224.47
	0.1	12.6	491	0.645	3.25	232.62	3817	30.62	242.8	3.4	222.35
	0.2	12.34	322	0.62	3.31	223.69	3669	29.37	230.83	3.5	211.54
	0.3	11.86	326	0.6072	3.29	216.29	3455	27.64	223.94	3.5	203.31
	0.4	11.43	354	0.568	3.56	192.64	3328	26.63	202.1	3.8	180.47
	0.5	11.1	357	0.521	3.61	184.49	3118	24.99	191.78	3.3	201.82
	0.6	10.57	336	0.512	3.79	167.34	2819	22.56	180.25	3.4	186.53
	0.7	10.07	175	0.484	3.93	153.74	2262	18.10	160.4	3.8	159.00
	0.75	9.61	214	0.468	4.01	143.79	2197	17.58	161.56	3.6	160.17
	0.8	8.58	148	0.438	3.99	129.02	1923	15.39	138.725	3.6	143.00
	0.85	8.12	177	0.439	3.89	125.24	1708	13.67	134.77	3.6	135.33
	0.87	7.36	126	0.449	4.24	104.15	1582	12.66	124.12	4.1	107.71
	0.9	7.18	81	0.427	4.41	97.69	1338	10.71	114.28	4.4	97.91
	0.92	6.4	82	0.409	3.83	100.26	1249	9.99	112.9	3.8	101.05
	0.95	5.67	50	0.367	3.82	89.06	1053	8.43	110.1	3.8	89.53

Test Results for ja=0.033 m/s

Jl (m/s)	r/R	α %	no of S. B	Uav(m/s)	Dav(mm)	IACav(1/m)	NOB	freq.(1/s)	IAC k (1/m)	Duga (mm)	IAC UGA
0.1	0	10.63	375	0.678	3.11	205.08	3349	26.90	235.94	3.3	193.27
	0.1	10.52	394	0.69	3.22	196.02	3276	26.25	219.89	3.3	191.27
	0.2	10.69	272	0.662	3.46	185.38	3272	26.18	204.33	3.8	168.79
	0.3	10.58	308	0.666	3.59	176.82	3207	25.66	191.44	3.9	162.77
	0.4	10.56	300	0.645	3.85	164.57	2988	23.91	185.43	4.1	154.54
	0.5	10.25	170	0.595	3.9	157.69	2762	22.10	175.42	3.5	175.71
	0.6	9.53	181	0.572	3.98	143.67	2620	20.97	165.257	3.6	158.83
	0.7	9.19	161	0.519	3.96	139.24	2332	18.66	150.69	3.5	157.54
	0.75	8.81	194	0.496	3.94	134.16	2127	17.02	139.11	3.4	155.47
	0.8	7.99	194	0.476	3.84	124.84	1821	14.57	129.75	3.4	141.00
	0.85	7.86	143	0.461	3.8	124.11	1784	14.28	134.73	3.4	138.71
	0.87	7.49	112	0.439	3.82	117.64	1551	12.41	118.42	3.42	131.40
	0.9	6.88	137	0.408	3.98	103.72	1490	11.93	125.85	3.95	104.51
	0.92	6.07	103	0.409	3.77	96.60	1286	10.29	124.7	3.9	93.38
	0.95	5.8	257	0.304	3.76	92.55	1223	9.79	123.12	3.5	99.43
0.2	0	9.45	168	0.689	2.98	190.27	3126	25.04	184.07	2.9	195.52
	0.1	9.38	169	0.684	3.11	180.96	3119	25.00	174.91	2.8	201.00
	0.2	9.28	244	0.683	3.28	169.76	3069	24.56	168.64	3.2	174.00
	0.3	9.21	392	0.673	3.33	165.95	2861	22.89	164.4	3.2	172.69
	0.4	9.11	216	0.662	3.6	151.83	2826	22.62	162.94	3.7	147.73
	0.5	8.51	230	0.664	3.62	141.05	2598	20.79	155.55	3.7	138.00
	0.6	8.17	234	0.649	3.83	127.99	2473	19.79	149.69	3.8	129.00
	0.7	7.74	221	0.603	3.89	119.38	2060	16.49	137.648	3.8	122.21
	0.75	7.68	189	0.57	3.99	115.49	1959	15.68	134.36	3.72	123.87
	0.8	7.12	185	0.569	3.85	110.96	1843	14.75	120.02	3.9	109.54
	0.85	6.52	177	0.536	3.81	102.68	1495	11.99	102.142	3.8	102.95
	0.87	6.33	139	0.483	3.82	99.42	1489	11.92	112.31	3.6	105.50
	0.9	5.91	105	0.477	3.89	91.16	1237	9.90	101.18	3.8	93.32
	0.92	5.58	112	0.426	3.92	85.41	1194	9.55	105.09	3.07	109.06
	0.95	5.38	88	0.445	3.91	82.56	1166	9.33	96.66	3.6	89.67

Test Results for ja=0.033 m/s

Jl (m/s)	r/R	α %	no of S. B	Uav(m/s)	Dav(mm)	IACav(1/m)	NOB	freq.(1/s)	IAC k (1/m)	Duga (mm)	IAC UGA
0.3	0	8.23	435	0.7238	2.79	176.99	2992	23.94	164.745	3	164.60
	0.1	8.37	173	0.716	2.98	168.52	2970	23.77	160.37	2.8	179.36
	0.2	8.23	328	0.715	3.21	153.83	2883	23.07	153.53	3.45	143.13
	0.3	7.92	268	0.709	3.23	147.12	2771	22.20	148.62	3.33	142.70
	0.4	7.61	241	0.682	3.23	141.36	2601	20.81	142.69	2.8	163.07
	0.5	7.27	163	0.674	3.26	133.80	2523	20.19	141.499	2.9	150.41
	0.6	6.72	286	0.67	3.366	119.79	2359	18.88	135.3	3.3	122.18
	0.7	6.52	175	0.638	3.51	111.45	2087	16.77	131.538	3.3	118.55
	0.75	6.41	181	0.608	3.61	106.54	1905	15.24	125.02	3.6	106.83
	0.8	6.06	134	0.575	3.52	103.30	1704	13.64	110.9	3.6	101.00
	0.85	5.4	135	0.56	3.53	91.78	1482	11.86	103.1	3.7	87.57
	0.87	6.1	109	0.549	3.77	97.08	1494	11.96	105.1	3.7	98.92
	0.9	5.67	80	0.526	3.98	85.48	1356	10.85	84.05	3.9	87.23
	0.92	5.02	91	0.517	4.28	70.37	1189	9.51	71.08	3.6	83.67
	0.95	4.38	73	0.509	4.51	58.27	1015	8.12	56.34	4.01	65.54
0.4	0	7.49	165	0.754	2.65	169.58	2983	23.93	144.78	2.6	172.85
	0.1	7.46	136	0.764	2.82	158.72	2926	23.52	146.27	2.9	154.34
	0.2	7.21	78	0.736	2.94	147.14	2875	23.01	143.69	2.6	166.38
	0.3	7.3	138	0.725	3.08	142.21	2760	22.13	140.75	2.9	151.03
	0.4	7.19	199	0.719	3.15	136.95	2685	21.49	134.24	2.9	148.76
	0.5	6.98	194	0.723	3.26	128.47	2443	19.55	134.3	3	139.60
	0.6	6.54	201	0.694	3.37	116.44	2341	18.73	126.5	3.2	122.63
	0.7	6.09	243	0.674	3.439	106.25	2007	16.15	120.9	3.6	101.50
	0.75	5.91	160	0.67	3.52	100.74	1879	15.08	110.83	3.4	104.29
	0.8	5.79	136	0.664	3.64	95.44	1744	13.99	110.38	3.4	102.18
	0.85	5.27	130	0.588	3.83	82.56	1633	13.10	108.73	3.5	90.34
	0.87	5.66	171	0.573	3.5	97.03	2017	16.30	116.79	3.3	102.91
	0.9	5.1	129	0.569	3.29	93.01	1556	12.47	101.78	3.5	87.43
	0.92	5.04	113	0.578	3.97	76.17	1360	10.92	84.46	3.6	84.00
	0.95	4.78	140	0.568	3.94	72.79	1496	11.99	97.08	3.5	81.94

Test Results for ja=0.033 m/s

Jl (m/s)	r/R	α %	no of S. B	Uav(m/s)	Dav(mm)	IACav(1/m)	NOB	freq.(1/s)	IAC I (1/m)	Duga (mm)	IAC UGA
0.02	0	16.82	400	0.757	4.48	225.27	4552	36.51	228.73	4.2	240.29
	0.1	16.3	373	0.755	4.4	222.27	4522	36.18	222.17	4.2	232.86
	0.2	15.99	512	0.751	4.52	212.26	4489	35.93	216.94	4.2	228.43
	0.3	16	501	0.746	4.699	204.30	4374	35.01	204	4.4	218.18
	0.4	15.4	476	0.732	4.95	186.67	4012	32.10	199.1	4.8	192.50
	0.5	15.1	495	0.713	4.98	181.93	3937	31.51	192.136	4.5	201.33
	0.6	14.1	345	0.688	5.05	167.52	3642	29.14	182.33	5	169.20
	0.7	12.8	267	0.618	5.155	148.98	3210	25.69	174.575	4.8	160.00
	0.75	11.94	271	0.604	5.11	140.20	3029	24.24	170.97	4.4	162.82
	0.8	10.65	189	0.553	5.01	127.54	2779	22.24	160.447	4.6	138.91
	0.85	9.59	165	0.527	5.079	113.29	2318	18.58	151.474	4.4	130.77
	0.87	8.9	146	0.4906	5.1	104.71	1939	15.52	143.957	4.3	124.19
	0.9	7.98	98	0.47	5.11	93.70	1869	14.95	144.07	4.4	108.82
	0.92	6.92	65	0.491	5.2	79.85	1720	13.83	128.8	4	103.80
	0.95	6.33	83	0.411	5.14	73.89	1257	10.07	113.33	4.1	92.63
0.06	0	15.35	393	0.797	4.42	208.37	4441	35.62	212.648	4.6	200.22
	0.1	15.07	356	0.799	4.41	205.03	4350	34.81	210.295	4.2	215.29
	0.2	14.74	730	0.79	4.52	195.66	4345	34.83	201.22	4.5	196.53
	0.3	14.5	654	0.778	4.55	191.21	4185	33.49	196.24	4.7	185.11
	0.4	14.06	480	0.77	4.7	179.49	3820	30.60	186.615	4.6	183.39
	0.5	14.19	349	0.746	4.91	173.40	3724	29.80	180.4	4.2	202.71
	0.6	13.65	362	0.7046	5.06	161.86	3371	27.06	176.489	5	163.80
	0.7	11.95	273	0.654	5.02	142.83	2936	23.53	170.686	4.5	159.33
	0.75	11.93	301	0.632	5.274	135.72	2623	20.99	167.29	4.8	149.13
	0.8	10.08	215	0.607	5.19	116.53	2181	17.45	156.438	4.8	126.00
	0.85	8.73	130	0.588	4.863	107.71	1910	15.31	149.97	4.3	121.81
	0.87	8.72	137	0.5775	4.95	105.70	1903	15.24	144.23	4.6	113.74
	0.9	7.95	138	0.548	5.122	93.13	1789	14.31	148.617	4.5	106.00
	0.92	6.6	106	0.531	4.96	79.84	1744	13.95	121.159	4.4	90.00
	0.95	5.79	66	0.539	4.75	73.14	1232	9.86	122.79	4.4	78.95

Test Results for ja=0.044 m/s

Jl (m/s)	r/R	α %	no of S. B	Uav(m/s)	Dav(mm)	IACav(1/m)	NOB	freq.(1/s)	IAC I (1/m)	Duga (mm)	IAC UGA
0.1	0	14.94	394	0.814	4.2	213.43	4332	34.74	207.45	3.6	249.00
	0.1	14.6	503	0.813	4.23	207.09	4287	34.34	204.46	4.2	208.57
	0.2	14.094	496	0.816	4.375	193.29	4185	33.49	193.99	3.8	222.54
	0.3	13.5	404	0.795	4.35	186.21	3941	31.54	187.50	3.9	207.69
	0.4	13.12	309	0.781	4.57	172.25	3684	29.49	179.00	3.9	201.85
	0.5	12.53	316	0.765	4.693	160.20	3429	27.44	169.60	4.5	167.07
	0.6	12.38	435	0.736	4.655	159.57	3269	26.16	165.09	4.5	165.07
	0.7	11.67	314	0.66	4.723	148.25	2874	23.06	160.04	4.4	159.14
	0.75	11.19	377	0.641	4.89	137.30	2639	21.14	164.95	4.8	139.88
	0.8	10.54	253	0.622	4.92	128.54	2448	19.59	151.10	4.5	140.53
	0.85	9.23	228	0.608	4.57	121.18	2214	17.71	141.60	4.5	123.07
	0.87	8.2	217	0.5494	4.967	99.05	1820	14.58	127.58	4.6	106.96
	0.9	7.95	162	0.558	5.199	91.75	1593	12.76	124.57	5.2	91.73
	0.92	6.794	154	0.543	5.237	77.84	1588	12.73	131.97	5.1	79.93
	0.95	5.65	100	0.513	4.5	75.33	1175	9.40	128.39	5	67.80
0.2	0	13.76	328	0.852	3.95	209.01	4282	34.34	201.379	3.55	232.56
	0.1	12.9	395	0.847	3.77	205.31	4203	33.69	192.899	3.8	203.68
	0.2	13.1	282	0.846	3.87	203.10	4151	33.21	190.315	3.8	206.84
	0.3	12.18	330	0.824	3.98	183.62	3892	31.14	182.965	3.9	187.38
	0.4	12	300	0.789	4.1	175.61	3630	29.04	180.352	3.3	218.18
	0.5	12.1	236	0.787	4.2	172.86	3403	27.23	167.376	3.3	220.00
	0.6	11.62	308	0.764	4.3	162.14	3201	25.61	163.356	3.5	199.20
	0.7	11.15	481	0.693	4.4	152.05	2705	21.64	155.82	3.5	191.14
	0.75	10.64	252	0.66	4.47	142.82	2753	22.05	151.94	4.5	141.87
	0.8	10.03	233	0.642	4.32	139.31	2212	17.70	137.47	4.19	143.63
	0.85	9.83	200	0.627	4.76	123.91	2204	17.63	128.09	4.4	134.05
	0.87	8.8	182	0.591	4.543	116.22	2126	17.01	124.17	4.5	117.33
	0.9	8.1	171	0.585	4.57	106.35	1757	14.06	116.189	4.5	108.00
	0.92	7.9	156	0.509	4.71	100.64	1654	13.23	130.032	4.3	110.23
	0.95	6.2	107	0.515	4.69	79.32	1415	11.32	130.391	4.1	90.73

Test Results for ja=0.044 m/s

Jl (m/s)	r/R	α %	no of S. B	Uav(m/s)	Dav(mm)	IACav(1/m)	NOB	freq.(1/s)	IAC I (1/m)	Duga (mm)	IAC UGA
0.3	0	11.9	161	0.91	3.749	190.45	3995	31.97	171.6	4.3	166.05
	0.1	11.33	610	0.915	3.645	186.50	3898	31.19	164.67	4.6	147.78
	0.2	10.93	402	0.903	3.71	176.77	3841	30.73	167.575	4	163.95
	0.3	10.61	484	0.882	3.9	163.23	3697	29.58	161.04	4.3	148.05
	0.4	10.63	397	0.862	4.06	157.09	3548	28.39	164.85	3.9	163.54
	0.5	10.35	285	0.818	4.18	148.56	3442	27.54	165.26	3.8	163.42
	0.6	9.859	491	0.803	4.6	128.60	3134	25.08	149.723	4.2	140.84
	0.7	9.64	326	0.757	4.67	123.85	2824	22.60	139.87	4.6	125.74
	0.75	8.677	327	0.718	4.686	111.10	2577	20.62	132.16	4.7	110.77
	0.8	8.46	352	0.696	4.779	106.21	2461	19.69	129.684	4.5	112.80
	0.85	8.46	334	0.683	4.72	107.54	2216	17.73	129.6	4.4	115.36
	0.87	8.89	160	0.675	5.02	106.25	2094	16.76	120.1499	4.8	111.13
	0.9	7.465	239	0.654	5.16	86.80	1908	15.27	116.496	4.6	97.37
	0.92	7.51	218	0.592	4.37	103.11	1764	14.11	113.53	4.4	102.41
	0.95	6.11	165	0.54	4.72	77.67	1488	11.91	103.932	4.4	83.32
0.4	0	10.72	344	0.94	3.69	174.31	3883	31.10	156.124	3.6	178.67
	0.1	10.51	513	0.949	3.67	171.83	3835	30.69	149.88	3.6	175.17
	0.2	10.02	629	0.947	3.66	164.26	3855	30.86	153.378	3.6	167.00
	0.3	10.11	500	0.926	3.777	160.60	3735	29.90	149.561	3.5	173.31
	0.4	9.9965	459	0.8957	3.835	156.40	3535	28.29	150.55	3.2	187.43
	0.5	9.91	353	0.872	3.983	149.28	3348	26.79	148.84	3.6	165.17
	0.6	9.28	341	0.85	4.0998	135.81	3134	25.11	142.394	3.9	142.77
	0.7	8.77	332	0.797	3.95	133.22	3060	24.50	135.129	3.6	146.17
	0.75	8.54	295	0.763	3.998	128.16	2614	20.92	131.93	3.9	131.38
	0.8	8.57	267	0.751	4.28	120.14	2641	21.14	127.733	4	128.55
	0.85	7.66	262	0.728	4.02	114.33	2324	18.60	117.9927	3.9	117.85
	0.87	7.63	251	0.695	4.348	105.29	2146	17.17	109.381	4.5	101.73
	0.9	7.34	253	0.7298	4.81	91.56	1994	15.96	101.335	4.2	104.86
	0.92	6.577	211	0.696	4.136	95.41	1798	14.41	89.679	4.7	83.96
	0.95	6.1	207	0.646	4.24	86.32	1589	12.71	98.735	4.4	83.18

Test Results for ja=0.044 m/s

Jl (m/s)	r/R	α %	no of S. B	Uav(m/s)	Dav(mm)	IACav(1/m)	NOB	freq.(1/s)	IAC k (1/m)	Duga (mm)	IAC UGA
0.02	0	17.75	637	0.93	4.9	217.34	5480	43.90	214.879	5	213.00
	0.1	17.54	376	0.9159	4.9	211.74	5257	42.09	209.93	4.9	214.78
	0.2	16.85	545	0.923	4.96	203.62	5072	40.73	214.874	5.2	194.42
	0.3	16.72	657	0.903	5.04	198.81	4987	40.03	210.048	5.3	189.28
	0.4	16.05	466	0.879	5.14	187.33	4403	35.30	205.11	5.1	188.82
	0.5	15.91	503	0.8558	5.45	174.91	4269	34.25	201.955	5.3	180.11
	0.6	14.45	416	0.775	5.29	163.83	3871	30.97	191.547	5.3	163.58
	0.7	13.74	509	0.749	5.68	145.12	3315	26.65	173.75	5.6	147.21
	0.75	12.64	434	0.7669	5.473	138.55	3224	25.87	167.69	5.7	133.05
	0.8	11.45	233	0.7589	5.73	119.78	2604	20.88	164.86	5.93	115.85
	0.85	10.73	200	0.716	6.22	103.40	2321	18.57	135.59	5.3	121.47
	0.87	10.3	251	0.6	6.1	101.30	2602	20.82	141.644	5.1	121.18
	0.9	9.01	173	0.668	5.75	93.95	2010	16.08	136.629	5.3	102.00
	0.92	8.29	163	0.637	6.17	80.52	1842	14.74	132.61	5.6	88.82
	0.95	6.59	95	0.5877	5.715	69.18	1466	11.73	105.8139	5.3	74.60
0.06	0	16.93	932	0.865	4.76	213.40	5093	40.77	202.649	4.95	205.21
	0.1	16.92	674	0.871	4.82	210.62	5300	42.46	201.342	4.83	210.19
	0.2	16.96	717	0.854	5.01	202.77	5462	43.71	203.058	4.5	226.13
	0.3	16.32	456	0.841	4.98	196.52	4992	40.07	199.782	4.9	199.84
	0.4	16.02	509	0.816	5.21	184.34	4565	36.53	197.41	4.4	218.45
	0.5	15.34	364	0.794	5.35	172.03	4162	33.31	194.658	5	184.08
	0.6	14.24	353	0.735	5.44	156.83	3900	31.21	183.98	4.55	187.78
	0.7	13.29	242	0.692	5.72	139.27	3328	26.63	172.11	4.6	173.35
	0.75	12.28	333	0.684	5.6	131.40	2917	23.37	158.719	4.9	150.37
	0.8	10.94	244	0.645	5.38	122.01	2326	18.65	148.077	4.98	131.81
	0.85	10.64	159	0.6198	5.96	107.11	2039	16.35	129.156	4.9	130.29
	0.87	9.95	167	0.581	5.77	103.47	2002	16.06	137.82	4.7	127.02
	0.9	8.756	132	0.557	5.92	88.74	1598	12.79	111.482	4.8	109.45
	0.92	7.94	135	0.5397	5.53	86.15	1430	11.47	112.99	5	95.28
	0.95	6.92	51	0.51	5.717	72.63	1149	9.19	79.99	5	83.04

Test Results for j_a=0.055 m/s

Jl (m/s)	r/R	α %	no of S. B	Uav(m/s)	Dav(mm)	IACav(1/m)	NOB	freq.(1/s)	IAC k (1/m)	Duga (mm)	IAC UGA
0.1	0	16.38	984	0.919	4.63	212.27	5355	42.85	200.829	4.8	204.75
	0.1	16.02	467	0.893	4.65	206.71	5381	43.11	195.04	4.3	223.53
	0.2	16.06	663	0.879	4.913	196.12	4818	38.56	192.78	4.7	205.02
	0.3	16.14	741	0.871	5.167	187.42	4884	39.10	189.629	5	193.68
	0.4	15.72	793	0.864	5.349	176.31	4551	36.46	186.99	5.2	181.38
	0.5	14.97	715	0.829	5.28	169.87	4168	33.37	182.49	5.1	176.12
	0.6	13.84	527	0.755	5.29	156.78	3849	30.81	171.517	4.9	169.47
	0.7	13.37	352	0.72	5.71	140.48	3339	26.75	162.56	4.7	170.68
	0.75	12.39	360	0.685	5.76	128.87	3122	24.99	155.32	4.8	154.88
	0.8	11.5	249	0.659	5.75	119.86	2840	22.75	146.826	4.7	146.81
	0.85	10.28	232	0.645	5.88	104.89	2258	18.07	122.537	5.2	118.62
	0.87	9.6	218	0.6328	4.689	122.84	2297	18.40	118.61	4.9	117.55
	0.9	9.057	136	0.695	5.517	98.49	2021	16.18	112.21	5	108.68
	0.92	7.91	124	0.722	6.19	76.60	1769	14.16	103.555	5.2	91.27
	0.95	6.64	129	0.508	5.09	78.27	1582	12.67	94.05	4.8	83.00
0.2	0	15.377	617	0.955	4.57	201.73	5293	42.54	190.866	4.5	205.03
	0.1	15.14	498	0.953	4.62	196.62	5058	40.51	185.16	4.9	185.39
	0.2	14.93	590	0.947	4.74	188.78	4831	38.66	183.84	4.75	188.59
	0.3	14.525	1144	0.932	4.88	178.56	4819	38.56	183.91	4.5	193.67
	0.4	14.51	660	0.8958	5.07	171.59	4170	33.37	178.08	5.1	170.71
	0.5	13.97	339	0.8479	5.26	159.16	3950	31.62	170.2	4.8	174.63
	0.6	13.12	348	0.7992	5.37	146.41	3565	28.53	166.067	4.8	164.00
	0.7	12.4	257	0.789	5.73	129.71	3098	24.79	151.09	4.8	155.00
	0.75	11.724	395	0.735	6.34	110.90	2993	23.95	137.926	5	140.69
	0.8	11.07	338	0.6987	6.21	106.79	2656	21.25	138.11	5	132.84
	0.85	10.27	289	0.669	6.189	99.55	2234	17.88	129.687	5.3	116.26
	0.87	9.81	252	0.636	6.56	89.59	2377	19.03	137.35	4.7	125.23
	0.9	8.319	207	0.622	5.54	89.94	1972	15.78	133.922	4.8	103.99
	0.92	7.74	156	0.494	6.13	75.69	1695	13.57	123.29	4.6	100.96
	0.95	7.07	111	0.547	5.49	77.22	1421	11.40	118.09	4.6	92.22

Test Results for j_a=0.055 m/s

Jl (m/s)	r/R	α %	no of S. B	Uav(m/s)	Dav(mm)	IACav(1/m)	NOB	freq.(1/s)	IAC k (1/m)	Duga (mm)	IAC UGA
0.3	0	13.76	945	1.01	4.29	192.45	5182	41.55	185.43	4.4	187.64
	0.1	14.12	1019	0.994	4.45	190.38	5276	42.42	180.15	4.1	206.63
	0.2	13.85	941	0.98	4.61	180.26	4845	38.77	180.62	4.6	180.65
	0.3	13.82	633	1	4.87	170.17	4779	38.24	180.229	4.8	172.75
	0.4	13.86	669	0.927	5.047	164.75	4527	36.22	176.77	4.7	176.94
	0.5	13.46	525	0.894	5.35	150.95	4280	34.25	167.52	4.7	171.83
	0.6	13	501	0.871	5.58	139.69	3838	30.71	162.1	4.8	162.50
	0.7	12.28	427	0.85	5.93	124.25	3408	27.27	147.44	4.8	153.50
	0.75	11.23	335	0.809	5.85	115.18	3086	24.70	138.395	5.4	124.78
	0.8	10.97	412	0.756	6.13	107.37	2852	22.82	139.287	5.2	126.58
	0.85	10.745	312	0.723	6.68	96.51	2600	20.81	130.62	5.2	123.98
	0.87	9.33	270	0.719	6.1	91.77	2402	19.25	126.2	5.1	109.76
	0.9	9.15	243	0.706	6.55	83.82	2145	17.19	114.63	5.2	105.58
	0.92	8.468	221	0.651	6.33	80.27	1820	14.57	104.373	5.2	97.71
	0.95	7.02	151	0.625	5.98	70.43	1377	11.04	83.71	4.9	85.96
0.4	0	12.16	1211	1.119	4.11	177.48	4960	39.69	177.8	4.1	177.95
	0.1	12.67	729	1.103	4.3	176.72	5009	40.17	168.15	4.6	165.26
	0.2	13.01	543	1.092	4.67	166.85	5143	41.15	169.9	4.1	190.39
	0.3	12.54	609	1.063	4.62	162.79	4774	38.20	160.25	4.1	183.51
	0.4	12.44	532	0.991	4.955	150.62	4638	37.16	158.28	4.1	182.05
	0.5	12.47	389	0.982	5.35	139.65	4311	34.51	155.62	4.3	174.00
	0.6	11.79	622	0.935	5.57	126.85	3989	31.93	151.93	4.4	160.77
	0.7	11.42	511	0.881	5.955	115.06	3603	28.83	147.22	4.4	155.73
	0.75	10.67	367	0.852	6.13	104.42	3159	25.28	126.67	4.8	133.38
	0.8	10.19	413	0.84	6.51	93.90	2874	23.01	117.21	4.8	127.38
	0.85	9.93	411	0.8	7.34	81.14	2837	22.70	127.85	4.7	126.77
	0.87	9.86	262	0.765	6.82	86.73	2572	20.58	114.61	4.6	128.61
	0.9	8.64	378	0.725	5.77	89.80	2226	17.81	112.34	4.6	112.70
	0.92	8	300	0.75	5.45	88.07	2029	16.24	88.3	5	96.00
	0.95	7.29	268	0.741	5.49	79.56	1815	14.52	94.385	5.6	78.11

Test Results for j_a=0.055 m/s

Appendix B

Area Averaged Experimental Results For 20 cm Diameter Pipe

Ja (m/s)	0.022					0.033				
Jl (m/s)	α %	Ub (m/s)	IAC Present Data	IAC Tabie et al. (1989)	IAC Akita and Yoshida (1974)	α %	Ub (m/s)	IAC Present Data	IAC Tabie et al. (1989)	IAC Akita and Yoshida (1974)
0.02	7.68	0.40	211.04	79.90	82.47	9.90	0.40	167.48	107.87	109.97
0.06	6.17	0.44	174.51	61.55	64.42	9.37	0.49	161.81	101.06	103.27
0.1	5.22	0.51	126.81	50.30	53.31	8.68	0.52	152.22	92.38	94.73
0.2	4.50	0.53	100.18	42.01	45.07	7.49	0.58	132.80	77.63	80.23
0.3	3.88	0.56	87.21	35.13	38.17	6.45	0.61	118.05	64.94	67.76
0.4	3.44	0.62	82.56	30.33	33.33	6.11	0.66	118.41	60.79	63.68

Ja (m/s)	0.044					0.055				
Jl (m/s)	α %	Ub (m/s)	IAC Present Data	IAC Tabie et al. (1989)	IAC Akita and Yoshida (1974)	α %	Ub (m/s)	IAC Present Data	IAC Tabie et al. (1989)	IAC Akita and Yoshida (1974)
0.02	11.85	0.61	169.31	132.85	134.74	12.70	0.76	169.40	143.84	145.74
0.06	11.18	0.65	164.54	124.20	126.14	12.43	0.69	158.28	140.32	142.21
0.1	10.69	0.66	156.83	117.93	119.92	12.27	0.73	151.07	138.29	140.18
0.2	10.39	0.68	151.36	114.14	116.17	11.64	0.75	150.80	130.17	132.08
0.3	9.12	0.74	138.87	98.01	100.26	11.46	0.81	143.91	127.80	129.72
0.4	8.58	0.80	128.60	91.21	93.58	10.73	0.88	133.88	118.48	120.46

Area Avearged Results for D=20 cm